Inaugural dissertation

for

obtaining the doctoral degree

of the

Combined Faculty of Mathematics, Engineering and Natural Sciences

of the

Ruprecht - Karls - University

Heidelberg

Presented by

M.Sc. Céline Saad

born in: Awkar, Lebanon

Oral examination: February 2026

Validating Novel Targets for Substrate Reduction Therapy in Glutaric Aciduria Type I

Referees: Prof. Dr. Christian Schaaf

Prof. Dr. Stefan Kölker

Summary

Glutaric aciduria type 1 (GA1) (OMIM #231670) is a rare autosomal recessive neurometabolic disorder caused by pathogenic variants in the *GCDH* gene (19p13.13). Deficiency of glutaryl-CoA dehydrogenase (GCDH) results in accumulation of neurotoxic glutaryl-CoA, glutaric acid, and 3-hydroxyglutaric acid. Clinically, GA1 features acute or insidious striatal damage causing variable movement disorders in infancy. Despite early diagnosis and treatment, current therapies remain suboptimal, and many patients develop dystonia, white-matter changes, intellectual impairment, and chronic kidney disease.

This study aimed to identify a target for substrate reduction therapy (SRT) focusing on lysine-degradation enzymes upstream of GCDH and to develop a human iPSC-based GA1 model. In vivo experiments used a *Gcdh* KO mouse combined with *Aass* or *Aadat* knockouts. All groups experienced metabolic stress using a high-lysine diet (HLD) to provoke the GA1 phenotype. Behavioral, histological, and biochemical assessments evaluated neuropathological and systemic alterations.

Analysis of *Gcdh/Aadat* KO and *Gcdh/Aass* KO mice showed that *Aadat* deletion did not ameliorate disease symptoms. Although neurotoxin reductions were seen in *Gcdh/Aadat* KO brains, this improvement was tissue-restricted, suggesting limited therapeutic coverage. Consistently, pharmacological AADAT inhibition with PF-04859989 had no benefit, demonstrating that AADAT is not a suitable monotherapy target. In contrast, *Aass* deletion provided systemic protection: *Gcdh/Aass* KO mice exhibited markedly reduced neurotoxins, attenuated neurological impairment, and improved overall condition under HLD stress. These findings indicate that blocking lysine metabolism effectively prevents neurotoxic metabolite formation.

Taken together, the findings support AASS inhibition or knockout as a promising SRT strategy for GA1, demonstrating metabolic and phenotypic benefits in preclinical models and providing a foundation for more effective therapies.

Zusammenfassung

Glutaraziduri Typ 1 (GA1) (OMIM #231670) ist eine seltene autosomal-rezessive neurometabolische Erkrankung, die durch pathogene Varianten im *GCDH*-Gen (19p13.13) verursacht wird. Ein Mangel an Glutaryl-CoA-Dehydrogenase (GCDH) führt zur Anreicherung von neurotoxischem Glutaryl-CoA, Glutarsäure und 3-Hydroxyglutarsäure. Klinisch ist GA1 durch eine akute oder schleichende Schädigung des Striatums gekennzeichnet, die zu unterschiedlichen Bewegungsstörungen im Säuglingsalter führt. Trotz frühzeitiger Diagnose und Behandlung sind die derzeitigen Therapien nach wie vor suboptimal, und viele Patienten entwickeln Dystonie, Veränderungen der weißen Substanz, geistige Beeinträchtigungen und chronische Nierenerkrankungen.

Ziel dieser Studie war es, einen Ansatzpunkt für eine Substratreduktionstherapie (SRT) zu identifizieren, die sich auf Lysin-abbauende Enzyme stromaufwärts von GCDH konzentriert, und ein auf humanen iPSC basierendes GA1-Modell zu entwickeln. In-vivo-Experimente wurden mit einer Gcdh-KO-Maus in Kombination mit Aass- oder Aadat-Knockouts durchgeführt. Alle Gruppen wurden einer metabolischen Belastung durch eine lysinreiche Ernährung (HLD) ausgesetzt, um den GA1-Phänotyp zu provozieren. Neuropathologische und systemische Veränderungen wurden anhand von Verhaltens-, histologischen und biochemischen Bewertungen beurteilt.

Die Analyse von *Gcdh/Aadat*-KO- und *Gcdh/Aass*-KO-Tieren zeigte, dass die Aadat-Deletion die Krankheitssymptome nicht linderte. Obwohl in *Gcdh/Aadat*-KO-Gehirnen eine Verringerung der Neurotoxine festgestellt wurde, war diese Verbesserung auf das Gewebe beschränkt, was auf eine begrenzte therapeutische Wirksamkeit hindeutet. In Übereinstimmung damit hatte die pharmakologische AADAT-Hemmung mit PF-04859989 keinen Nutzen, was zeigt, dass AADAT kein geeignetes Ziel für eine Monotherapie ist. Im Gegensatz dazu bot die *Aass*-Deletion einen systemischen Schutz: *Gcdh/Aass*-KO-Mäuse zeigten unter HLD-Stress deutlich reduzierte Neurotoxine, abgeschwächte neurologische Beeinträchtigungen und einen verbesserten

Gesamtzustand. Diese Ergebnisse deuten darauf hin, dass die Blockierung des Lysin-Stoffwechsels die Bildung neurotoxischer Metaboliten wirksam verhindert.

Zusammengenommen stützen die Ergebnisse die Hemmung oder das Knockout von AASS als vielversprechende SRT-Strategie für GA1, da sie metabolische und phänotypische Vorteile in präklinischen Modellen zeigen und eine Grundlage für wirksamere Therapien bieten.

Table of Content

Abbreviations

2AA	2-Aminoadipic acid
2OA	2-Oxoadipic acid
3OHGA	3-Hydroxyglutaric acid
AASS	2-Aminoadipate semialdehyde synthase
AADAT	2-Aminoadipate aminotransferase
ACADS	Short-chain acyl-CoA dehydrogenase
ALDH7A1	Aldehyde dehydrogenase 7 family, member A1
BBB	Blood-brain barrier
BSA	Bovine serum albumin
C5DC	Glutarylcarnitine
c-MYC	Protooncogene coding for transcription factors
CoA	Coenzyme A
CRISPR/Cas9	Clustered regularly interspaced short palindromic repeats/CRISPR-associated protein 9
DAPI	4’,6-Diamidino-2-phenylindol
DBS	Dried blot spot
DHTKD1	Dehydrogenase E1 and transketolase domain-containing protein 1
DMEM	Dulbecco’s modified Eagle medium
DNA	Deoxyribonucleic acid
DNase	Deoxyribonuclease
DTT	Dithiothreitol
dNTPs	Deoxyribonucleotide triphosphate
dH2O	Distilled water
EBs	embryoid bodies
E. coli	Escherichia coli
EDTA	Ethylenediaminetetraacetic acid
ESCs	Embryonic stem cells
et al.	et altera (i.e., and others)

ETF	Electron transfer flavoprotein
FAD	Flavin adenine dinucleotide
FCS	Fetal calf serum
GA	Glutaric acid
GA1	Glutaric aciduria type 1
GABA	Gamma-aminobutyric Acid
GAPDH	Glyceraldehyde-3-phosphate dehydrogenase
GC/MS	Gas chromatography / Mass spectrometry
GCDH	Glutaryl-CoA dehydrogenase
HE	High excreters
HepG2	Human liver cancer cell line
HLD	High lysine diet
HTS	High-throughput screening
iPSCs	Induced pluripotent stem cells
IVD	Isovaleryl-CoA dehydrogenase
KA	Kynurenic acid
KAT II	kynurenine aminotransferase II
KLF4	Krüppel-like factor 4
KO	Knockout
LE	Low excreters
LOR	Lysine-oxoglutarate reductase
MCAD	Medium-chain acyl-CoA dehydrogenase
NaCl	Sodium chloride
NBS	Newborn screening
NMDA	N-Methyl-D-Aspartate
NPC	Neuron progenitor cell
PBS	Phosphate Buffer saline
PCR	Polymerase chain reaction
pH	Potential of hydrogen
PIPOX	Pipecolic acid and sarcosine oxidase
PLP	Pyridoxal phosphate

POI	Protein of interest
RT	Room temperature
RT-qPCR	Real-time polymerase chain reaction
RNA	Ribonucleic acid
rpm	Rounds per minute
SCHAD	Short-chain 3-hydroxyacyl-CoA dehydrogenase
SD	Standard deviation
SDH	Saccharopine dehydrogenase
SDS	Sodium dodecyl sulfate
SDS-PAGE	Sodium dodecyl sulfate–polyacrylamide gel electrophoresis
SNPs	Single nucleotide polymorphism
SOX2	(Sex-determining region Y)-box 2
SUGCT	Succinyl-CoA:glutarate-CoA transferase
Taq	Thermus aquaticus
TBST	Tris-buffered saline with Tween-20 detergent
TCA	Tricarboxylic acid
TEMED	Tetramethylethylenediamine
Tris	Tris(hydroxymethyl)aminomethane
Triton X100	t-Octyl phenoxy polyethoxy ethanol
OCT4	Octamer-binding transcription factor 4
2AA	2-Aminoadipic acid
2OA	Oxoadipic acid
3OHGA	3-Hydroxyglutaric acid
ON	Over night
w	Weeks
WT	Wild type
vs.	Versus

Symbols

c	centi (10^{-2})
Da	Dalton
°C	Degree Celsius
N	Experiment number
g	Gram
h	Hour
l	Kilo (10^{3})
L	Liter
M	Meter
µ	Micro (10^{-6})
M	Milli (10^{-3})
min	Minute
M	Molar (mol/l)
n	Nano (10^{-9})
%	Percent
mol	SI unit of the amount of substance

Introduction

Glutaric aciduria type 1: clinical presentation

Glutaric aciduria type 1 (GA1; MIM #231670) is a rare autosomal recessive neurometabolic disorder caused by pathogenic variants in the *GCDH* gene (NCBI gene ID: 2639; cytogenic location: 19p13.13). It encodes the mitochondrial enzyme glutaryl-CoA dehydrogenase (GCDH; EC 1.3.8.6). This enzyme plays an important role in the catabolism of the amino acids L-lysine, L-hydroxylysine, and L-tryptophan [1]. Deficiency of GCDH results in the accumulation of neurotoxic glutaryl-CoA, glutaric acid (GA), 3-hydroxyglutaric acid (3OHGA), and nontoxic glutarylcarnitine (C5DC). Accumulation of neurotoxic dicarboxylic compounds in the brain compartment affects the central nervous system, specifically the striatum [2] due to synergistically acting inhibition of mitochondrial energy metabolism and neurotransmitter homeostasis as well as increased oxidative stress. As a consequence, affected infants develop a complex movement disorder with predominant dystonia with variable impact on motor function and neuro-development [3]. Clinical outcomes depend on the age of diagnosis and start of treatment [4], and adherence to recommended dietary and emergency treatment.

One of the earliest signs is macrocephaly, often present at birth or developing within the first few months of life. However, it is absent in approximately 25% of affected individuals. Slight muscular hypotonia is also often found in infants but can be fully reversible [5, 6]. If not diagnosed and treated early, the majority of affected individuals experience acute- or insidious-onset of striatal damage with subsequent dystonia during a critical time window between 6 and 36 months of age [7]. Clinical manifestations with acute encephalopathic crises are commonly precipitated by catabolic stressors such as fever, intercurrent infectious disease, prolonged fasting, or surgery. They are marked by sudden-onset dystonia, rigidity, and loss of previously acquired motor skills. Commonly, these physical changes correlate with bilateral necrosis of the caudate and putamen on MRI [8]. The damage sustained during these episodes is often irreversible, resulting in severe motor disabilities and loss of acquired motor functions [8]. Some individuals experience an insidious disease course, characterized by gradually progressive dystonia

and motor impairment in the absence of a clear metabolic decompensation episode [9]. In early treated individuals, insidious onset has been associated with non-adherence to low-lysine diet [10, 11].

Based on biochemical findings, GA1 patients have been arbitrarily distinguished into high excreters (HE) or low excreters (LE) [12]. The HE group shows markedly elevated urinary GA levels exceeding 100 mmol/mol creatinine [12]. These patients generally have near-complete loss of GCDH enzyme function. Patients in the LE group are characterized by urinary GA concentrations below 100 mmol/mol creatinine and residual enzyme activity between 3-30% of controls [9]. Despite these biochemical differences, both LE and HE patients have a strongly increased risk of striatal damage during infancy and, therefore, LE patients should not be mistaken as having an attenuated clinical phenotype [13]. However, despite initial similarity HE patients are more likely to develop a progressive clinical phenotype, involving white matter, cognitive function, peripheral nervous system, and renal function than LE patients in the long run [9, 11, 13].

While enzyme activity and excretion profiles can offer some insight into the metabolic background of the disorder, genotype-phenotype correlations in GA1 remain unclear [14]. Several studies have shown that patients with identical *GCDH* mutations can have different clinical outcomes [15]. This suggests the involvement of additional modifying factors such as impairment of mitochondrial function due to lysine glutarylation of mitochondrial proteins [16]. Understanding these variable clinical and biochemical manifestations highlights the need for precise diagnostic methods and early intervention strategies.

Metabolic work-up and newborn screening program

The diagnosis of GA1 can be established through two main routes: the clinical investigation of symptomatic patients and the identification of asymptomatic individuals via newborn screening (NBS). In symptomatic individuals, diagnostic confirmation relies on a combination of biochemical and molecular analyses that collectively characterize the metabolic block in amino acids catabolism. Organic acid analysis of urine using gas chromatography–mass spectrometry (GC-MS) typically reveals the accumulation of GA and 3OHGA, which are hallmark metabolites of GA1 and serve as the primary diagnostic indicators [17]. In parallel, acylcarnitine profiling in dried blood spots (DBS) using tandem mass spectrometry (MS/MS) often demonstrates elevated levels of C5DC, providing supportive evidence for the diagnosis [18].

In cases where biochemical results are ambiguous, such as in patients with LE phenotypes, measurement of residual GCDH enzyme activity in cultured fibroblasts or leukocytes can provide functional confirmation [19]. Furthermore, molecular genetic testing of the *GCDH* gene allows for the identification of (likely) pathogenic variants, enabling definitive diagnosis [20]. The integration of these complementary diagnostic approaches ensures high diagnostic accuracy, particularly in atypical or borderline biochemical presentations.

In addition to the diagnostic work-up of symptomatic cases, population-based NBS has proven transformative. The increasing introduction of GA1 to NBS programs worldwide has significantly transformed the early detection and clinical management of GA1 [21]. Through the quantification of C5DC as first tier in neonatal DBS samples by MS/MS, NBS enables the identification of affected infants before the onset of clinical symptoms [12]. The major advantage of NBS lies in its capacity to prevent irreversible neurological injury through the prompt initiation of dietary lysine restriction and carnitine supplementation [22]. Large-scale population studies have demonstrated that patients diagnosed pre-symptomatically through NBS exhibit markedly improved neurological outcomes and reduced incidence of dystonia and motor regression compared to those diagnosed after symptom onset [11].

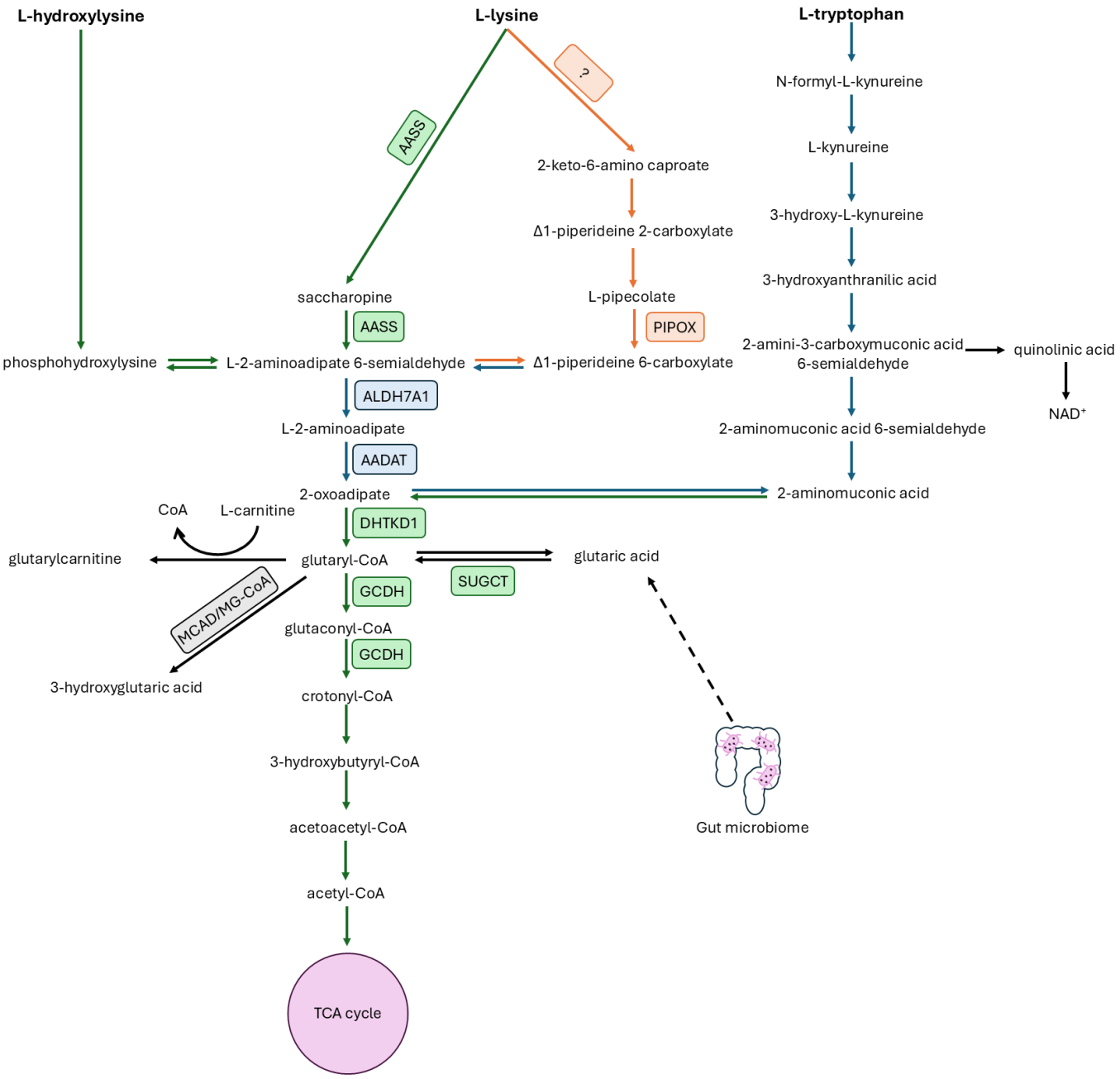

Figure 1. Degradation pathways of L-lysine, L-hydroxylysine and L-tryptophan. The deficiency of glutaryl-CoA dehydrogenase (GCDH) results in the accumulation and urinary excretion of the metabolites glutaric acid (GA), 3-hydroxyglutaric acid (3 OH-GA), and glutarylcarnitine (C5DC). Abbreviations used: AASS, aminoadipic acid semialdehyde synthase; ALDH7A1, Aldehyde dehydrogenase 7; AADAT, 2-aminoadipate aminotransferase; DHTKD1, dehydrogenase E1 and transketolase domain containing protein 1; MCAD, medium-chain acyl-CoA dehydrogenase; TCA cycle, tricarboxylic acid cycle. Enzymes are represented by squares. In orange are the enzymatic reactions happening in peroxisomes, in blue in the cytoplasm, in green in the mitochondria

Disruption of the catabolic pathways of L-lysine, L-tryptophan, and L-hydroxylysine pathways in GA1 and its consequences

The metabolic abnormalities in GA1 originate from a disruption in the mitochondrial degradation of L-lysine, L-tryptophan, and L-hydroxylysine. These amino acids catabolic pathways are essential metabolic routes that play an important role in cell function [23]. This catabolic breakdown transforms their carbon backbones into usable energy and metabolic intermediates. Disruptions in these pathways can lead to the accumulation of toxic byproducts, as is seen in GA1 [24]. In healthy individuals, lysine degradation is primarily initiated through the saccharopine branch, while a quantitatively minor route utilizes the pipecolic acid branch of this pathway, both ultimately leading to the formation of glutaryl-CoA. The latter is then converted by GCDH through oxidative decarboxylation into crotonyl-CoA, a precursor of acetyl-CoA that can enter the tricarboxylic acid (TCA) cycle [23]. Tryptophan, another essential amino acid, is primarily metabolized through the kynurenine pathway, which converges with the lysine oxidative pathway at the level of 2-oxoadipate. Similarly, hydroxylysine, a derivative of lysine found mainly in collagen, is metabolized in a pathway that converges with lysine degradation. Finally, all three catabolic pathways can produce glutaryl-CoA; however, there is a fourth route: GA produced by gut bacteria can be re-absorbed in the intestines and activated back into glutaryl-CoA via succinyl-CoA:glutarate-CoA transferase (SUGCT), the enzyme deficient in glutaric aciduria type 3 [25, 26]. GCDH deficiency leads to failure in processing glutaryl-CoA effectively. Consequently, glutaryl-CoA accumulates and is hydrolyzed non-enzymatically or via side reactions into GA and 3OHGA. The blockage at the glutaryl-CoA step therefore represents an obstacle in the catabolism of all three amino acids disrupting cellular energy balance and generating damaging intermediates.

Metabolic disruption has both systemic and tissue-specific consequences, particularly in energy-demanding organs like the brain [14]. Lysine and tryptophan, being essential amino acids, must be obtained from diet and are actively transported across the blood-brain barrier (BBB) [27]. Once in the brain, their catabolism is tightly regulated. Similarly, lysine metabolism contributes to carnitine homeostasis, and its impairment may reduce available carnitine pools, further impairing mitochondrial fatty acid oxidation and energy

production [28]. The excessive formation of these glutarylated intermediates promotes the conjugation of glutaryl residues to free carnitine, forming C5DC, which in turn leads to secondary depletion of systemic carnitine pools. This reduction in available carnitine further compromises mitochondrial β-oxidation and energy metabolism, exacerbating metabolic stress in affected tissues [29].

During periods of metabolic stress such as intercurrent illness, fasting, or high-protein intake, the demand for amino acid catabolism increases [30]. In GA1 patients, this can lead to a strong increase in toxic metabolite production, overwhelming the body's capacity to excrete these compounds and triggering acute neurological crises [31]. Neurons exposed to elevated levels of GA and 3OHGA show increased oxidative stress, disrupted calcium homeostasis, and mitochondrial swelling, all of which are hallmarks of neurotoxicity [31]. These effects are most prominent in the developing brain, coinciding with the peak vulnerability window for striatal damage in GA1 [32].

Neurotoxicity of glutaryl-CoA, GA and 3OHGA

Glutaryl-CoA is a central mitochondrial toxin in GA1. GCDH deficiency prevents glutaryl-CoA conversion to crotonyl-CoA, causing glutaryl-CoA accumulation in mitochondria. This buildup competes with other acyl-CoA species for CoA, reducing free CoA needed for the TCA cycle and β-oxidation, thereby impairing energy metabolism [33]. Glutaryl-CoA also drives non-enzymatic protein glutarylation of lysine residues in mitochondrial enzymes, destabilizing protein structure, impairing enzyme activity, and disrupting electron transport, which reduces ATP generation and increases reactive oxygen species (ROS) [16].

Secondary metabolites GA and 3OHGA further compromise mitochondrial function, increasing ROS production and oxidative stress [34]. Medium-spiny neurons, the most abundant neuronal species in the striatum, are highly susceptible due to high metabolic demands, strong excitatory glutamatergic input, and limited antioxidant defenses [2] [34]. GA and 3OHGA disrupt mitochondrial membrane potential and inhibit electron transport chain enzymes, reducing ATP and promoting superoxide generation and thus facilitating the formation of peroxynitrite. This leads to lipid peroxidation, protein carbonylation, DNA

damage, and activation of intrinsic apoptotic pathways, resulting in neuronal death. Oxidative stress also triggers glial activation and inflammatory cytokine release, exacerbating neuroinflammation [34].

GA and 3OHGA also impair neurotransmission, particularly glutamatergic signaling [35]. They inhibit astrocytic glutamate uptake, elevating extracellular glutamate and enhancing excitotoxicity [2]. Excess glutamate over-activates NMDA and AMPA receptors, causing calcium influx, protease activation, and further mitochondrial stress. In the developing brain, this disrupts synaptic pruning and neuroplasticity [35]. GA additionally impairs GABAergic transmission by inhibiting glutamate decarboxylase, potentially contributing to excitatory/inhibitory imbalance, which may underline movement disorders and cognitive deficits in GA1 [2, 36].

Prolonged GA and 3OHGA exposure also affect BBB integrity [37]. Elevated levels can disrupt tight junction proteins and trigger endothelial inflammation, increasing BBB permeability and facilitating neurotoxic and immune cell infiltration [2, 35]. Accumulation of these metabolites in cerebrospinal fluid and brain parenchyma can disturb osmotic balance, causing cellular swelling and vacuolization, particularly in striatal neurons, which exhibit degenerative changes consistent with metabolic encephalopathy [3]. These pathologies reflect combined effects of mitochondrial dysfunction, excitotoxicity, oxidative stress, and ion imbalance.

The “entrapment hypothesis” explains the selective accumulation of GA and 3OHGA in the brain. The BBB has low permeability for di- and tricarboxylic acids due to absent high-capacity transporters, preventing efficient efflux of GA and 3OHGA from the CNS. Local production from glutaryl-CoA in neurons and astrocytes leads to progressive intraparenchymal accumulation, especially in metabolically active regions like the striatum [2]. These metabolites exert cytotoxic effects through mitochondrial dehydrogenase inhibition, energy disruption, and oxidative/excitotoxic stress, creating a self-reinforcing loop of metabolic entrapment, mitochondrial impairment, neuroinflammation, and neuronal loss. This provides a biochemical and anatomical explanation for the brain-specific vulnerability in GA1 despite systemic presence of the metabolites [2, 38]. Together, these pathophysiological mechanisms explain the selective

vulnerability of the striatum and provide the rationale for developing experimental and animal models that reproduce these neuropathological features.

GA1 mouse model

To better understand disease mechanisms and evaluate potential treatments, a mouse model of GA1 has been established. The most frequently studied mouse model for GA1 is a genetic knockout (KO) of the *Gcdh* gene with complete loss of enzymatic GCDH activity [39]. This model recapitulates key metabolic features of the human disease, such as accumulation of GA and 3OHGA, particularly in brain, peripheral tissues, and body fluids [39]. However, under standard dietary conditions, these mice do not spontaneously develop a neurological phenotype that resembles acute- or insidious-onset striatal damage in individuals with GA1. This has led to the introduction of dietary stressor, the high lysine diet (HLD), to trigger disease-relevant phenotypes. Feeding *Gcdh* KO mice a HLD challenges their metabolic capacity and mimics catabolic conditions in GA1 patients [40]. Under these conditions, mice exhibit significant metabolic disturbances, including elevated levels of GA and 3OHGA, increased oxidative stress, and energy imbalance [40]. Neurologically, HLD leads to neuronal vacuolation, reactive gliosis, and degeneration primarily in brain regions analogous to the striatum and hippocampus [2]. Moreover, movement changes were noted, mirroring the neurodegenerative patterns seen in patients during acute encephalopathic crises. The administration of lysine-rich diets therefore serves as a functional model to induce pathology and study mechanisms underlying disease progression and potential therapeutic interventions.

The choice of mouse genetic background may relevantly influence the resulting clinical phenotype; however, their potential impact is often underestimated. Common laboratory strains such as C57BL/6N and SV129 have distinct genetic architectures that impact metabolic pathways, immune responses, and neural development. For instance, C57BL/6N mice are known to exhibit distinct mitochondrial function profiles and have a generally higher baseline oxidative stress compared to SV129 mice. In contrast, SV129 mice may have differing levels of baseline carnitine, glutathione, and other metabolic regulators, which can influence how they respond to disruptions in lysine degradation or

oxidative metabolism [41-44]. Neurologically, strain differences manifest in neurodevelopmental timing, synaptic plasticity, and neuronal vulnerability to stressors [44, 45]. C57BL/6N mice, for example, often show higher baseline activity in certain behavioral tests [46] but are more prone to neurodegeneration under oxidative or excitotoxic conditions [45]. SV129 mice, on the other hand, may exhibit delayed but more prolonged responses to similar insults [47]. These intrinsic differences can result in varying degrees of susceptibility to GA1-like pathology.

These genetic background effects are crucial not only for interpreting experimental results but also for the translational relevance of findings. An intervention that is effective in one strain may fail in another due to these baseline differences, which may or may not reflect human variability [48]. Therefore, selecting an appropriate genetic background is essential for aligning the animal model with specific research question whether it concerns acute neurotoxicity, chronic disease progression, or therapeutic efficacy. These considerations are vital for designing robust, reproducible, and translatable experiments in the context of GA1 and metabolic diseases in general. Selecting the most appropriate genetic background and understanding its inherent characteristics ensures that the mouse model faithfully reflects the human disease features under study [48]. In the establishment of a standardized HLD model for GA1, various factors have been carefully considered to ensure reproducibility and translational relevance, including dietary lysine content and developmental stage at exposure. Sauer et al. systematically evaluated these parameters to optimize the induction of neuropathological features consistent with the human phenotype, thereby providing a reliable preclinical framework for studying disease mechanisms and therapeutic interventions [49]. These models provide an essential experimental framework to test new therapeutic concepts and understand the biochemical complexity of GA1 at the organismal level.

Recommended metabolic therapy for GA1 and its limitations

Currently recommended therapy for GA1 aims at preventing irreversible brain damage though reduced production and accumulation of toxic metabolites and the preservation of anabolism, especially during infancy and early childhood. To achieve this goal individuals with GA1 receive low-lysine diet, carnitine supplementation, and intermittent emergency

treatment during putatively threatening episodes that are likely to induce catabolism [50]. Therapy initiated in symptomatic patients with GA1 after the manifestation of striatal damage is ineffective since brain damage is irreversible [4]. Therefore, the efficacy of any therapy for GA1 critically depends on the availability of NBS programs for GA1.

The low-lysine diet is designed to minimize the substrate load entering the defective metabolic pathway and hence the formation of toxic metabolites. Specialized medical formulas devoid of lysine and low in tryptophan are added to provide adequate supply with all essential nutrients and micronutrients [50]. While this dietary therapy has been shown to reduce the incidence of acute striatal injury when started in asymptomatic newborns and infants, it is not curative and requires precise adherence to the prescribed treatment and supervision by an multiprofessional team [51].

Furthermore, carnitine supplementation is used to prevent secondary carnitine depletion and to support the formation and urinary excretion of non-toxic C5DC (as seen in figure 1) [52]. While this intervention can lower the intracellular burden of glutaryl-CoA, GA, and 3OHGA and may have a mild detoxifying effect, it does not fully prevent neurotoxicity or the progression of neurological symptoms in all patients [53].

Emergency treatment protocols are employed during times of catabolic stress and typically include intravenous glucose to suppress endogenous protein breakdown, temporary protein restriction, and increased carnitine dosing [52].

Despite these interventions, the efficacy of current therapies remains suboptimal [54]. Some patients, even those who identified early through NBS and are treated proactively, still go on to develop movement disorders such as dystonia, white matter changes, and even chronic kidney disease [53]. This partial therapeutic inefficacy is explained by challenges in achieving consistent dietary adherence and the inability of current therapies to protect against effects of neurotoxins throughout life [54].

Upstream enzymes of GCDH in the lysine degradation pathway as potential therapeutic targets

As a consequence of incomplete protection against short- and long-term negative consequences of GA1, more reliable therapeutic strategies are needed. One of the currently evaluated strategies is substrate reduction therapy (SRT) aiming to minimize flux through the defective pathway by inhibition of enzyme or transporters upstream of the defective enzyme. It is important to target key enzymes in the lysine degradation pathway, specifically the saccharopine pathway, which serve to catabolize lysine into intermediates that feed into the tricarboxylic acid (TCA) cycle [21].

DHTKD1 is involved in converting 2-oxoadipate to glutaryl-CoA. While DHTKD1 inhibition was hypothesized to reduce glutaryl-CoA levels and mitigate GA1 symptoms, studies have shown that genetic deletion of *Dhtkd1* in *Gcdh* KO mice did not alleviate the biochemical and clinical manifestations of GA1. These *Gcdh/Dhtkd1* KO mice exhibited similar metabolite accumulations as *Gcdh* KO mice, indicating that DHTKD1 inhibition alone is insufficient to treat GA1. This is explained by 2-oxoglutarate dehydrogenase complex in the TCA, which can also accept 2-oxoadipate at lower substrate activity and thus opens an alternative route that circumvents the induced inhibition in DHTKD1 [55]. The failure to rescue the GA1 phenotype highlights the need for an alternative therapeutic approach targeting different enzymes is necessary.

Aminoadipate aminotransferase (AADAT), also known as kynurenine aminotransferase II (KAT II), is a pyridoxal-5'-phosphate (PLP)-dependent enzyme that plays a dual role in metabolism [56]. In the lysine degradation pathway, it converts 2-aminoadipate to 2-ketoadipate in the final step of the saccharopine pathway [23]. More prominently, AADAT is critically involved in the kynurenine pathway of tryptophan metabolism, where it catalyzes the transamination of kynurenine to kynurenic acid (KA), a neuroactive metabolite with known roles in modulating glutamatergic neurotransmission and neuroinflammation [57]. AADAT is expressed in several tissues [56] including liver, kidney, and the brain [58]. Currently, no pathogenic variants in the human *AADAT* gene are known [56].

Aminoadipate-semialdehyde synthase (AASS) is a bifunctional mitochondrial enzyme that catalyzes the first two steps of the saccharopine pathway: it first converts lysine and 2-ketoglutarate into saccharopine via its lysine-oxoglutarate reductase (LOR) domain and then transforms saccharopine into aminoadipic semialdehyde via its saccharopine dehydrogenase (SDH) domain. AASS is primarily expressed in the liver, particularly in mitochondria-rich tissues, and has a tightly regulated expression profile to ensure lysine homeostasis. Dysfunction in AASS can lead to hyperlysinemia type 1 or 2, rare autosomal recessive metabolic disorder characterized by elevated plasma lysine levels [59]. Hyperlysinemia type 1 results from mutations affecting both LKR and SDH activities. It is often considered benign, with most affected individuals being asymptomatic [59]. Hyperlysinemia type 2, which is even rarer and sometimes debated as a distinct entity, is associated with an isolated defect in SDH activity. Clinically, it may have a more pronounced metabolites dysregulation due to saccharopine accumulation, although its clinical significance remains less well-defined. Despite the elevation of lysine due to AASS deficiency, hyperlysinemia is generally considered a benign condition[59].

In the context of GA1, targeting AASS expression or activity, for instance, has been proposed as a metabolic modulation strategy to reduce substrate load in GA1, potentially decreasing GA accumulation and related neurotoxicity [60]. Similarly, in conditions where tryptophan metabolism is disrupted or KA levels are dysregulated, modulation of AADAT could represent a therapeutic strategy, either by enhancing neuroprotection or by restoring neurotransmitter balance [57].

To investigate whether AADAT and/or AASS can modulate GA1 disease phenotype, two double knockout mouse models (*Gcdh/Aadat* KO and *Gcdh/Aass* KO) should be developed and studied to enable preclinical testing under physiologically relevant conditions. The next step would be to translate the results pharmacologically. PF-04859989 is a potent and selective small-molecule inhibitor of KAT II [61]. PF-04859989 was developed to specifically target and reduce KA [62] since elevated KA levels have been implicated in several neuropsychiatric disorders and certain neurodegenerative diseases [63]. By inhibiting KAT II, PF-04859989 reduces KA levels [62], which have been shown in to enhance glutamatergic and cholinergic neurotransmission and improve

cognitive performance in rat models [64]. The compound has been described for its brain penetration, pharmacokinetic properties, and selective enzyme inhibition, making it a useful pharmacological tool [61]. While it has not advanced to clinical use, PF-04859989 remains a valuable molecule for research into metabolic contributions to psychiatric and neurological disorders.

Aim of the study

There is a great need for safe and effective long-term treatment for individuals with GA1 caused by inherited deficiency of GCDH, which plays a key role in the catabolism of lysine, hydroxylysine, and tryptophan. The overarching aim of this thesis is to study whether the enzymes AADAT and AASS, which are located upstream of GCDH in the deficient pathway, could serve as a potential target for a substrate reduction therapy for GA1.

To test this overarching hypothesis, the study follows three specific objectives:

1. Standardize the GA1 mouse model under standard and HLD conditions:
    a. Studying the effect of different mouse genetic backgrounds (C57BL6/ SV129) on GA1 disease progression
    b. Explore phenotypic differences between male and female in GA1 disease
2. To prevent formation and accumulation of downstream neurotoxins the target is to block Alpha-aminoadipate aminotransferase (AADAT) or Alpha-aminoadipic semialdehyde synthase (AASS) or glutaric acid-producing gut bacteria producing:
    a. To validate that targeted inhibition of AADAT is a plausible therapeutic approach for GA1 patients through comparing *Gcdh/Aadat* double knockout mouse model (rescue) to *Gcdh* knockout mouse model (disease).
    b. Administer AADAT inhibitor as a potential pharmacological treatment.
    c. To validate that targeted inhibition of AASS is a plausible therapeutic approach for GA1 patients through comparing *Gcdh/Aass* double knockout mouse model (rescue) to *Gcdh* knockout mouse model (disease).
    d. Study the role of microbiota on GA1 toxicity through administering Enrofloxacin antibiotic.

2. Materials and Methods

2.1. Materials

2.1.1. Chemicals

Chemical	Manufacturer
Acetic acid	Carl Roth
Acetonitrile	Carl Roth
Agarose NEEO Ultra-Quality	Carl Roth
Aluminum Sulfate	Carl Roth
Ampicillin	Sigma Aldrich
Ammonium persulfate (APS)	Sigma Aldrich
Bacteriological Agar	Sigma Aldrich
Bromophenol blue sodium salt	Sigma Aldrich
Bovine Serum Albumin	Serva
Chloroform	Carl Roth
Dulbecco's Modified Eagle Medium (DMEM)	ThermoFisher Scientific
Dulbecco's phosphate buffered saline (DPBS, no calcium, no magnesium)	ThermoFisher Scientific
Ethylenediaminetetraacetic acid (EDTA)	Carl Roth
Ethanol	Carl Roth
Ethidium bromide	AppliChem
Fetal Calf Serum (FCS)	ThermoFisher Scientific
Glutaraldehyde solution, 25% in H_2O	Sigma Aldrich
Glycerol	Sigma Aldrich
Glycine	Carl Roth
Hydrochloric acid	Carl Roth
Isopropanol	Carl Roth
Magnesium chloride ($MgCl_2$)	Carl Roth
Methanol	Carl Roth
β-Mercaptoethanol	Merck
Opti-MEM Medium	ThermoFisher Scientific
Penicillin-Streptomycin (10000 U/ml)	ThermoFisher Scientific
Paraformaldehyde (PFA)	Carl Roth
Sodium acetate	Merck
Sodium chloride	Sigma Aldrich

Sodium-Dodecyl-Sulfate (SDS)	Carl Roth
Tetramethylethylenediamine (TEMED)	Carl Roth
Tris-Base	Carl Roth
Tris-HCl	Carl Roth
Trypsin-EDTA (0.25%), phenol red	ThermoFisher Scientific
Tween	Carl Roth
Xylol	Carl Roth

Table 1. Chemicals used in the study

2.1.2. Consumables

Reagent	Manufacturer
100 bp DNA Ladder	ThermoFisher Scientific
Cover glasses (15mm)	Geyer
Broad Range Prestained Protein Marker	Proteintech
Lipofectamine 2000 Reagent	ThermoFisher Scientific
Nitrocellulose Blotting Membrane, pore size 0.45 µm	GE Healthcare Life science
Optimal temperature compound (OCT)	Tissuetech (Sakura)
PerfeCTa SYBR Green FastMix	QIAGEN
Pierce ECL Western Blotting Substrate	ThermoFisher Scientific
Quick Start Bovine Serum Albumin Standard	Bio-Rad
PageRuler Prestained Protein Ladder	ThermoFisher Scientific
DNase I, RNase-free	ThermoFisher Scientific
Phusion High-Fidelity DNA Polymerase	ThermoFisher Scientific
Proteinase K	Carl Roth
Q5 Polymerase	New England Biolabs
Roti® - Mount Mounting medium	Roth
Superfrost™ Plus adhesion Microscope slides	Epredia
T4 DNA Ligase	New England Biolabs

Table 2. Reagents used in this study

2.1.3. Commercially available kits

Kit	Manufacturer
PCR clean up Gel extraction kit	QIAGEN
GeneJET Plasmid-Midiprep Kit	ThermoFisher Scientific
Maxima first strand cDNA synthesis kit for RT-qPCR	ThermoFisher Scientific
Was it not GeneJET MiniPrep	ThermoFisher Scientific
RNeasy Mini Kit	QIAGEN

Table 3. Kits used in this study

Type	Manufacturer
pGEM®-T Easy Vector system I	Promega
pX459	Addgene
DH5 alpha Competent *E. Coli* (High Efficiency)	New England Biolabs
HEK293Tcells	ATCC
HeLa cells	ATCC
SCC058A iPSC	Sabine Jung-Klawitter

Table 4. Vectors, bacterial strain and cell lines used

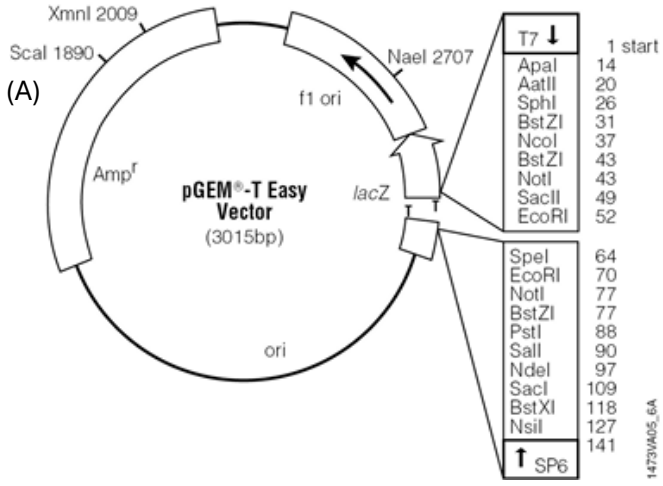

Figure 2. Vector maps. (A) pGEM®-T easy vector (Promega)

2.1.4. List of primers

Primers for RT-qPCR		
Primer	Sequence	Annealing T (°C)
***Gcdh* forward**	TCGGGGCTTCATACTGGAGA	65,5
***Gcdh* reverse**	GCACATTCTCCTCAGGCACT	65,3
***Aass* forward**	GTCTTCACAGGGACTGGCAA	65,2
***Aass* reverse**	GCGACTTAACACCGTCCCAT	65,4
***Aadat* forward**	GGGTTGAGAGTAGGGTTTATG	60,7
***Aadat* reverse**	GAATCCCTCTGGTTCTTGTAG	60,7
***Gapdh* forward**	TGCACCACCAACTGCTTAG	63,3
***Gapdh* reverse**	GGATGCAGGGATGATGTTC	61,1
Primers for PCR		
Primer	Sequence	
***β-ACTIN* forward**	CATGGAGAAAATCTGGCACCAC	64,6
***β-ACTIN* reverse**	GCACAGCTTCTCCTTAATGTCAC	64,7
***Gcdh* WT forward**	CTTCCGTAACTACTGGCAGGAGCGG	71,1
***Gcdh* WT reverse**	AGCTCTCGGGTCAGAAGCCCATAGG	72,1
***Gcdh* KO forward**	GCGGTGGGCTCTATGGCTTCTGAGG	73,2
***Gcdh* KO reverse**	CCCAGAACTCAGGAGGAAGAGGCAG	70,7
***Aass* WT forward**	GATATGCAGACAGGAGAGGTTAACC	65,5
***Aass* KO forward**	CCTTCAGGTTGAGAACTGGTGTT	65,7
***Aass* reverse**	CAGAGCCAGAACAATAAGAAGACC	64,1
***Aadat* forward**	GCCACTATTTCTTCTCTGCCG	63,9
***Aadat* reverse**	GTGTACCTGCCTTGTGTGTG	64
Sp1 forward	TAATACGACTCACTATAGGG	55.9
Sp2 reverse	CATTTAGGTGACACTATAG	52.7
Primers for cloning sgRNA in pSpCAS9(BB)-2A-Puro		
Primer	Sequence	
GCDH exon5 forward	caccGGAGATCATTTCGGAGATGG	
GCDH exon5 reverse	aaacCCATCTCCGAAATGATCTCC	
GCDH exon6 forward	caccGATAGGGTGCATGACGAGGG	
GCDH exon6 reverse	aaacCCCTCGTCATGCACCCTATC	

Table 5. List of Primers used in the study

2.1.5. Antibodies

Product	Manufacturer	Catalog no.
AADAT Polyclonal Antibody (Rabbit)	Proteintech	13031-1-AB
AASS Polyclonal Antibody (Rabbit)	Atlas	HPA 020734
GAPDH Polyclonal Antibody (mouse)	Life	AM4300
GCDH Polyclonal Antibody (Rabbit)	Atlas	HPA 043252

Table 6. Antibodies used in this study

2.1.6. Inhibitors

Inhibitor	Manufacturer
PF-04859989	Pfizer CAS No: 34783-48-7
Protease Inhibitor	Roche cOmplete™ Tabs, EDTA free

Table 7. Inhibitors used in the study

2.1.7. Buffers

Buffer	Composition
Anode buffer	25 mM TRIS-Base, 20% (v/v) Methanol
Cathode buffer	25 mM TRIS-Base, 40 mM 6-Aminohexanoic acid, 20% (v/v) Methanol
GCDH-assay buffer (pH 7.2)	100 mM Sodium phosphate, 50 µM Glutaryl-CoA, 200 µM Fc+PF-6, 0.1 mM FAD,0.5 mM N-ethylmaleimide, 5mM $MgCl_2$
6× Laemmli sample buffer	7.0 ml 4× Tris-Base/SDS (pH 6.8), 3.6 ml Glycerol, 1 g SDS, 0.93 g DTT, 1.2 mg Bromophenol blue
LB-Agar plates	1 L LB-Medium, 15 g Agar, 50 mg Ampicillin
Luria broth (LB)-Medium (pH 7.4)	10 g/L Tryptone, 5 g/L Yeast extract, 5 g/L NaCl
Lysis buffer	50mM TrisHCl, 50mM EDTA, 100mM NaCl, 0.5% SDS
7× Protease Inhibitor Solution	1 tablet cOmplete™, Mini EDTA-free Protease inhibitor cocktail, 2 ml DPBS
PFA 4%	4g of PFA in 100 mL of PBS
Protein extraction buffer	120 µL RIPA buffer, 15 µL 7× Protease Inhibitor Solution
Radioimmunoprecipitation assay (RIPA) Buffer (pH 7.2)	150 mM NaCl, 5 mM EDTA, 1% Nonidet P-40, 0.05% (w/v) SDS, 0.5% (w/v) Na-Deoxycholate, 50 mM Tris-HCl
5× Running buffer	15.1 g/L TRIS-Base, 72 g/L Glycine, 5 g/L SDS
Sucrose 15%	15g sucrose in 100ml PBS
Sucrose 30%	30g sucrose in 100ml PBS
10× TBST (pH 7.6)	24 g/L Tris-HCl, 5.6 g/L TRIS-Base, 88 g/L NaCl, 1% (v/v) Tween
Tris Acetate EDTA Buffer (pH=8.0)	40mM Tris Base, 2mM EDTA, pH=8.0 with glacial acetic acid
25× Tris-Glycine transfer buffer (pH 8.3)	12 mM TRIS-Base, 96 mM Glycine
4× Tris-HCl/SDS (pH 6.8)	0.5 M TRIS-Base, SDS 0.4% (w/v)
4× Tris-HCl/SDS (pH 8.8)	1.5 M TRIS-Base, SDS 0.4% (w/v)

Table 8. General Buffers used in the study

2.1.2. Gels for gel electrophoresis

Separating gel (10%)

Reagent	Volume
dH_2O	2.6 mL
40% Acrylamide	3.0 mL
4x Tris-HCL (pH=8.8)	1.8 mL
10% APS	25 µL
TEMED	5 µL

Stacking gel

Reagent	Volume
dH_2O	2.6 mL
40% Acrylamide	3.0 mL
4x Tris-HCL (pH=6.8)	1.8 mL
10% APS	25 µL
TEMED	5 µL

Agarose gel

Reagent	Volume/Weight
1X TEA buffer	200 mL
1,5% Agarose	3 g

Table 9. Components of Western blot separating and stacking gels and electrophoresis agarose gel

2.1.8. Instruments

Instruments and Software	Manufacturer
Bacteria Incubator	Memmert
Cell Culture incubator	Binder
Centrifuge pico17	ThermoFisher Scientific
Centrifuge plate and tubes	Rotina 420R
C1000 Touch Thermal Cycler	Bio-Rad
CFX Connect 180 Real-Time cycler	Bio-Rad
Cryotome CM1900	Leica
Fusion X7 Chemiluminescence imaging system	Peqlab Biotechnology
Fusion SL Imaging System	Peqlab Biotechnology
Prism	GraphPad Software Inc.
Immunofluorescent Microscope	Leica microsystem
TH-15 Control Bacteria shaker	Edmund Buehler
Light microscope DMi1	Leica
Leica LASX software	Leica microsystem
Heat block and shaker TS-100	ThermoFisher Scientific
Membrane shaker	Sunlab
Nanodrop Lite Spectrophotometer	ThermoFisher Scientific
OMNI Beads 19-646-3	OMNI International
Power Pac 300 (for Agarose-Gel electrophoresis)	Bio-Rad
Power Pac 1000 Electrophoresis Power supply (for Western blotting)	Bio-Rad
rotary microtome (Leica CM1900)	Leica
SnapGene Viewer	Dotmatics
Sonifier 450 ultrasonic processor and cell disruptor	Branson
Trans-Blot SD Semi Dry Transfer Cell	Bio-Rad
Tissue Bead Mill Homogenizer	OMNI International
Tecan Spark	Tecan
VF2 Vortex	Janke & Kunkel IKA laboratory technology
ImageJ, Version 1.53	https://imagej.nih.gov/ij/

Table 10. Instruments and Software used in the study

2.2. Methods

2.2.1. Animal Husbandry

2.2.1.1. Mouse models

This study was performed in strict accordance with the Principles of Laboratory Animal Care, and the Animal Protection Commission (Tierschutzkommission), as approved by the Ethical Committee for the Care and Use of Laboratory Animals of the Heidelberg University (G-95/19, G-10/21). All efforts were made to minimize suffering, discomfort, stress and the number of mice necessary to produce reliable scientific data.

2.2.1.2. Mouse strains and treatment groups

Male and female wild-type (WT), *Gcdh* KO, *Gcdh/Aadat* KO, and *Gcdh/Aass* KO mice on C57BL6N background or SV129 background (4 weeks old) were held at IBF Animal Care Facility. Mice were housed in 22×37×18 cm acrylic glass cages (up to five mice per cage) in an acclimatized room (22– 26℃) with a 12hour light/dark cycle. Water and standard ("normal"; 20% protein, 0.9% lysine) or high lysine (20% protein, 4.7% lysine) diet was provided *ad libidum*.

Genotype	Genetic Background	Role	Group n.	Standard diet	High Lysine diet
WT	C57BL/6N	Control	1	+	-
			2	-	+
WT	Sv129	Control	3	+	-
			4	-	+
Gcdh KO	C57BL/6N	GA1 mouse model	5	+	-
			6	-	+
Gcdh KO	Sv129	GA1 mouse model	7	+	-
			8	-	+
Gcdh/Aadat KO	C57BL/6N	Rescue model 1 of GA1	9	+	-
			10	-	+
Gcdh/Aass KO	C57BL/6N	Rescue model 2 of GA1	11	+	-
			12	-	+
Gcdh KO	C57BL/6N	Enrofloxacin (Antibiotic)	13	+	-
			14	-	+

Table 11. Summary of the experimental groups used in the study and the underlying genetic background.

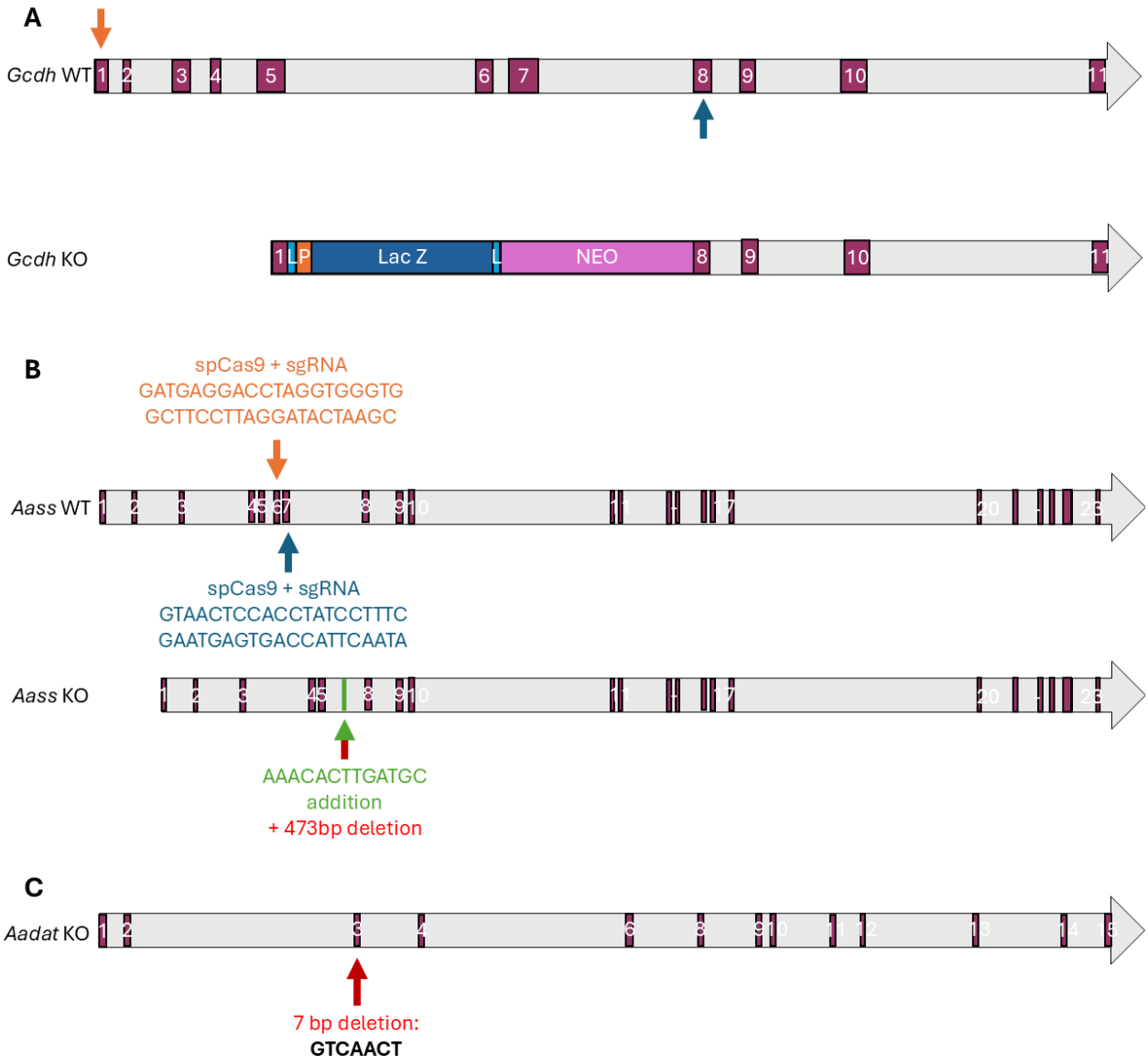

Figure 3. Genotype in the *Gcdh*, *Aass* and *Aadat* KO mice. (A) In the *Gcdh* KO mice the LacZ and Neo cassette replace the WT sequence from mid-exon 1 to exon 8 (B) *Aass* gene editing through CRISPR/Cas9 combined with sgRNA target exon 6 and 7 leaving the gene with a 473 bp deletion and an insertion of 13 bp (AAACACTTGATGC). (C) Within the *Aadat* gene a 7 bp deletion was inserted in exon 3 at nucleotide position 10110-10116. Abbreviations: P: Promoter region. O: Operator region.

To analyze whether *Aass* or *Aadat* knockout can rescue the metabolic and behavioral phenotype of *Gcdh* knockout, mice were divided into different experimental groups (comprising 3 males and 3 females each) according to the diet they received (figure 4; Table 11)

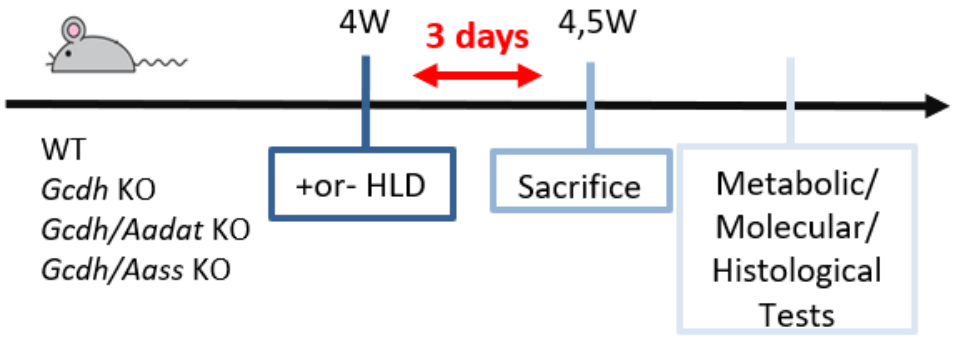

Figure 4. Treatment scheme for testing the effect of *Aass* or *Aadat* knockout on *Gcdh* knockout mice under standard or HLD conditions. All mice groups WT, *Gcdh* KO, *Gcdh/Aadat* KO, or *Gcdh/Aass* KO received either normal diet (n = 3 males and 3 females) or HLD for three days (n = 3 males and 3 females) Abbreviations: HLD, high lysine diet; KO, knockout; WT, wild-type.

To study the role of the gut microbiome on the production of glutaric acid (GA) and the total GA concentration present in a patient´s plasma, the microbiome was erased by antibiotics treatment, and the concentrations of GA were measured. Therefore, two additional treatment groups were added (figure 5).

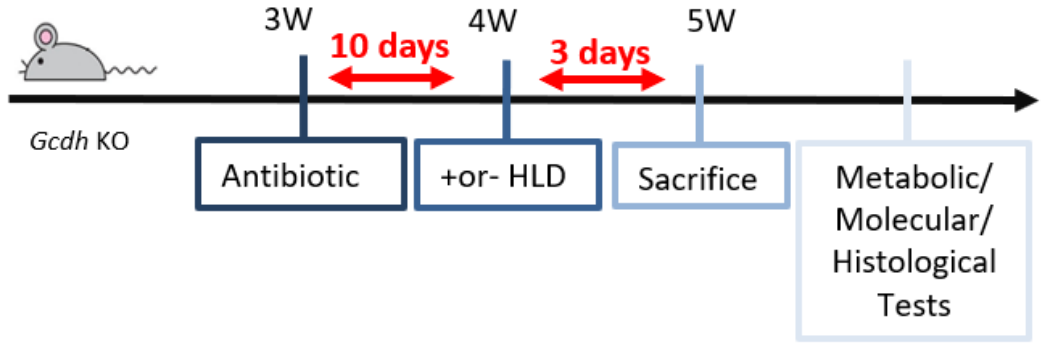

Figure 5. Treatment scheme for testing the role of the microbiome in the production of toxic metabolites in *Gcdh* knockout mice. The *Gcdh* KO group was subjected to antibiotic treatment for 10 days receiving normal diet (n = 3 males and 3 females). Afterwards, the *Gcdh* KO received or not a high lysine diet for three days (n = 3 males and 3 females). Abbreviations: HLD, high lysine diet; KO, knockout.

To investigate whether inhibition of the first enzyme in lysine degradation, AADAT, can prevent accumulation of GA and 3OHGA efficiently, PF-04859989, an AADAT Inhibitor, was tested. Before trying the drug *in vivo,* it was tested *in vitro* as described in 2.2.3.8. In the GA1 mouse model, first, a dosage finding study was performed (table 13, figure 6). 4 mice per group were injected subcutaneously with either 3.2, 10, or 32 mg/kg PF-04859989 dissolved in NaCl. After 1, 4, or 24h, mice were sacrificed and organs and body

fluids were collected to be used for metabolic analysis that included the measurement of GA and 3OHGA concentrations, but also for the enzyme substrate aminoadipic acid (2AA) and its product oxoadipic acid (2OA) concentrations were measured to test for the production of toxic metabolites and the AADAT inhibition efficiency in different organs (brain, liver, and kidney) and body fluids (plasma and urine).

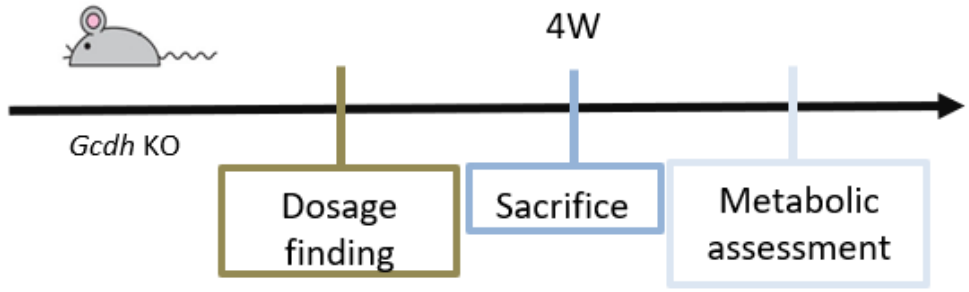

Figure 6. Treatment scheme for testing the efficiency of PF-04859989 on the production of toxic metabolites and inhibition of AADAT in *Gcdh* knockout mice. *Gcdh* KO mice received a PF-04859989 inhibitor treatment with normal diet for 1h, 4h, or 24h with a dose of 3.2, 10, or 32 mg/kg (n = 4 males). Abbreviations: HLD, high lysine diet; KO, knockout; WT, wild-type.

Sacrifice after Injection	Dose 1 (mg/kg)	Dose 2 (mg/kg)	Dose 3 (mg/kg)
1h	3.2	10	32
4h	3.2	10	32
24h	3.2	10	32

Table 12. Dosage finding study design includes 9 groups, n=4 each. 3 groups were under 1 mg/kg treatment, 3 groups were under 10 mg/kg, and the last 3 groups with 32mg/kg.

2.2.1.3. Mouse monitoring through the mouse score sheet

To monitor the health status of the mice under high lysine diet, a mouse score sheet was used. This sheet assessed motor activity, weight loss, and seizure-like behavior development. The scoring consists of the measurement of the three parameters (table 14) weight, seizure-like behavior, and overall condition. The score counts from 0 to 3 with 0 (no symptoms) up to 3 (severe symptoms). The overall condition is determined via summing up the scores of the three monitored parameters mouse movement and activity, seizure-like behavior and the calculation of the percentage weight changes throughout the experiment. Also, the mice were observed almost every 4 hours for 15 min during the

day. The weight measurements for the calculations have been performed once in the morning.

Mouse weight(g)	Seizure score (0-3):	Overall condition (0-3):
Keep record of mouse weight for three days And calculate the percentage of weight loss. If >15% weight loss a termination of the experiment should take place.	0: no seizure 1: punctual seizures 2: spontaneous, short-lived seizures; full recovery between episodes 3: persistent tremor with weight loss; prolonged periods of seizures	0: no weight loss Normal grooming activity 1: <10% weight loss Movement and activity changes 2:10-15% weight loss Decrease in movement 3: >15% weight loss No movement

Table 13. Mouse score sheet analysis. This sheet is used to monitor the mice and record the weight measurement, seizure-like behavior and movement observations. These conditions are scored from 0 to 3. If 3 points are achieved in one of the categories, the end of the test was initialized.

2.2.1.4. Histological Processing and Hematoxylin & Eosin (H&E) Staining

At the designated endpoints, mice were euthanized following institutional ethical guidelines, and the brain was carefully extracted. One of the hemispheres was immediately fixed in 4% paraformaldehyde (PFA) for 24 hours at room temperature to preserve tissue architecture. The second hemisphere was used for molecular tests. Following fixation, tissues were washed, dehydrated in 15% sucrose for 16 hours and then in 30% sucrose for up to 1 week at 4°C.

Dehydrated tissues were then embedded in optimal cutting temperature compound (OCT) overnight at -20°C and stored at -80° C until sectioning. Tissue blocks were sectioned at a thickness of 6µm using a rotary microtome (Leica CM1900). Sections were mounted on Superfrost™ Plus microscope slides. Slides were allowed to air-dry overnight or incubated at 37°C for at least 2 hours prior to staining.

For staining, the slides were rehydrated through a descending ethanol series (100%, 95%, 80%, and 70%, each for 2 minutes) and rinsed in running distilled water. Next, they were immersed in Mayer's hematoxylin for 5 minutes. Rinsing steps in tap water followed

for 5–10 minutes to allow color development. The slides were briefly dipped (3–5 seconds) in 0.3% acid alcohol (1% HCl in 70% ethanol), then rinsed again in tap water. Then immersed in 1% eosin Y solution for 2 minutes. Dehydration step took place through a graded ethanol series (70%, 95%, 100%, each for 1–2 minutes), cleared in xylene (2 × 5 minutes), and air-dried. Stained slides were mounted with Rotimount® (Roth) mounting medium and covered with glass coverslips. Slides were allowed to dry at 4 °C overnight. Brightfield images were acquired using a light microscope (Zeiss) equipped with a digital camera at various magnifications (5x, 10x, 20x). Images were processed minimally using ImageJ for contrast and scale bar addition, without altering raw data.

2.2.2. Biochemical analysis

2.2.2.1. Metabolomic analysis

Quantification of glutaric acid, 3-hydroxy glutaric acid, and glutarylcarnitine and other metabolites in liver, brain, kidney, plasma, and urine of mice was performed in cooperation with Prof. Giancarlo Lamarca (Florence, Italy). Organic acids were measured by liquid chromatography tandem mass spectrometry LC-MS/MS. Urine creatinine was measured on an AU480 (Beckman Coulter) at the Dietmar Hopp Metabolic Center. Tissue organic acid was determined using the same analysis procedure with a homogenate in water containing approximately 30 mg wet weight as matrix. Values were normalized for protein content in tissues, and to creatinine in urine.

Compound	Abbreviation
Glutaric acid	GA
3-hydroxyglutaric acid	3OHGA
Glutarylcarnitine	C5DC
Kynurenic acid	KA
Oxoadipic acid	2OA
Aminoadipic acid	2AA
Quinolinic acid	QA
Picolinic acid	PA

Table 14. Metabolites measured

2.2.2.2. Oxoadipate measurement in cell culture

After seeding, cells were grown to confluence. Afterwards, the medium was removed from cells, 300µL acetonitrile was added in the well for the different time points. The cells were collected and sonicated and flash frozen in liquid nitrogen. 10µL of this mixture was used to count the cells and the rest was centrifuged at 10.000 rpm for 5 min. Samples were then measured for oxoadipate levels by GC-MS performed by the newborn screening lab at the Dietmar Hopp Metabolic Center.

2.2.2.3. GCDH activity measurement

The GCDH-assay buffer (section 2.1.7) and stock solutions were prepared. Fc+PF-6, glutaryl-CoA and N-ethylmaleimide stock solutions were prepared immediately before use. FAD stock solution was stored at −20°C, sodium phosphate and $MgCl_2$ stock solutions were stored at room temperature. $Fc^{+}PF^{-6}$ was dissolved in 10mM HCl, all other components were dissolved in Millipore water. The pH value of the GCDH assay buffer was adjusted to pH7.2. The prepared solution was stored on ice, and prewarmed to 37°C before use. The spectrophotometric GCDH assay followed the reduction of the ferricenium ion and was adapted from Lehman et al. [65]. Assays were performed in a 96-well plate at 37°C. In each well, 50µL cell lysate containing 187.5 µg protein was loaded. The lysate of WT untreated cells served as a negative control. The GCDH assay was started by adding 250µL GCDH-assay buffer (section 2.1.7). The absorbance at 300 nm was determined in for 2min. To calculate GCDH activity, the activity at the final timepoint was subtracted from the initial activity measured. Each sample was measured in triplicate.

2.2.3. Cell culture

2.2.3.1. Cultivation of HEK293Tcells

HEK293Tcells were cultivated in T75 flasks at 37°C with 5% CO_2. Cell culture medium was HeLa medium (as described in table 9). Cell culture medium was changed every two or three days, cells were splitted every three or four days. To passage the cells, cells were first dissociated from the flask by incubating with 1mL Trypsin solution (ThermoFisher Scientific) for 5 min, then diluted at 1:10 with fresh medium. To seed cells for transfection, cells were counted at 3 x 10^5 cells per 6 well plate with 2 ml fresh medium.

2.2.3.2. Inhibitor treatment of HEK293T cells with or without high lysine

HEK293T cells were used to test the effect of the AADAT inhibitor PF-04859989 on AADAT activity. 5x10^6 cells per 6well were seeded and grown until confluence. Cells were starved overnight in medium with 1% FCS and on the following day, cells were treated with increasing concentrations of inhibitor PF-04859989 (1µM, 5µM, or 10µM) prepared in DPBS (without calcium or magnesium) and incubated for 72h. Afterwards, the cells were collected for the measurement of oxoadipate (see 2.2.2.1.), or collected for protein measurements (see 2.2.4.6.). In addition, the same test was performed agin in high lysine conditions. L-lysine was dissolved in DPBS to a final concentration of 0,1mM, 0,5mM, 1mM, 2mM, or 5mM. The cells were collected with trypsin after 24h, 48h, or 72 h. The cells were pelleted and the cell pellet was taken for RNA extraction followed by PCR analysis (see 2.2.4.5) or used for protein extraction followed by Western Blot (see 2.2.4.6.) or for GCDH enzyme activity assay (see 2.2.2.1.).

2.2.3.3. Cell culture plates coating

Gelatin coating was performed to enhance cell attachment. Briefly, a 0.1% (w/v) gelatin solution was prepared by dissolving gelatin (Type A, Sigma-Aldrich) in sterile distilled water and sterilized by filtering. Each well of a 6-well plate was coated with 1.5 mL of the gelatin solution and incubated at 37°C for 2h. Excess gelatin was removed by aspirating the solution, and the wells were allowed to air-dry under sterile conditions in a biosafety cabinet before cell seeding.

Matrigel coating was performed to provide an extracellular matrix environment. 1 mL Matrigel was thawed on ice at 4 °C and mixed with 55 mL DMEM Knockout media. Each

well of a 6-well plate was coated with 1.5 mL of Matrigel, ensuring even coverage of the surface. The plates were incubated at 37 °C for 30 minutes to allow gelation. After gelation, excess Matrigel was gently aspirated, and the wells were immediately used for cell seeding.

2.2.4. Molecular Biology

2.2.2.4.1 Transformation of bacteria for extraction of plasmid DNA

To obtain a large quantity of plasmid DNA, the plasmid was transformed into competent DH5-α *E. coli* (NEB). Thus, 2µL of plasmid was added to 50µL chemically competent *E. coli* cells, followed by incubation on ice for 20min, heat shock at 42°C for 30sec, incubation on ice for 5min, and incubation in 500µL LB-medium at 37°C for 30 min with shaking. Afterwards, 100µL of the suspension was spread on a LB plate containing ampicillin (50µg/mL) and incubated overnight at 37°C. Single colonies were picked and grown overnight in 3 mL LB media with 3 µL Ampicillin at 37°C in a shaking incubator. This bacterial mixture was used for either a mini prep or a midi prep according to the manufacturer´s instructions.

2.2.2.4.2 Preparation of plasmid DNA

For a mini prep, individual clones were expanded in 5 mL LB media containing 100µg/mL ampicillin and incubated at 37°C with shaking for 12–16 hours. The plasmid DNA was extracted using the mediCore Plasmid Miniprep Kit I (VWR International) adhering to the manufacturer’s protocol. The bacterial culture was first centrifuged at 13.000 rpm for one minute to pellet the cells, which were then resuspended in 250µL of Solution I (containing RNaseA). Cell lysis was performed by adding 250µL of Solution II, followed by neutralization with 350µL of Solution III. The sample was centrifuged at 13.000 rpm for 10 minutes, and the resulting supernatant was transferred to a spin column. After a 1-minute centrifugation at 13.000 rpm, the flow-through was discarded. The purification process included one wash with 500µL of Wash Solution I and two washes with 750 µL of Wash Solution II. The column was dried by centrifugation at 13.000 rpm for 2 minutes, and plasmid DNA was eluted with 50µL of elution buffer by centrifuging at 7.500 rpm for

1 minute. The purified plasmid DNA was stored at −20°C. All steps were performed at room temperature.

To obtain larger quantities of a plasmid, clones were cultured overnight at 37°C in 50mL of LB medium containing 50 µg/mL ampicillin with shaking at 170 rpm. The culture was subsequently purified using the GeneJET Plasmid-Midiprep Kit following the manufacturer's protocol. Cells were pelleted by centrifugation for 10 minutes at 5.000 × g. 2mL of Resuspension Solution containing RNase A was used to resuspend the resulting cell pellet, followed by lysis with 2mL of Lysis Solution and neutralization with 2mL of Neutralization Solution. Endotoxins were removed using 0.5mL of Endotoxin Binding Reagent. After the addition of 3mL of 96% ethanol, the mixture was centrifuged for 40 minutes at 4.000 × g. The supernatant was combined with another 3mL of 96% ethanol, transferred to a binding column, and centrifuged for 3 minutes at 2.000 × g to facilitate the binding of plasmid DNA to the column. The column was washed once with Wash Solution I, followed by two washes with Wash Solution II, and then dried by centrifugation for 5 minutes at 3.000 × g. 0.35mL of Elution Buffer was used to elute the plasmid DNA by adding to the column, incubating at room temperature for two minutes, and centrifuging for 5 minutes at 3.000 × g. To enhance the yield, the elution process was repeated with 0,15 mL of Elution Buffer. Following quantification with the Nanodrop1000, the purified plasmid DNA was stored at −20°C.

2.2.4.1. DNA extraction

For genotyping of the mice, DNA was extracted from ear punches. To each ear punch, 500µL Lysis buffer with 50µL Proteinase K (10mg/ml) was added and then incubated while shaking for at least 2h at 56°C. Afterwards, the DNA was precipitated from the supernatant using 1,4mL ethanol (99%) and centrifuged at 12.000rpm for 20 min. The DNA pellet was washed with 500µL 70% ethanol and dried for 15-30 min before the addition of 50µL dH_2O and then stored at -20 °C.

Genomic DNA from cell cultures was extracted using 500µL DNAzol® reagent per well of a 6 well plate. After homogenization, the mixture was incubated for 10 min at RT. Afterwards, the samples were centrifuged at 8000 rpm for 10 min, and the supernatant

was mixed with 250µL 99,9% Ethanol and incubated for 5 min at RT. Next, the DNA was precipitated via 10 min centrifugation at 8000 rpm. DNA was washed with 75% Ethanol and dried before adding 30µL of water to redissolve it.

2.2.4.2. RNA extraction

30 mg of tissue from liver, kidney, heart, or brain, was homogenized with TRIzol™ reagent (Invitrogen) using beads in the tissue homogenizer (OMNI). Then, chloroform was added with a ratio of 2:1 and incubated for 3 min at RT. The mixture was centrifuged for 20 min at 13.300 rpm at 4°C. The solution then separates into 3 phases: upper clear supernatant containing RNA, middle cloudy phase containing cell debris and proteins, and lower pink phase containing DNA. The clear supernatant was carefully extracted and mixed with 500µL isopropanol. After incubation for 10 min at RT, the mixture was centrifuged for 10 min at 13.300 rpm at 4°C to allow RNA precipitation. The supernatant was discarded, and the pellet was washed with 500µL 75% Ethanol. After centrifugation for 5 min at 13.300 rpm at 4°C, the RNA pellet was dissolved in 15-30µL RNAse free water.

2.2.4.3. Measurement of DNA and RNA concentration

The concentration of double stranded DNA and of RNA was measured at 260 nm (A260) and 280nm (A280) with a Nanodrop Lite Spectrophotometer. The ratio of absorbance 260nm/280nm was used to access the purity of the samples. The A260/A280 ratio should be between 1.8 and 2.0 for purified DNA or RNA.

2.2.4.4. cDNA transcription

2.2.4.5.1 DNAse I digestion

After isolation, RNA was treated with DNase I (RNase-free) at 37°C for 30 min. The mixture was prepared as described in table 18. To inactivate DNase I, 2.5µL 50mM EDTA was added into the reaction mixture, and incubated at 65°C for 10 min.

Reagent	Amount
DNAse I buffer	1µL
DNAse I Enzyme	1µL
RNA	1µg
RNase-free H_2O	Add to 10µL
After 30 min at RT add:	
Reagent	Amount
EDTA	1µL
Incubate at 65°C for 10 min	

Table 15. DNase treatment reagents

2.2.4.5.2 First Strand cDNA synthesis

1µg of DNAse I digested RNA was immediately subjected to cDNA synthesis. Using the purified RNA, the first strand cDNA was synthesized with the Maxima first strand cDNA synthesis kit. The reaction mixture (table 19) was incubated at 65°C for 5 min for denaturation. Afterwards, reverse transcriptase was added and incubated at 50°C for 1h, followed by 70°C for 15 min to stop the reaction. The reaction was run on a c1000 Touch Thermal-Cycler. The synthesized cDNA was immediately subjected to RT-qPCR analysis or stored at −20°C for a week or at -80 °C for long-term storage.

For first strand cDNA synthesis add:	
Reagent	Amount
DNAse I treated RNA	10µL
Random Primer	1µL
dNTP-mix	1µL
After denaturation at 65°C for 5 min add:	
Reagent	Amount
First strand buffer (FS)	4µL
DTT	1µL
RNAseOUT	1µL
Superscript III transcriptase	1µL
Incubate at 50°C for 1h, then 70°C for 15min	

Table 16. First strand cDNA synthesis reagents

2.2.4.5. qRT-PCR and RT-PCR

2.2.4.6.1 RT-qPCR

To detect expression of *Gcdh, Aass,* and *Aadat* transcripts in mouse brain, kidney, heart and liver, qRT–PCR was done with total DNAse I digested RNA isolated from these tissues. Specific TaqMan probes for mouse *Gcdh* (MM00433541_m1 Gcdh) and

18SrRNA (ThermoFischer 4310875) (housekeeping gene) were used in this study. Also, Luna script polymerase in combination with corresponding primers were used to quantify the amount of *Gcdh*, *Aass* and *Aadat* with normalization to *Gapdh* levels. Relative gene expression was calculated using the ΔΔCt method [66], using WT mice at each time point as control.

Cycle Step	Cycles	Temperature	Time
initial denaturation	1 cycle	50°C	2min
Enzyme activation	1 cycle	95°C	10min
Denaturation	40 cycles	95°C	15s
Annealing/Extension		60°C	1min

Table 17. PCR parameters for qRT-PCR using TaqMan probes

PCR parameters using Luna script:

Cycle Step	Cycles	Temperature	Time
Initial denaturation	1 cycle	95°C	1min
Denaturation	40 cycles	95°C	15s
Extension		60°C	30s
Melt Curve	1 cycle	60-95°C	various

Table 18. PCR parameters for qRT-PCR using SYBRgreen and Luna Script

2.2.4.6.2 PCR

After measuring the DNA concentration with the Nanodrop, it was diluted to a concentration of 200 ng/µL. For PCR 1 µL of measured DNA, 1 µL forward, 1 µL reverse primer, and 10 µL MyTaq enzyme polymerase was added and filled to a total volume of 20 µL with water using one of the settings described in table 22-26.

Cycle Step	Cycles	Temperature	Time
Initial denaturation	1 cycle	95°C	5 min
Denaturation	35 cycles	95°C	30s
Annealing		59°C	30s
Elongation		72°C	30s
Final Elongation	1 cycle	72°C	5 min
Storage		4°C	∞

Table 22. PCR parameters for Aadat genotyping

Cycle Step	Cycles	Temperature	Time
Initial denaturation	1 cycle	95°C	5 min
Denaturation	35 cycles	95°C	30s
Annealing		53°C	30s
Elongation		72°C	30s
Final Elongation	1 cycle	72°C	5 min
Storage		4°C	∞

Table 19. PCR parameters for *Aass* genotyping

Cycle Step	Cycles	Temperature	Time
Initial denaturation	1 cycle	95°C	5 min
Denaturation	34 cycles	95°C	30s
Annealing		69°C	30s
Elongation		72°C	120s
Final Elongation	1 cycle	72°C	5 min
Storage		4°C	∞

Table 20. PCR parameters for *Gcdh* genotyping

Cycle Step	Cycles	Temperature	Time
Initial denaturation	1 cycle	94°C	2min
Denaturation	35 cycles	94°C	30s
Annealing		56°C	30s
Extension		72°C	30s
Final Extension	1 cycle	72°C	5min
Storage		4°C	∞

Table 21. PCR parameters for *GCDH* gene detection

Cycle Step	Cycles	Temperature	Time
Initial denaturation	1 cycle	95°C	30s
Denaturation	35 cycles	95°C	30s
Annealing		56°C	1min
Extension		68°C	1min
Final Extension	1 cycle	68°C	5min
Storage		4°C	∞

Table 22. PCR parameters for Pluripotency markers

2.2.4.6.3 PCR purification or Gel extraction

PCR products were run on 1,5% agarose gels to determine whether the genotype is homozygote WT (*Gcdh* WT band size: 500 bp; *Aass* WT band size: 250 bp), homozygote KO (*Gcdh* KO band size: 750 bp; *Aass* WT band size: 500 bp), or heterozygote for *Gcdh* and *Aass* (with both bands WT and KO of each gene present on the gel). For *Aadat*, Sanger Sequencing was required to verify the genotype using the expected band size of 350 bp. The band was excised from the gel and extracted using the Quiagen gel extraction kit according to the manufacturer's instructions.

2.2.4.6.4 Sanger Sequencing

For sequencing, the PCR product (Length 401 - 900 bp; 4 - 17ng/µl) and a forward primer (20µM) were mixed and used for sequencing in a total volume of 15µl. For plasmid DNA, 40–100ng/µl was mixed with either forward or reverse primer (20µM) in a final volume of 15µl. Both mixtures were sent for Sanger sequencing to Microsynth. The FASTA sequence result was analyzed with Snapgene Viewer software.

2.2.4.6. Protein biochemistry

2.2.4.7.1 Preparation of tissue homogenates

30mg of tissue from the liver, kidney, heart, brain, spleen or skeletal muscle was homogenized with 500µL RIPA buffer using beads in the tissue homogenizer at RT. The mixture was centrifuged for 20 min with 14.000 rpm at 4°C. The supernatant containing the proteins was collected for further analysis and stored at -20 °C.

2.2.4.7.2 Protein extraction from cells

Cell pellets were lysed in 300µL RIPA buffer and homogenized with a 23Gauge syringe in order to extract the proteins. Next, the mixture was centrifuged for 10min with 14.000 rpm at 4°C. The supernatant containing the proteins was collected for further analysis and stored at -20 °C.

2.2.4.6.3 Determination of the protein concentration

To determine the protein concentration, a Lowry assay was performed [67]. Bovine Serum Albumin (BSA) was used as a standard with a concentration range of 0 to

10mg/ml. In a 96 well plate, 5µL of lysate was mixed with a combination of 25µl of reagent A/S, for every 1 ml of reagent A 20µL of reagent S is added, to avoid a high background due to the solvents present in RIPA buffer. Additionally, 200µL reagent B are added. After 15 min incubation, the absorbance was measured at 750nm with a TECAN SPARK reader. Using the standard curve, protein concentrations were calculated.

2.2.4.6.4 Western Blot

For immunoblotting, 40µg of proteins were used from animal tissue or 30µg from cell lysates were mixed with SDS page loading dye and heated to 95°C for 5 min to linearize the protein. Then the mixture is separated on a 10% polyacrylamide gel for 90 min at 100 Volt. Proteins were transferred to PVDF nitrocellulose membranes (Bio-Rad Laboratory, CA, USA) pre-activated in methanol for 2 min. Using a semi-wet system, the activated membrane was inserted between 2 layers of filters, the lower one incubated with anode buffer and the upper with cathode buffer (2.1.7). The transfer was run for 90 min on 120 milliampere. Afterwards, membranes were blocked with 5% BSA in TBST for 60 min to reduce non-specific antibody binding before immunodetection. Then, the membrane was incubated with rabbit polyclonal anti-GCDH antibody (1:10.000, Sigma), rabbit polyclonal anti-AASS antibody (1:2.000, Sigma), or rabbit polyclonal anti-AADAT antibody (1:2000, ProteinTech) overnight at 4°C prepared in 5% BSA. The next day, blots were washed three times with TBST buffer at room temperature for 5min. The HRP-coupled secondary antibodies were diluted 1:10.000 in TBST and incubated for 60 min at room temperature on a shaker. Afterwards, the blots were washed three times with TBST at room temperature for 5min. Proteins were detected using ECL. β-Actin or GAPDH were used as loading controls. Densitometric analysis was performed using Image J software to determine the protein band area normalized to the area of loading control protein area.

The expression of the protein of interest was calculated as follows:

$$\frac{\text{POI signal of KO}}{\text{POI signal of control}} \Big/ \frac{\text{GAPDH signal of KO}}{\text{GAPDH signal of control}}$$

2.2.5. Statistical Analysis

Results are expressed as mean ± SD for behavioral tests and for molecular experiments. For all assessments, normality tests were done to ensure that the sample distributions of both the groups of mice are normal. Statistical significance was assessed using both one-way and two-way ANOVA to test the efficacy of the administered treatments across all groups. P-value <0.05 is considered statistically significant.

3.Results

3.1. Standardization and characterization of the *Gcdh* KO mouse model under standard and high-lysine conditions

3.1.1 Validation of the *Gcdh* knockout model in C57BL/6N

As the genotyping of the *Gcdh* KO mice did not always work properly, the locus was re-sequenced to have the exact sequence and position of the knockout available to design new primer pairs for genotyping. Figure 9 summarizes the results of the re-sequencing of the locus which validated the presence of the lacZ and Neo cassette between exon 1 and 8 of the *Gcdh* gene with a size of around 3 Kbp. Nucleotide position 9070 to 9494 located in exon 1 are present, the next 120 bp are a polylinker region with a nuclear localization sequence. Next there is a promoter region for 330 bps followed by a LacZ region of 1055 bps, then another linker region of 580 bp. Finally, the neo cassette is present with around 1270 nucleotides followed by the start of exon 8.

Figure 7. *Gcdh* gene locus as present in *Gcdh* KO mice. As previously described by Zinnanti et al. (2010), It could be confirmed that the Lac Z and NEO cassette replace the WT sequence from 9070 nucleotide position mid-exon 1 to end of intron 8. This sequence is as follows, a polylinker region (120 bp); promoter region (330 bp); LacZ region (1100 bp); Polylinker region (580 bp); and lastly a NEO Cassette region (1260). The data was generated with the help of SnapGene Viewer software.

3.1.2 Establishment of a genotyping procedure for *Gcdh* KO

To faithfully identify mice with either a *Gcdh* heterozygous or homozygous genotype, a PCR was established based on the number of band and the band size of the PCR products. Here, primers were designed to bind within or outside deletion site (nucleotide position 9070 – 13055) and to distinguish between heterozygous and homozygous knock out mice. If the fragment size was 500bp, this corresponds to the WT allele, whereas a fragment size of 750bp is present in the knockout. Heterozygous mice present with two bands of 750bp and 500bp, respectively. Figure 10 shows one representative gel image of all possible genotypes.

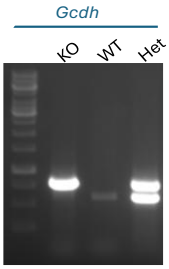

Figure 8. Genotyping results of *Gcdh* gene. Data shows the expression of *Gcdh* gene in different mice genotype. Line 1 is homozygote knockout, line 2 is homozygote WT, and line 3 is heterozygote Het.

3.1.3 Gcdh KO induces morphological changes in specific brain regions of *Gcdh* KO mice

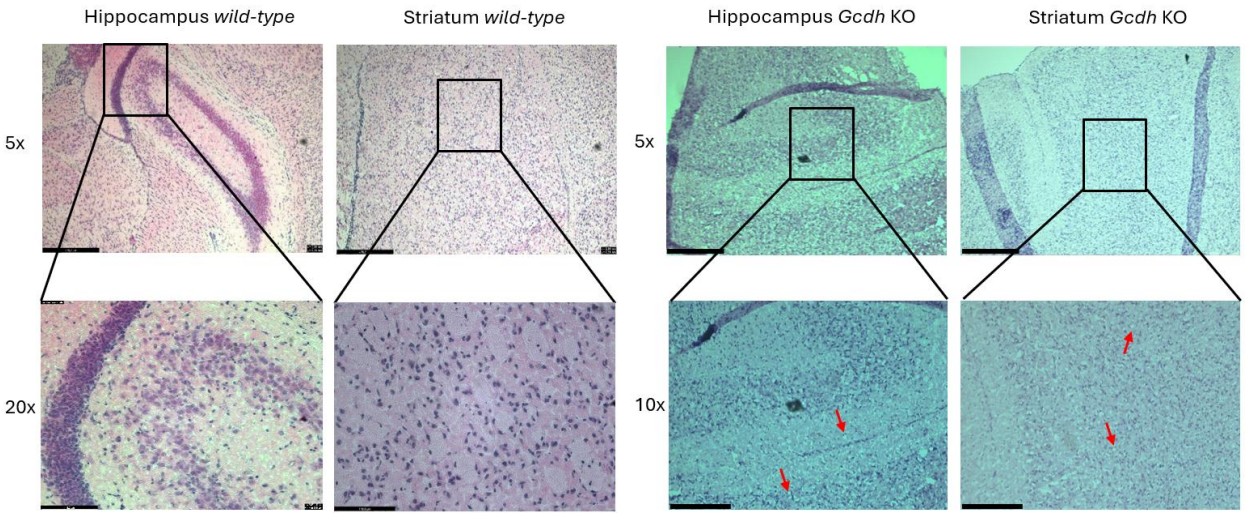

Figure 9. Representative images of hematoxylin and eosin-stained sagittal brain sections from a male WT, and a *Gcdh* KO mouse at 4 weeks of age under standard diet. The *Gcdh* KO mouse presented with vacuoles (arrows; insets) in several brain regions (hippocampus and striatum), which were absent in the WT mouse (top panel: scale bar 2.5mm, 5x magnification, panels below: left side, scale bar 100µm, 20x magnification, right side 10x magnification, scale bar 200µm).

To investigate potential neuropathological alterations associated with GA1, I examined brain tissue from the GA1 model using hematoxylin and eosin (H&E) staining. This approach allowed to assess general tissue architecture, cellular integrity, and the presence of morphological abnormalities that may underline the disease phenotype. Nevertheless, not all studies confirm the presence of striatal damage in this mouse model after lysine intake. Sauer et al. shows spongiform alterations in the hippocampal area of the *Gcdh* KO mouse model [49]. Histological analyses of H&E staining reveal vacuoles in the striatal tissue. These vacuoles indicate cell damage or death [35]. These vacuoles could reflect disrupted cellular architecture and loss of neuronal integrity. Compared to WT mouse, the striatal region in WT brains appear more homogenous with absence of vacuoles. The hippocampus of the tested GA1 mouse shows signs of structural damage compared to WT brain showing some vacuoles. Unfortunately, the slides were not taken at the same magnification hindering the ability to compare clearly the regions' differences. Also, the comparison under HLD is missing.

Understanding these region-specific vulnerabilities is crucial for developing targeted neuroprotective strategies, particularly those aimed at early intervention before irreversible damage occurs in the striatum and hippocampus.

As seen in figure 12, the expression of *Gcdh* in different areas of the WT brain is similar to whole brain homogenate. Similar results are seen on the protein expression. Thus, whole brain homogenate was used for further analysis.

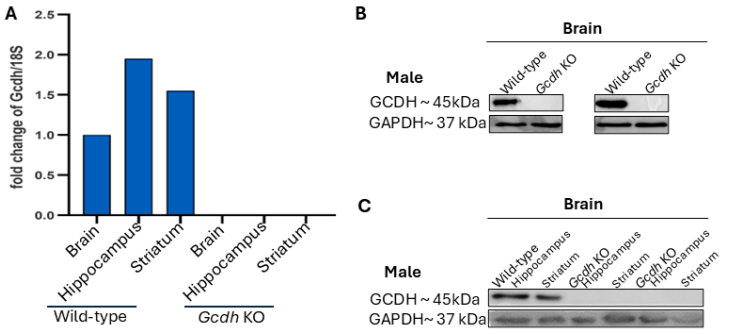

Figure 10. GCDH protein expression in the brain of WT and *Gcdh* KO mice from C57BL/6N background. (A) Comparison of the RNA level between whole brain homogenate, hippocampus, and striatum regions. (C) GCDH protein expression in the different brain regions.

3.1.4 Expression of the *Gcdh* gene is differentially regulated in different mouse genetic backgrounds

As different mouse strains show varying degrees of susceptibility to brain injury and differences in the blood brain barrier [46], I investigated whether there are also differences present in the expression of the enzymes involved in lysine degradation enzyme between mice of C57BL/6N or SV129 genetic background. Therefore, mRNA and protein expression of *Gcdh* between WT and *Gcdh* KO mouse models from both genetic backgrounds with or without HLD were analyzed. C57BL/6N WT mice expressed *Gcdh* mRNA under standard diet. *Gcdh* KO mice from both backgrounds did not express *Gcdh* mRNA. Interestingly, SV129 animal do not express *Gcdh* mRNA under standard diet. Under high lysine diet, WT mice from SV129 background induce expression of *Gcdh* which is then expressed in a similar way as in healthy WT mice without HLD from C57BL/6N background in liver, kidney, brain, and heart.

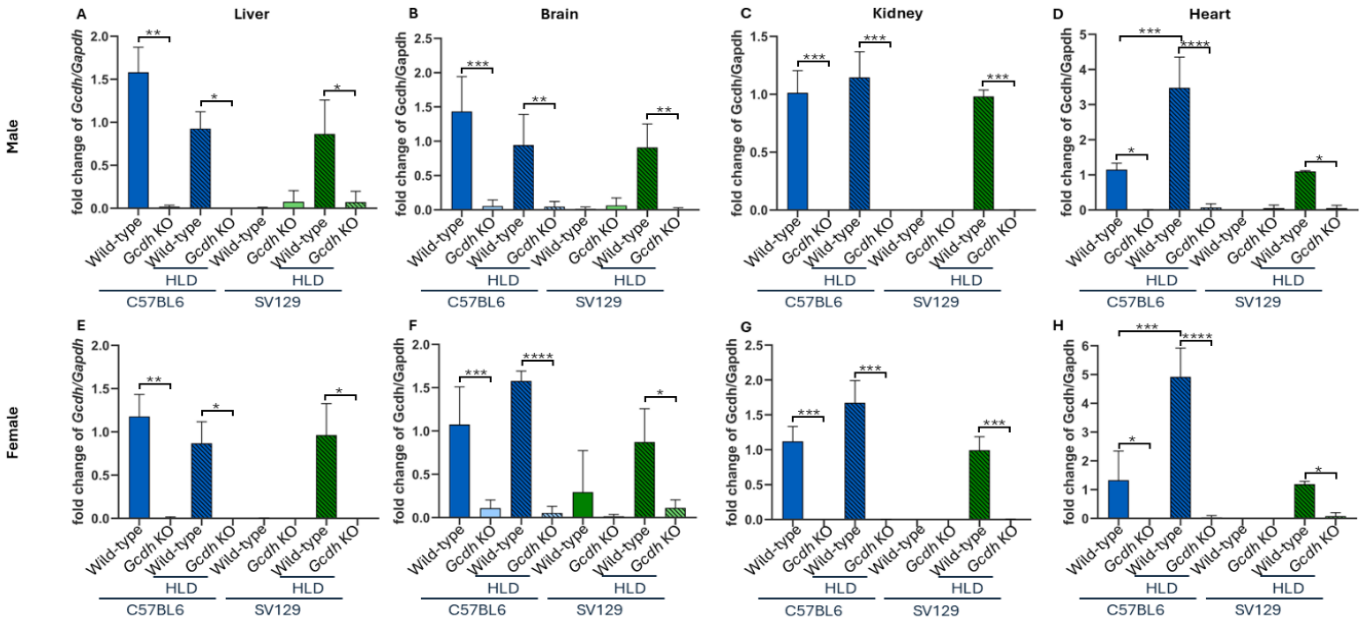

Figure 21. mRNA expression of *Gcdh* under standard and high lysine diet. Analysis of *Gcdh* (A-H) mRNA expression in brain (A, E), liver (B, F), kidney (C, G), and heart (D, H) of male and female WT and *Gcdh* KO mice with or without HLD and normalized to *Gapdh* expression with WT set as 1. Significance calculated with One-way ANOVA test with * p <0.05; ** p ≤0.01; *** p ≤0.001; **** p ≤ 0.0001; n=3 for all groups. Abbreviations: blue bar, WT mice on a C57BL/6N background; light blue bar, *Gcdh* KO from C57BL/6N background; green bar, WT from SV129 background; light green bar, *Gcdh* KO from SV129 background; striped bar, groups under HLD

To validate the mRNA data on the protein level, Western Blot analyses were performed in two different genetic backgrounds and confirmed the mRNA data. Similar results were seen in male and female groups (figure 14).

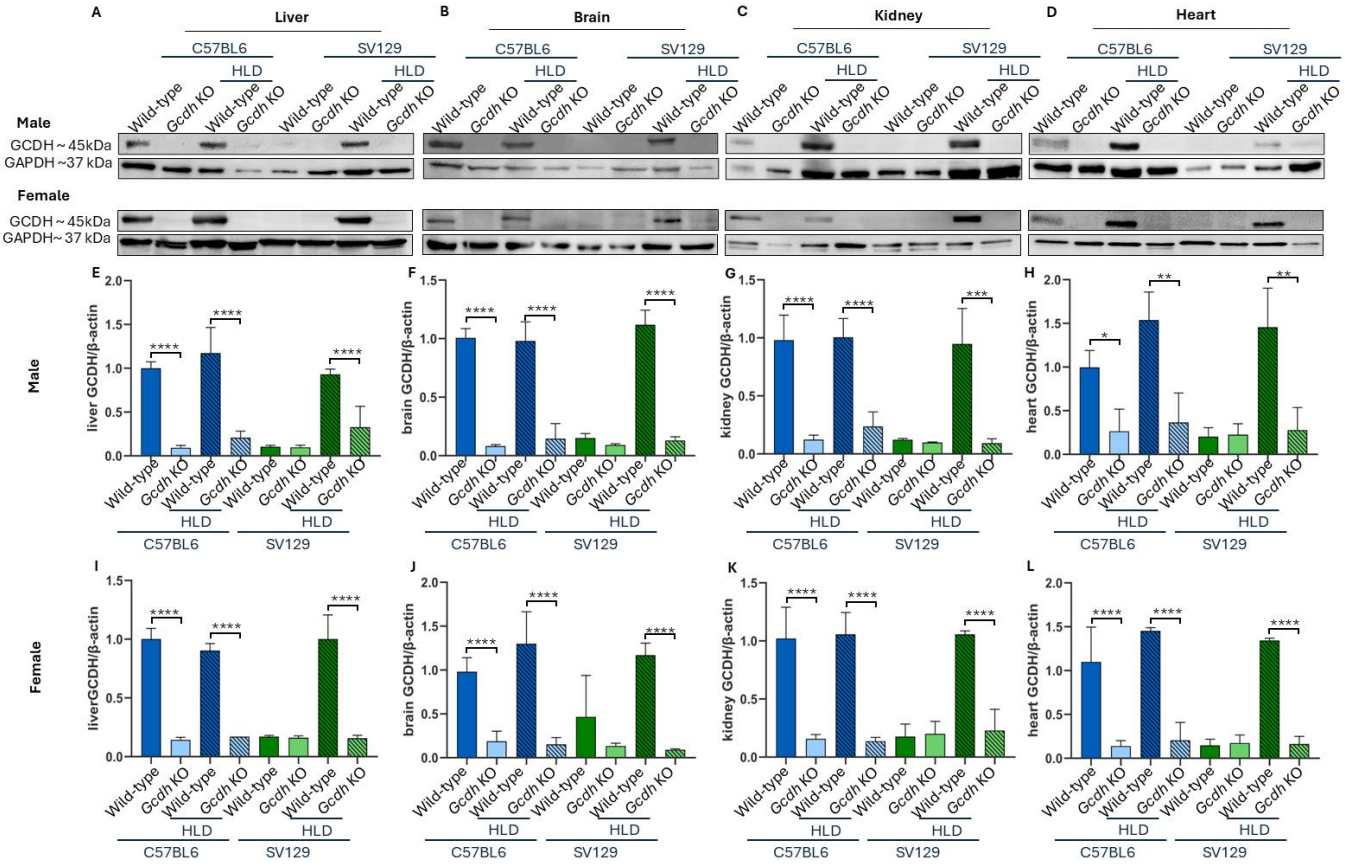

Figure 32. Protein expression of GCDH under standard and high lysine diet. (A-D) GCDH protein expression in liver (A), brain (B), kidney (C), and heart (D) of male and female mice with or without HLD with GAPDH used as loading control. The quantification of the GCDH protein is represented in E-L. Significance calculated with One-way ANOVA test with * $p < 0.05$; ** $p \leq 0.01$; *** $p \leq 0.001$; **** $p \leq 0.0001$; n=3 for all groups. Abbreviations: blue bar, WT from C57BL/6N background; light blue bar, *Gcdh* KO from C57BL/6N background; green bar, WT from SV129 background; light green bar, *Gcdh* KO from SV129 background; striped bar, groups under HLD.

3.1.5 The underlying genotype affects the metabolic response of *Gcdh* KO mice to HLD and their constitution

To study the severity of the clinical phenotype induced by HLD in *Gcdh* KO mice, these KO mice were fed a high lysine diet for three days. In literature, the untreated mice show an increase in the concentration of the neurotoxic metabolites GA and 3OHGA in plasma, urine, and tissues. However, there is no acute formation of neurological symptoms [39]. To initiate these manifestations, a high-lysine diet is essential [39]. The induced clinical phenotype has similarities to the human disease, including encephalopathy, motor deficits, and seizure-like behavior. As increased exposure to this diet increases the mortality rate the high lysine diet has to be stopped after three days, and mice have to be monitored closely.

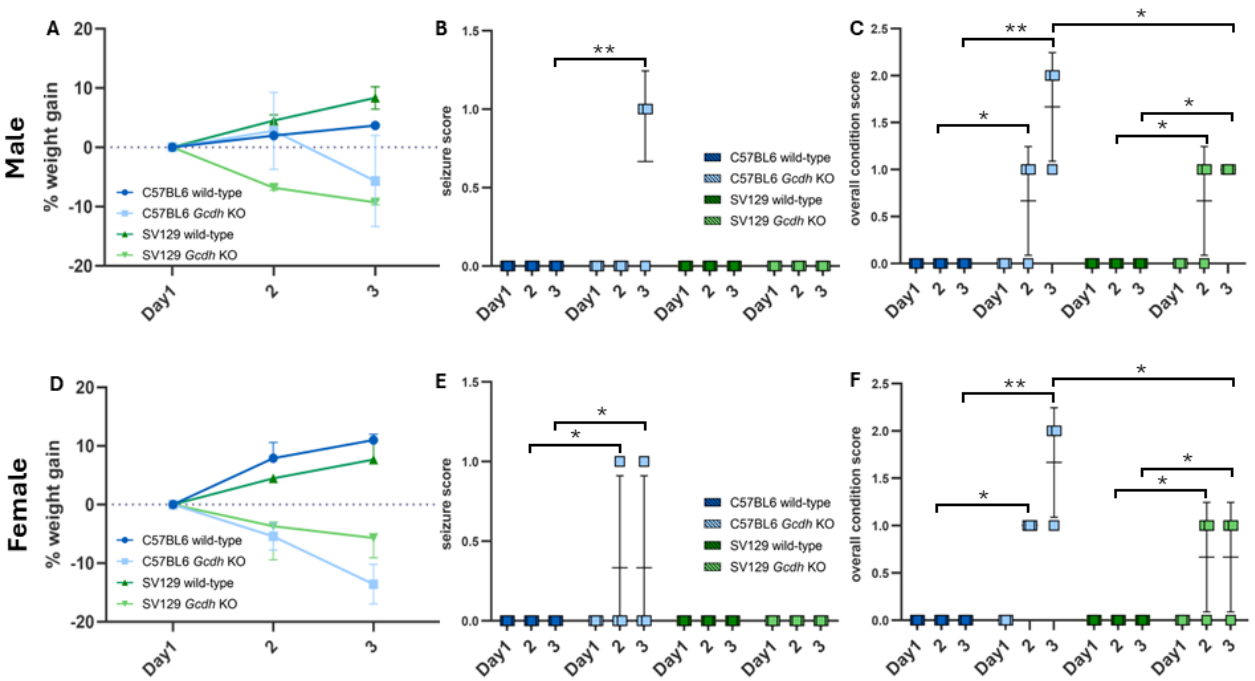

Figure 13. Monitoring of well-being and distress induced by HLD in healthy and *Gcdh* KO mice. Mouse score sheet in 4-week-old mice summarizing the measurements of the weight change during HLD in male (A) and females (D), the seizure-like behavior development during HLD in male (B) and females (E), and the overall condition (that includes the average score of percentage of weight loss, seizure like behavior, and the decrease in movement) in males (C) and females (F). The significance was calculated with One-way ANOVA test with * $p < 0.05$; ** $p \leq 0.001$; n=3 for all groups. Abbreviations: blue bar, WT from C57BL/6N background; light blue bar, *Gcdh* KO from C57BL/6N background; green bar, WT from SV129 background; light green bar, *Gcdh* KO from SV129 background; striped bar, groups under HLD.

As seen in figure 13, *Gcdh* KO mice on HLD lose weight (statistically not significant) compared to healthy WT either from C57BL/6N or SV19 background. Moreover, the overall condition of *Gcdh* KO mice from both backgrounds worsened compared to WT, exemplified by decreased movement of *Gcdh* KO mice. However, only *Gcdh* KO mice from C57BL/6N background developed seizure-like behavior, demonstrating a higher level of distress in *Gcdh* KO mice from C57BL/6N background compared to SV129 background.

To assess the impact of the observed differential gene expression in Godh KO mice of C57BL/6 and SV129 background the metabolite levels of all metabolites involved into the pathophysiology of GA1 were determined in collaboration with Prof. Giancarlo Lamarca (Florence, Italy). Since disease manifestation is not restricted to the brain but can also involve other tissues [68], metabolite concentrations in different organs (brain, liver, kidney and heart) and body fluids (urine, plasma) have been assessed. When comparing the WT mice of both genetic backgrounds, WT C57BL/6N mice excreted low concentrations of GA, 3OHGA and glutaryl carnitine (C5DC) (figure 14), while WT SV129 mice under standard diet excreted high amounts of GA, 30HGA, and C5DC. On the contrary, exposure to HLD resulted in a decrease of these metabolites to normal range in WT SV129 mice. Neurotoxic GA and 30HGA as well as non-toxic C5DC were clearly elevated in Godh KO mice from both genetic backgrounds under a standard diet and further increased during exposure to HLD. Similar results were found in male and female groups. Quinolinic acid (QA) shows no significant changes in all groups and tissues analyzed. Only in the plasma of Godh KO mice with C57BL/6N background a significant increase in the concentration of QA was detectable as compared to WT under both standard and HLD.

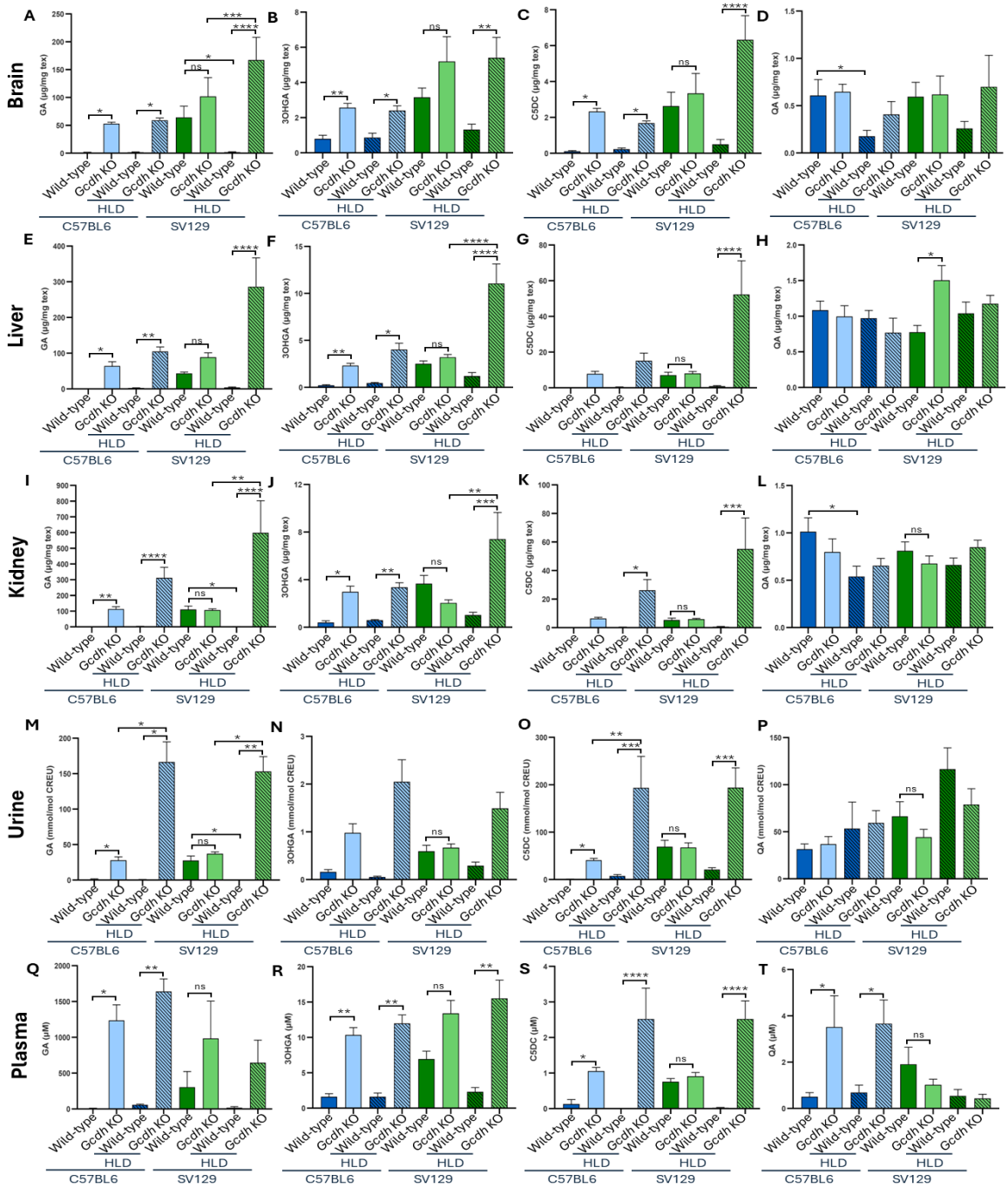

Figure 44. Measurement of metabolites concentrations in C57BL/6N and SV129 mice under standard or HLD. The figure shows the metabolomic analysis measured by Prof. Giancarlo Lamarca (Florence, Italy) and analyzed by me was performed on 4-week-old WT and *Gcdh* KO mice in tissues and body fluids. The concentrations were measured in brain (GA (A), 3OHGA (B), C5DC (C), and QA (D)), liver (GA (E), 3OHGA (F), C5DC (G), and QA (H)), kidney (GA (I), 3OHGA (J), C5DC (K), and QA (L)), urine (GA (M), 3OHGA (N), C5DC (O), and QA (P)), and plasma (GA (Q), 3OHGA (R), C5DC (S), and QA (T)). n=6 for all groups with 3 males and 3 females where male and female results were statistically not significant, thus the results were combined. The significance was calculated with One-way ANOVA test with * $p < 0.05$; ** $p \leq 0.01$; *** $p \leq 0.001$; **** $p \leq 0.0001$. Abbreviations: blue bar, WT from C57BL/6N background; light blue bar, *Gcdh* KO from C57BL/6N background; green bar, WT from SV129 background; light green bar, *Gcdh* KO from SV129 background; striped bar, groups under HLD.

3.1.6 Strain-Specific Regulation of *Gcdh* gene expression possibly due to alternative enzyme or genetic differences

Based on the differences in mRNA and protein expression of key enzymes in the lysine degradation pathway seen in SV129 background compared to C57BL/6N mice, this might be explained by the capability of other enzymes to degrade lysine or its metabolites. To test this hypothesis, I searched for enzymes capable of metabolizing the intermediate metabolite glutaryl-CoA of the lysine degradation. Three enzymes could be identified based on structural similarities of their main substrates to glutaryl-CoA (appendix figure 43). These include isovaleryl-CoA dehydrogenase (IVD), butyryl-CoA dehydrogenase (SCAD), and medium-chain acyl-CoA dehydrogenase (MCAD).

Substrate	Molecular formula	Enzyme	Location of the Enzyme
Glutaryl-CoA	$C_{26}H_{42}N_7O_{19}P_3S$	GCDH	Catalyzes the oxidative decarboxylation of glutaryl-CoA in the degradative pathway of L-lysine, L-hydroxylysine, and L-tryptophan metabolism in the mitochondria
Adipoyl-CoA	$C_{27}H_{44}N_7O_{19}P_3S$	MCAD	Involved in fatty acid oxidation in the Mitochondria
Isovaleryl-CoA	$C_{26}H_{44}N_7O_{17}P_3S$	IVD	Transforms isovaleryl-CoA to 3-methylcrotonyl-CoA in the mitochondria
Crotonyl-CoA	$C_{25}H_{40}N_7O_{17}P_3S$	SCAD	The Weizmann process in the mitochondria

Table 23. Potential candidates for degradation of glutaryl-CoA in animals or cells devoid of *Gcdh*.

To test the hypothesis, expression of these enzymes in the different mouse strains and KO models was validated in liver and brain on the mRNA level (figure 17). SCAD was expressed in the liver of WT and KO mice from SV129 background, and KO mice from C57BL/6N background, but not in WT mice from C57BL/6N background. In the brain, SCAD was expressed in all groups. It is worth noting that there are two known isoforms of SCAD and expression of both was measured. The other two enzymes were not expressed in either organ analyzed here. Since SCAD is expressed in the absence of GCDH in the *Gcdh* KO mice, this could imply that SCAD might serve as additional scavenger of glutaryl-CoA.

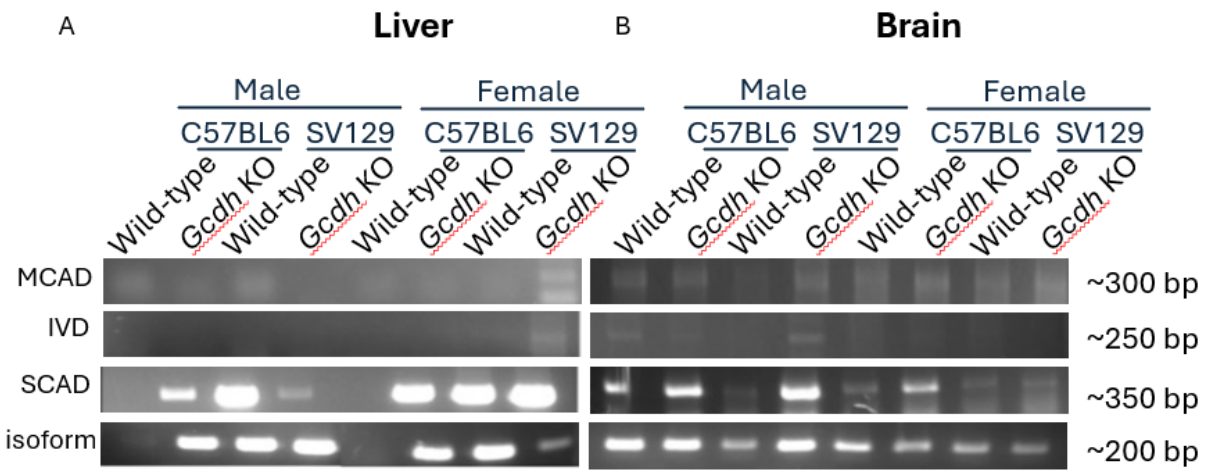

Figure 15. Expression of *Mcad*, *Ivd*, *Scad* and *Scad* isoform mRNA in *Gcdh* KO mice liver(A) and brain (B) from SV129, C57BL/6N background.

However, as SV129 WT mice under standard conditions accumulated GA and 3OHGA and this could be reversed under HLD by upregulation of *Gcdh* expression, this implies that SCAD is not involved in breakdown of surplus glutaryl-CoA. As the differences might also be caused epigenetically, differences in histone modifications have been hypothesized. Besides the facts that the position of the SV129 gene is shifted by around 3 kbp on the chromosomal level compared to C57BL/6N (figure 18), and the size of intron 4 is larger in SV129 mice, 177 single nucleotides polymorphisms are present between the two mouse strains, mainly situated around the promoter region of *Gcdh* gene, explaining the differential gene regulation present between the two genetic backgrounds. Due to these genetic differences, C57BL/6N background was used for further animal testing and therapeutic strategies trials.

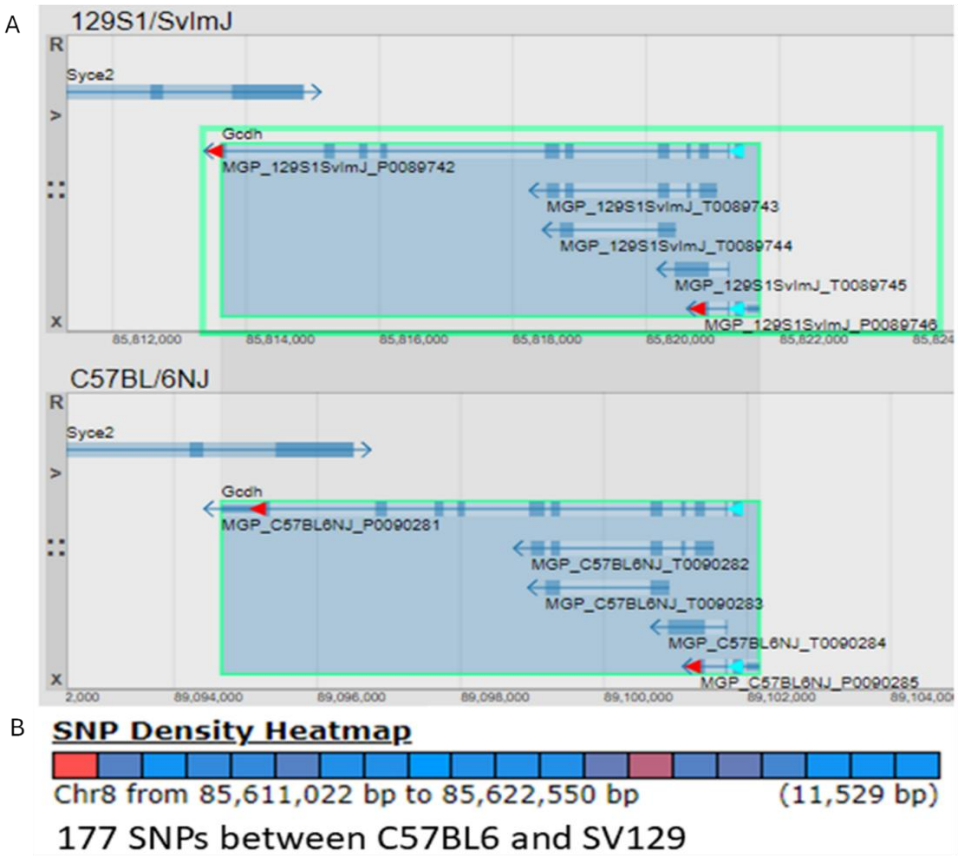

Figure 16. Comparison of the genomic locus of the *Gcdh* gene in C57BL/6 and SV129 mouse strains. Data has been provided by the Mouse Genome Informatics (MGI). (A) location of *Gcdh* gene on chromosome 19 in both SV129 and C57BL/6 backgrounds. (B) heat map showing the concentration of single nucleotide polymorphism (SNPs) between both backgrounds with a color range from red meaning high number of SNPs to light blue meaning low to no SNPs.

3.2. Evaluation of substrate reduction by gene knockout of upstream enzymes of the lysine degradation pathway for therapy

3.2.1. Generation of *Gcdh/Aadat* KO mice and validation via genotyping

To test whether substrate reduction might be an effective therapeutic strategy in GA1, I generated an *Aadat/Gcdh* DKO mouse model. *Aadat* KO mice were obtained from Prof. Robert Schwarcz (University of Maryland School of Medicine, U.S.). *Aadat* KO mice are well characterized [5] and, according to the stress assessment in Heidelberg, did not develop a clinical phenotype. To generate the double KO mice, heterozygous *Gcdh* mice were crossed with heterozygous *Aadat* mice, both maintained on the same C57BL/6N genetic background, in order to establish a breeding colony. Breeding pairs were selected and monitored under standard housing and husbandry conditions, with genotyping performed on ear biopsies. To confirm the presence of the respective KO in the *Gcdh* and *Aadat* genes, a genotyping PCR was performed, followed by Sanger Sequencing as the *Aadat* KO is based on a 7bp deletion which cannot be monitored on an agarose gel.

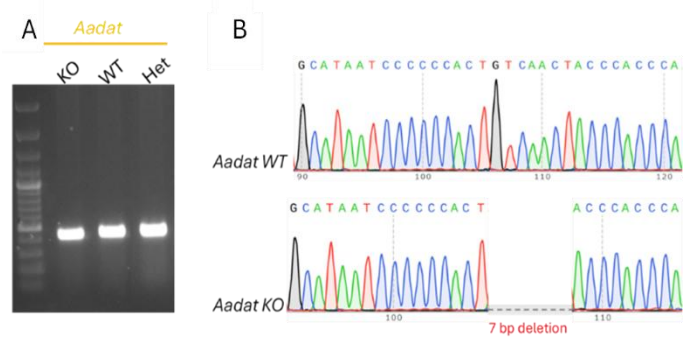

Figure 17. Genotyping strategy to monitor KO of *Gcdh* and *Aadat* genes. (A) Data presented from *Aadat* gene expression in different mice genotype at ~400bp. Line 1 is homozygous knockout, line 2 is WT, and line 3 is heterozygous. Since the deletion cannot be seen on a gel, the bands were extracted and sequenced. (B) Sequencing results of a WT allele compared to a KO allele carrying the 7bp deletion.

3.2.2. Analysis of *Gcdh* and *Aadat* mRNA and protein expression under standard and high lysine diet

Regulation of upstream enzyme of GCDH can alter downstream reaction and impact disease severity. α-Aminoadipate aminotransferase (AADAT), also known as kynurenine aminotransferase II (KAT II) (figure 1) is the first target to be studied. The first step in this strategy was to confirm the validity of the mouse model by measuring the amount of transcript and protein expressed. As seen in figure 20, WT mice expressed both *Gcdh* and *Aadat* transcripts. As expected, the *Gcdh* KO mice expressed *Aadat* but not *Gcdh* mRNA. *Gcdh/Aadat* DKO mice expressed neither *Gcdh* nor *Aadat* mRNA. These results were seen under both standard and HLD.

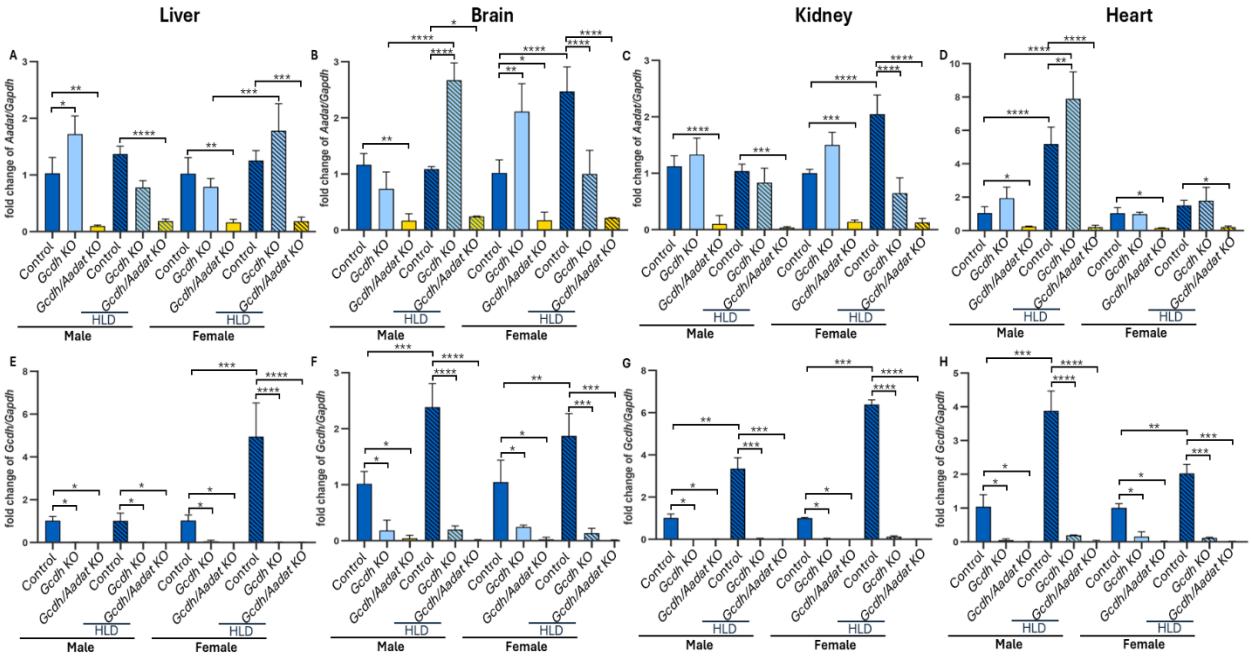

Figure 18. Quantification of *Gcdh* and *Aadat* mRNA expression via qRT-PCR in the different genotypes. Analysis of *Aadat* (A-D) and *Gcdh* (E-H) mRNA expression in liver (A, E), brain (B, F), kidney (C, G), and heart (D, H) of male and female WT, *Gcdh* KO, and *Gcdh/Aass* KO mice with or without HLD and normalized to *Gapdh* with WT group set as 1. Significance calculated with One-way ANOVA test with * p <0.05; ** p ≤0.01; *** p ≤0.001; **** p ≤ 0.0001; n=3 for all groups. Abbreviations: blue bar, WT; light blue bar, *Gcdh* KO; yellow bar, *Gcdh/Aadat* KO; striped bar, groups under HLD.

When comparing the protein expression in WT, *Gcdh* KO, and *Gcdh/Aadat* KO groups, GCDH protein was only expressed in WT mice but not in KO mice as expected. AADAT protein expression in kidney and liver of WT mice increased under HLD (figure 21). In *Gcdh/Aadat* KO mice, AADAT protein was not expressed in any organ under standard or HLD. In brain and heart, GCDH increased under HLD, while AADAT was not clearly detected in these tissues. Furthermore, AADAT protein was not present in *Gcdh* KO mice in the liver and kidney.

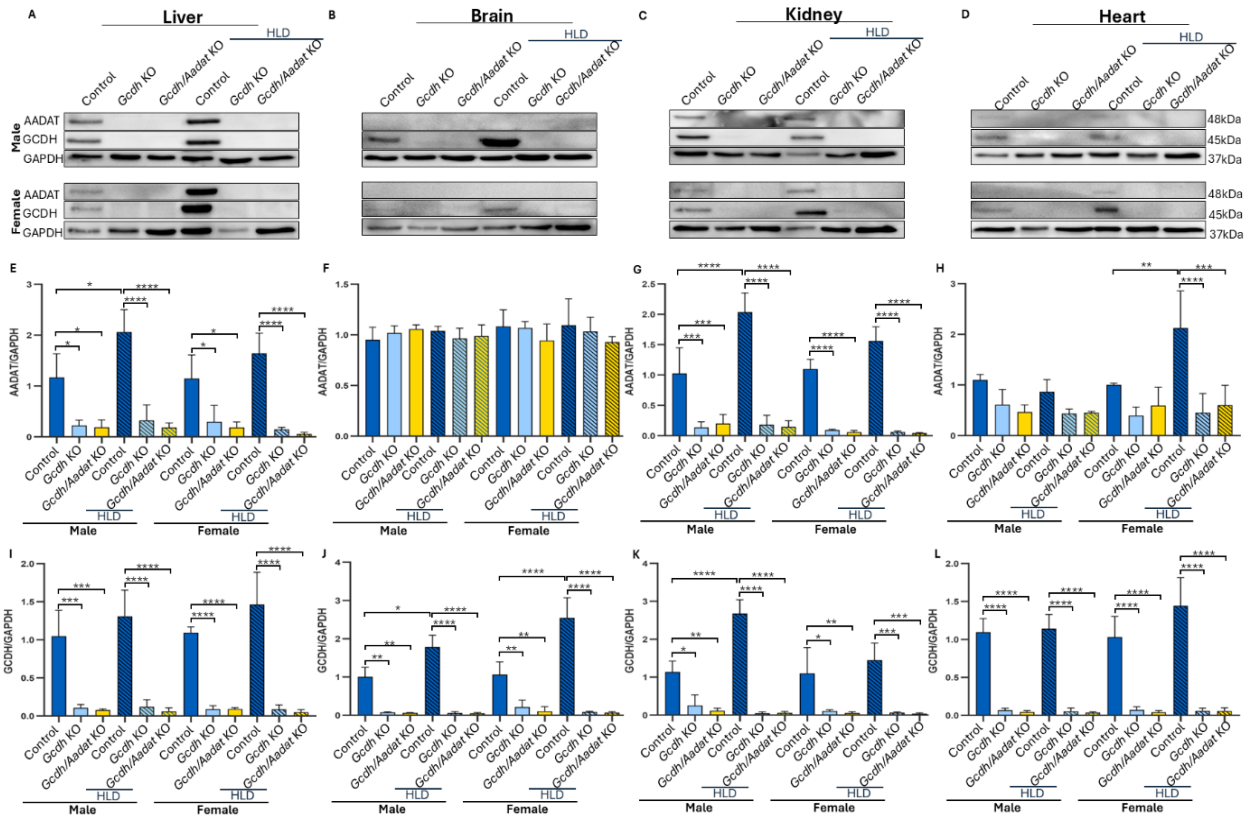

Figure 19. Quantification of GCDH and AADAT protein expression. In A-D AADAT and GCDH proteins expression blots in organs (liver (A), brain (B), kidney (C), and heart (D)) of male and female mice with or without HLD are shown. GAPDH was used as loading control and for normalization of AADAT (E-H) and GCDH (I-L) blot results. Significance was calculated with One-way ANOVA test with * $p < 0.05$; ** $p \leq 0.01$; *** $p \leq 0.001$; **** $p \leq 0.0001$; n=3 for all groups. Abbreviations: blue bar, WT; light blue bar, *Gcdh* KO; yellow bar, *Gcdh/Aadat* KO; striped bar, groups under HLD.

3.2.3. Partial protection against high-lysine diet in *Gcdh/Aadat* KO mice

To test whether *Gcdh/Aadat* KO mice were protected against the induction of a severe biochemical and clinical phenotype, I exposed them for three days to a HLD. As seen in figure 22, compared to *Gcdh* KO mice, *Gcdh/Aadat* KO mice were protected against the negative effects of HLD on body weight, seizures-like behavior, and motor behavior. The overall condition measurement, combining all three criteria that are the percentage of weight loss, seizure-like behavior, and the decrease in movement shows significant decrease for *Gcdh/Aadat* KO group similar to WT compared to *Gcdh* KO group.

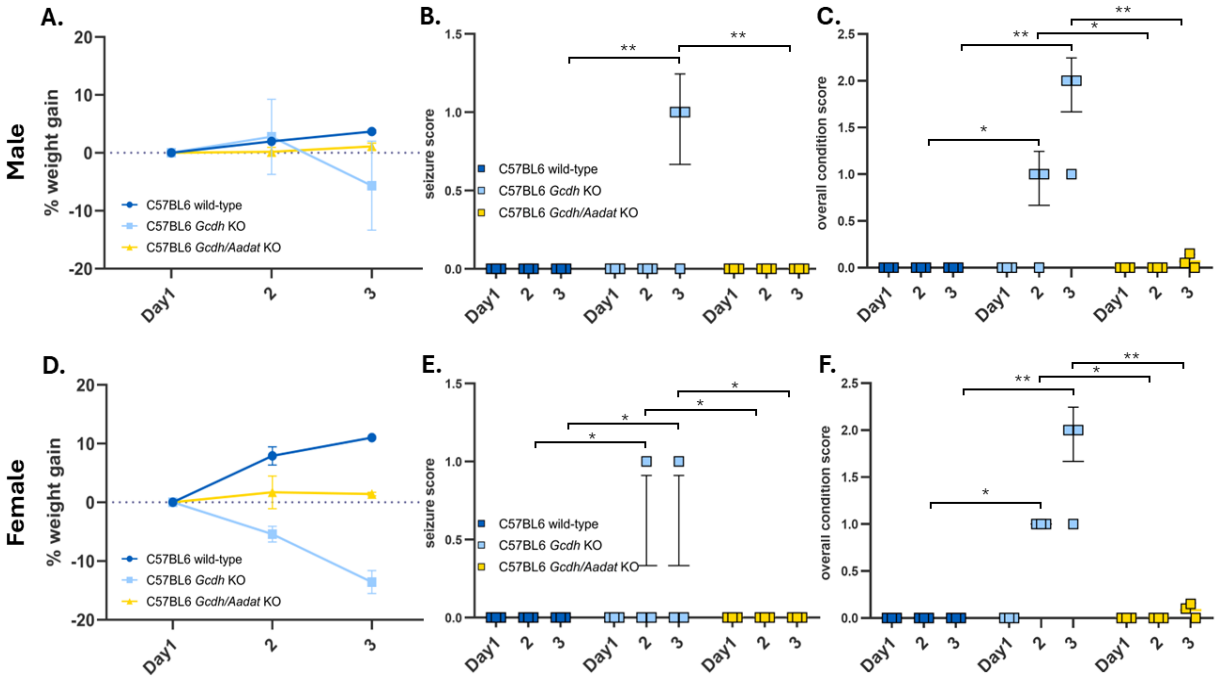

Figure 20. Rescue of *Gcdh* KO mice by *Aadat* KO on the physical level. Mouse score sheet in 4-week-old mice shows the weight change in male (A) and female (D) mice, the seizure-like behavior development in male (B) and females (E), and overall condition in males (C) and females (F) during HLD. The overall condition is the calculation of the averaged score of three criteria that are the percentage of weight loss, seizure-like behavior, and the decrease in movement. The significance was calculated with One-way ANOVA test with * p <0.05; ** p ≤0.01; n=3 for all groups. Abbreviations: blue bar, WT; light blue bar, *Gcdh* KO; yellow bar, *Gcdh/Aadat* KO; striped bar, groups under HLD.

To evaluate the impact of targeting AADAT, and to check if AADAT is a suitable therapeutic target, metabolite analysis was performed in cooperation with Prof. Giancarlo Lamarca (Florence, Italy). GA, 3OHGA, and C5DC were measured in WT, *Gcdh* KO and *Gcdh/Aadat* KO in various tissues and body fluids (figure 23). In the brain and urine of *Gcdh/Aadat* KO mice a downregulation of GA,3OHGA, and the none-toxic C5DC is seen under a standard diet. However, in the rest of the organs and in plasma of *Gcdh/Aadat* KO mice GA, 3OHGA, and C5DC levels were high similar to *Gcdh* KO when compared to WT. Under HLD, only the brain of *Gcdh/Aadat* KO mice shows a decrease in metabolites accumulation. In contrast, in the rest of the organs, GA, 3OHGA, and C5DC concentrations were upregulated in *Gcdh/Aadat* KO group to levels even higher than those observed in the *Gcdh* KO group. These results display a tissue specific effect.

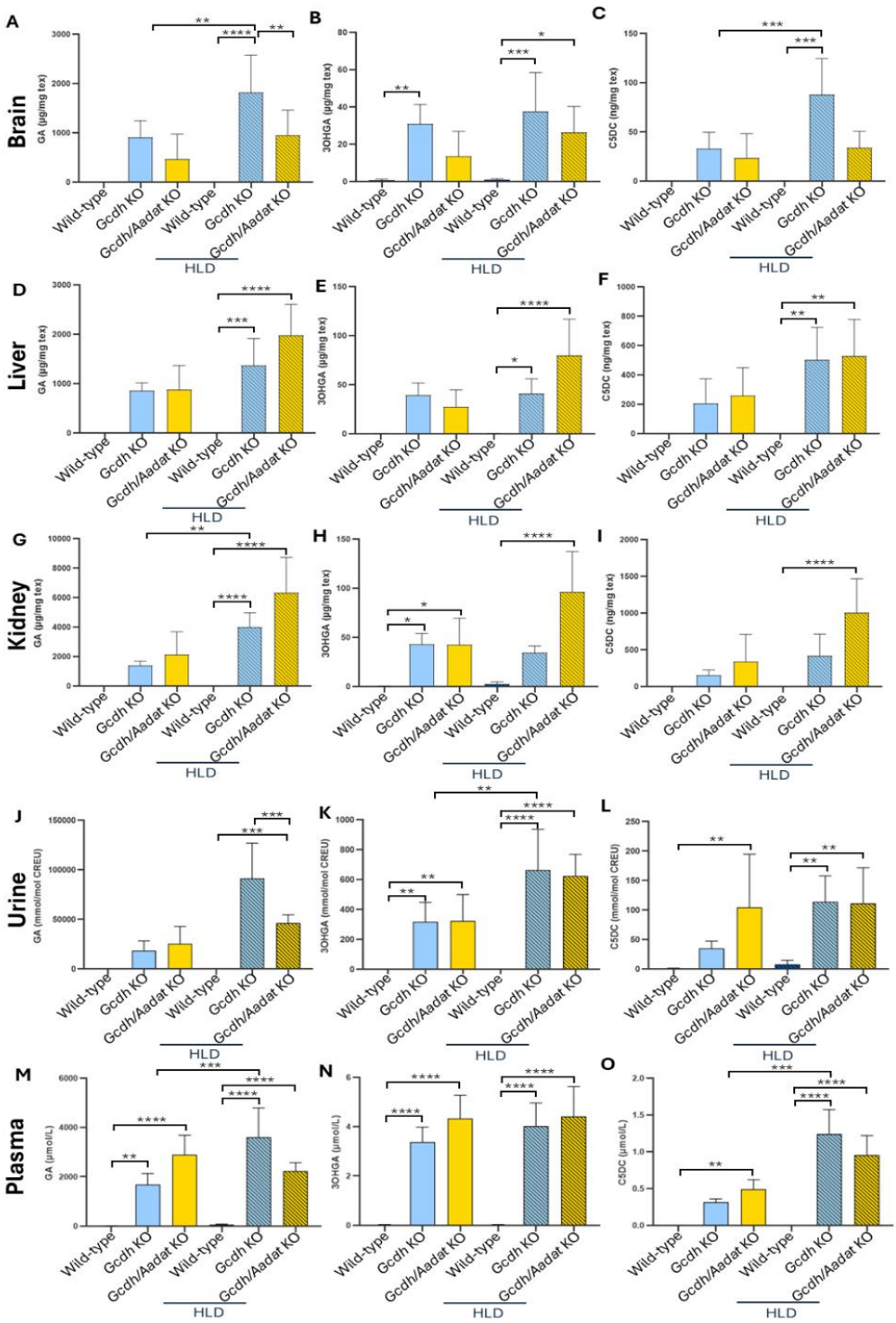

Figure 21. Metabolic changes in WT, *Gcdh* KO, and *Gcdh/Aadat* KO under standard or HLD. Metabolomic analysis measured by Prof. Giancarlo Lamarca (Florence, Italy) and analyzed by me was performed in 4-week-old mice tissues and body fluids including brain GA (A), 3OHGA (B), and C5DC (C), liver GA (D), 3OHGA (E), and C5DC (F), kidney GA (G), 3OHGA (H), and C5DC (I), urine GA (J), 3OHGA (K), and C5DC (L), and plasma GA (M), 3OHGA (N), and C5DC (O). n=6 for all groups with 3 males and 3 females, male and female results were statistically nonsignificant, thus the results were combined. The significance calculated with One-way Anova test with * $p < 0.05$; ** $p \leq 0.01$; *** $p \leq 0.001$; *** $p \leq 0.0001$. Abbreviations: striped bar, groups under HLD; KO, knockout; HLD, high lysine diet.

3.2.4. Suitability of PF-04859989, an AADAT inhibitor, for the treatment of GA1

One of the goals in this study was to test the AADAT inhibitor already developed pharmaceutically. PF-04859989 was not tried in mouse model before. Therefore, before trying on the mouse model, the efficacy of PF-04859989 was tested *in vitro* through the measurement of AADAT activity by quantifying its substrate in HEK293T cell model. In the study of Kozak et al. (2014), after a detailed pharmacokinetic analysis of PF-04859989, a dose of 10 mg/kg was determined to be effective in rats [69], as it led to a concentration of 10 mM PF-04859989 in the plasma and 5mM in the brain directly after injection. In order to replicate the condition in cell culture to be able to study the feasibility of the dosage finding approach, I decided on using an increasing concentration of PF-04859989 from 0 to a maximum of 10mM. In HEK293T cells different doses of the inhibitor were tested to see if there is a dose dependent response. No information on the dose establishment *in vitro* was found in literature. Thus, a range of doses was tested. The AADAT activity was measured by analyzing the concentration of its substrate 2AA upon inhibition.

To know which concentration of lysine to use on the cells, a study on required lysine concentration took place. 0.1 mM, 0.5, 1 mM, 2 mM, or 5 mM of lysine were used on HEK293T cells. GCDH activity was measured as an indicator of which conditions caused the highest activation of the lysine degradation pathway.

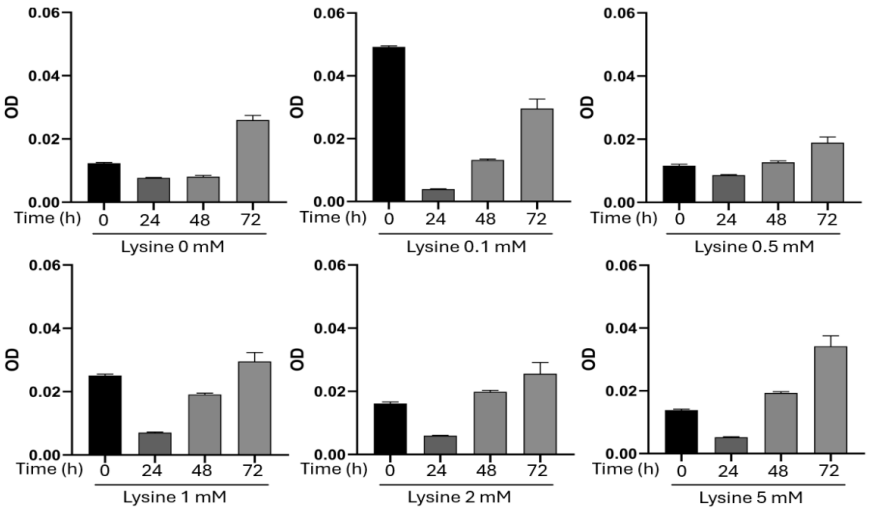

Figure 22. Dose response experiments to find a suitable dose for L-lysine in cell culture. GCDH activity results in HEK293T cells. Data from GCDH activity measured by the optical density at λ=350nm in cells with increasing lysine concentration in the media (0,1 mM, 0,5 mM, 1 mM, 2 mM, 5mM) after 24h, 48h, and 72h. n=3. Normalization was done to total protein concentration.

As seen in figure 24, GCDH activity peaks after 72 h in all treated groups. After 72 h, 5 mM lysine caused the highest GCDH activity. Thus, 5 mM lysine for 72 h treatment was chosen for further experiments.

Next, HEK293T cells were treated for 72 h with PF-04859989, an AADAT inhibitor with or without 5mM lysine. Then AADAT activity was determined via the measurement of 2AA concentration in the cell lysate in collaboration with Dr. Rossmann (Dietmar Hopp Metabolic Center Heidelberg). As seen in figure 25, there is a dose dependent inhibition observed as the concentration of 2AA increase with increasing concentrations of AADAT inhibitor. 2AA without additional lysine accumulates at level of 0,5 µmol/L compared to 2 µmol/L with 10 mM inhibitor. Under high lysine conditions, 2AA accumulates in healthy HEK293T at level of 0,8 µmol/L compared to 3 µmol/L in treated cells. In both cases there is an increase of around 4 folds of substrate. Also, there is a tendency of increase in substrate level when lysine is added as there is a higher activation of lysine degradation pathway with increased lysine availability. The levels were normalized to total protein content.

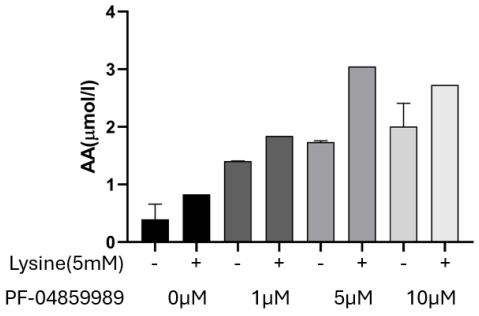

Figure 23. AADAT activity in HEK293T cells. (A) PCR analysis confirming the expression of *AASS*, *AADAT*, and *GCDH* transcripts in HEK293T. (B) Data from AADAT activity measurements in µmol/L with 2 samples used per condition showing an increase in AADAT inhibition with increased in inhibitor concentration.

Next, I checked whether the inhibitor would work in the same manner on the animal model. The inhibitor used was already established by Pfizer and has been tested in rats [69] and not in mice. PF-04859989 is a potent inhibitor that covalently binds to the PLP within the active site of AADAT enzyme. To find a suitable dosing for the AADAT inhibitor in the GA1 mouse model, a dose finding study was conducted. The same doses chosen were tried in the rat study and acknowledged as safe [69]. A subcutaneous single shot of 3 different doses (3.2 mg/kg, 10 mg/kg, 32 mg/kg) of PF-04859989 was injected and then then organs were harvested 1 h, 4 h, or 24 h after injection. The organs (liver, brain, and kidney) and body fluids were sent for metabolomics analysis to Prof. Giancarlo Lamarca (Florence, Italy) and analyzed by me. To confirm the activity of the inhibitor and its efficiency in inhibiting AADAT, the concentrations of 2AA and the product 2OA were determined (figure 24) in treated groups compared to WT. Additionally, the concentrations of GA and 3OHGA were measured (figure 25).

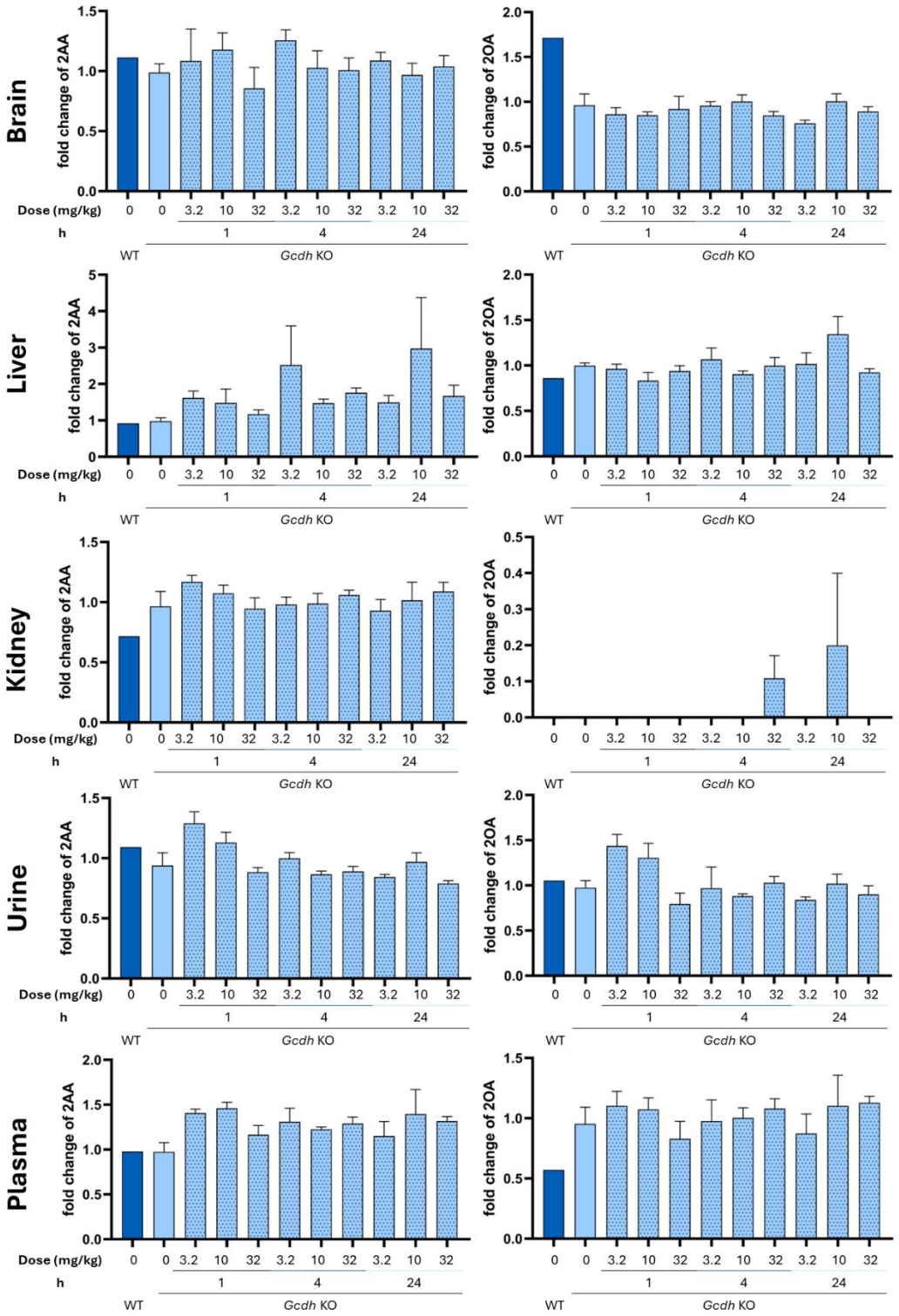

Figure 24. Impact of PF-04859989 Treatment on AADAT Metabolite Profile in Mice. Bar charts represent the fold change of AADAT substrate 2-aminoadipic acid (2AA) and its product 2-oxoadipic acid (2OA). The concentrations were measured in collaboration Prof. Giancarlo Lamarca (Florence, Italy) and analyzed by me in mouse tissue: brain (A, B), liver (C, D), and kidney (E, F) and body fluids urine (G, H) and plasma (I, J) of each group with a dose of 3.2, 10, or 32 mg/kg after 1h, 4h, or 24h with n=4 mice per group.

Figure 24 summarizes the efficiency of PF-04859989 in inhibiting AADAT. 2AA was not significantly increased with the presence of the inhibitor in any of the organs. Also, 2OA was not significantly decreased in any of the organs under any of the inhibitor concentrations. Thus, there was no clear dose dependent activity *in vivo*.

Moreover, in tissues and body fluids, there was an increase in the concentrations of GA and 3OHGA (figure 25) in treated groups compared to WT. This implies that the used dosing and treatment approach is not capable in inhibiting AADAT. Therefore, if the inhibitor is intended to be further developed for therapy, additional experiments are needed to define a suitable dose and timing.

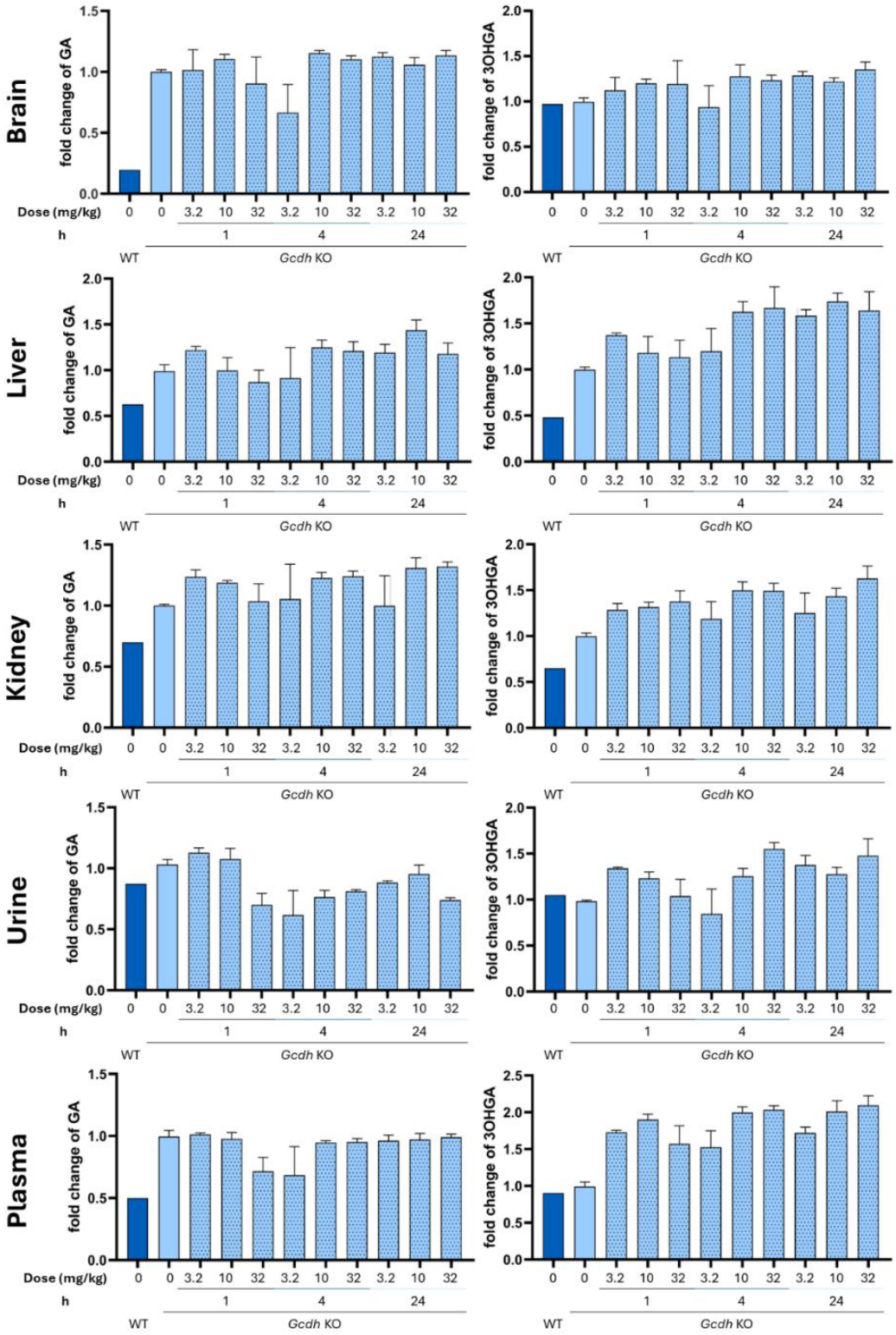

Figure 25. Observed changes in neurotoxins concentrations in multiple tissues following single-dose PF-04859989 administration. Bar charts represent the fold change of GA and 3OHGA measured in brain (A, B), liver (C, D), kidney (E, F), urine (G, H) and plasma (I, J) of each group with single doses of 3.2 mg/kg, 10 mg/kg, or 32mg/kg measured 1 h, 4 h, or 24 h after injection. The measurements were done by Prof. Giancarlo Lamarca (Florence, Italy) and analyzed by me. n=4 mice per group

3.2.5. Breeding strategy to generate *Gcdh/Aass* KO mice and genotyping strategy

Next, I tested the suitability of AASS as a target for substrate reduction in a mouse model. *Aass* KO mice on a C57BL/6N background, previously generated and described by Prof. S. Houten (Icahn School of Medicine at Mount Sinai, New York, United States) were transferred to the German Mouse Clinic (GMC) in Munich. To generate *Gcdh/Aass* KO mice, heterozygous *Gcdh* mice were crossed with heterozygous *Aass* mice, and *Gcdh/Aass* were transferred to the IBF at Heidelberg University. All pups were genotyped before starting the experiments. *Gcdh* gene genotyping was performed as shown before (in 3.1.1) This was done by gel electrophoresis. Figure 28 shows one exemplary gel image. For *Aass* genotyping, primers were designed to amplify a sequence surrounding the KO locus generating either a 250bp fragment (WT allele) or a fragment of 500bp (KO allele). PCR products were separated on an agarose gel, and a typical result is shown in figure 28.

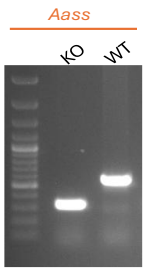

Figure 26. Genotyping results of *Aass* genes. PCR-based genotyping results for *Aass* alleles showing the presence of WT and homozygous KO genotypes.

3.2.6. Analysis of mRNA and protein expression of *Gcdh* and *Aass* in *Gcdh* KO, *Gcdh/Aass* KO and WT mice under standard and HLD

Next, mRNA and protein expression were determined to validate the animal model. As seen in figure 29, WT mice expressed *Gcdh* and *Aass* mRNA, while *Gcdh* KO mice expressed *Aass* but not *Gcdh* mRNA since they carry a *Gcdh* KO. Mice with *Gcdh/Aass* KO expressed no *Gcdh* nor *Aass* mRNA. Even under HLD, similar results were observed as under standard diet in all groups.

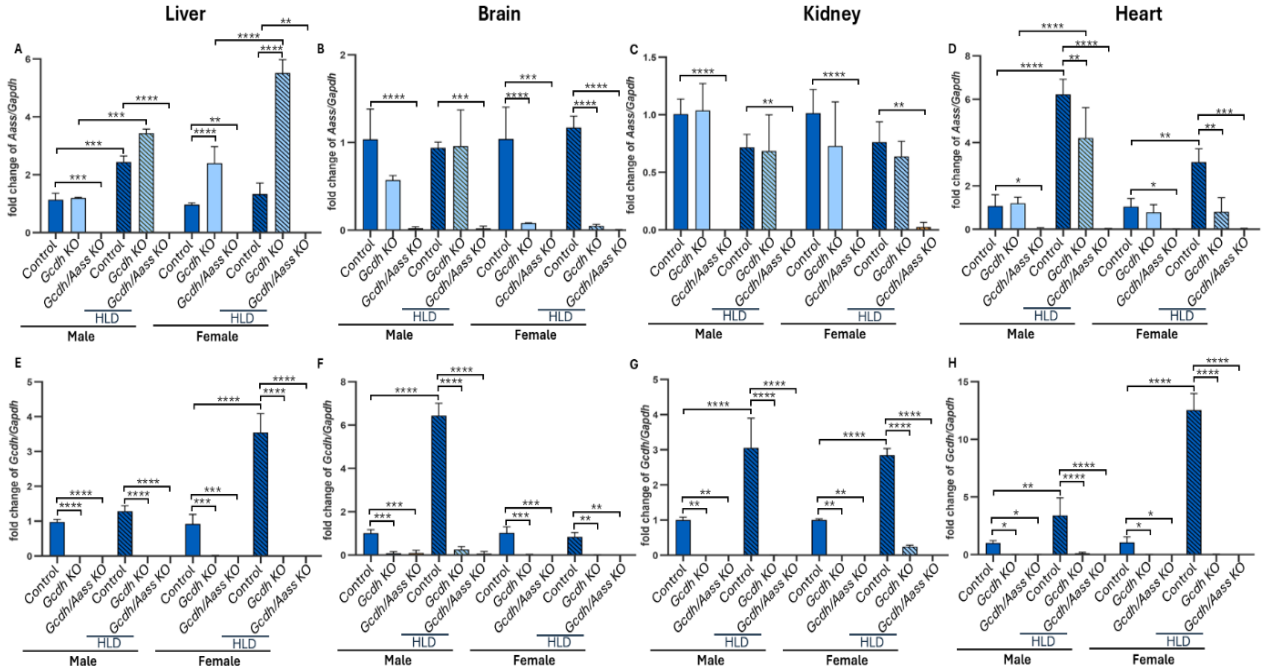

Figure 27. mRNA expression of *Gcdh* and *Aass* in the WT, *Gcdh* KO, and *Gcdh/Aass* KO mice. Analysis of *Aass* (A-D) and *Gcdh* (E-H) mRNA expression in brain (A,E), liver (B.F), kidney (C,G), and heart (D,H) of male and female WT, *Gcdh* KO, and *Gcdh/Aass* KO mice with or without HLD. The measurements were normalized to *Gapdh* with WT group set as 1. Significance was calculated using One-way ANOVA test with * p <0.05; ** p ≤0.01; *** p ≤0.001; **** p ≤ 0.0001; n=3 for all groups. Abbreviations: striped bar, groups under HLD; KO, knockout; HLD, high lysine diet.

When comparing the GCDH protein expression in WT, *Gcdh* KO, and *Gcdh/Aass* KO groups, GCDH protein was only expressed in WT mice. Mice carrying a *Gcdh* knockout showed no GCDH protein expression compared to the WT group. Regarding AASS protein expression (figure 28), there was an upregulation under HLD in the kidney and liver in WT and *Gcdh* KO mice. In the brain and heart, GCDH protein showed an increase in the WT mice under HLD; however, AASS protein was not detected due to the antibody showing unspecific bands.

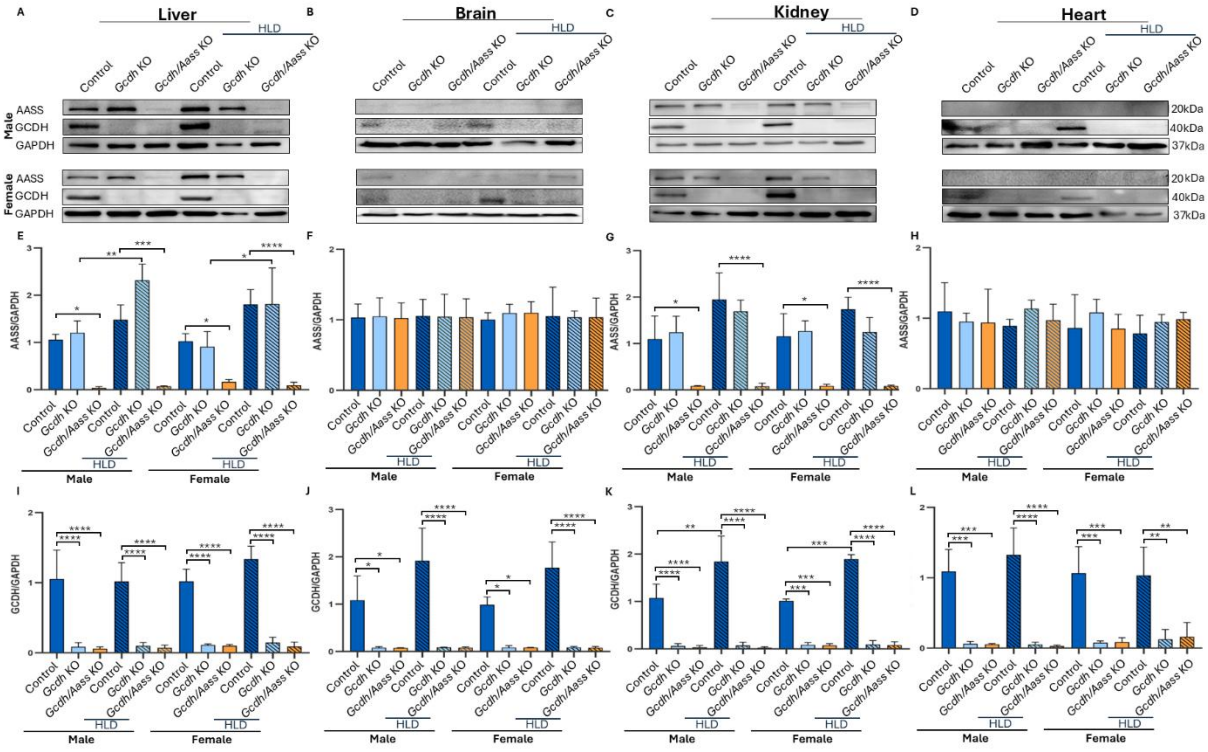

Figure 28. Protein expression of GCDH and AASS in the WT, *Gcdh* KO, and *Gcdh/Aass* KO mice. A-D shows the protein expression of AASS and GCDH in liver (A), brain (B), kidney (C), and heart (D) of male and female mice with or without HLD with GAPDH used as loading control. The quantification of AASS protein can be seen in E-H and GCDH from I-L. Significance calculated with One-way ANOVA test with * p <0.05; ** p ≤0.01; *** p ≤0.001; **** p ≤ 0.0001; n=3 for all groups. Abbreviations: striped bar, groups under HLD; KO, knockout; HLD, high lysine diet.

3.2.7. *Gcdh/Aass* KO are protected against biochemical and clinical deterioration under high-lysine diet

To investigate whether targeting AASS could provide therapeutic benefit in GA1, the generated *Gcdh/Aass* KO mice were studied. Studying these mice allowed to evaluate whether substrate reduction via AASS inhibition could mitigate GA1 associated metabolic imbalances and phenotypic outcomes. First the mice were subjected to HLD for three days. During this time, they were closely monitored while measuring their weight changes, development of seizure-like behaviors or movement deficits. The behavior of *Gcdh* KO mice aggravated under HLD compared to WT group while *Gcdh/Aass* double KO mice presented with a significantly attenuated clinical phenotype under HLD. *Gcdh/Aass* KO mice demonstrated no seizure-like behavior nor decrease in movement. Their overall condition was similar to WT group (Figure 29).

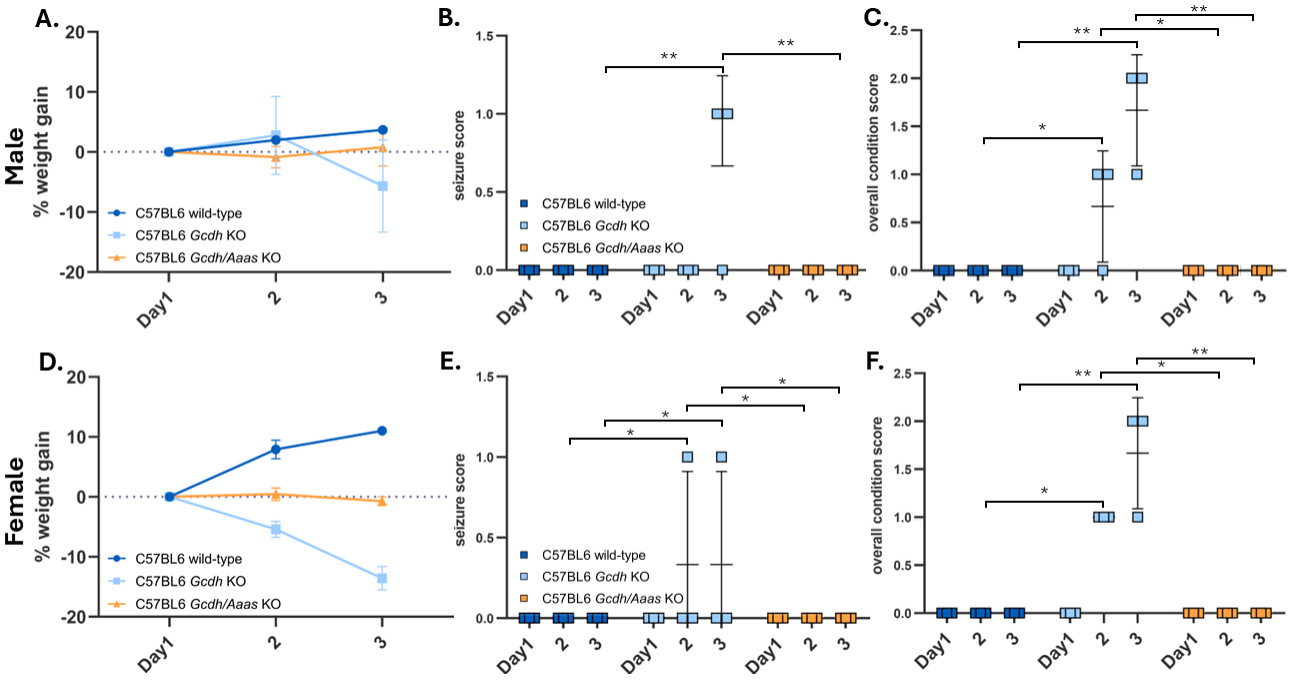

Figure 29. *Aass* KO leads to a rescue of the clinical phenotype seen in *Gcdh* KO mice. Mouse score sheet in 4-week-old mice recorded the: weight change during HLD in male (A) and females (D), seizure-like behavior development during HLD in male (B) and females (E), and overall condition (that includes the average score of percentage of weight loss, seizure like behavior, and the decrease in movement) in males (C) and females (F). Significance was calculated with One-way ANOVA test with * p <0.05; ** p ≤0.01; with n=3 for all groups. Abbreviations: striped bar, groups under HLD; KO, knockout; HLD, high lysine diet.

Next, we compared the metabolic response to HLD in both mouse models determining the concentrations of key metabolites of GA1 in urine and plasma, as well as in brain, liver, and kidney (figure 30). Since no significant differences were identified in male and female mice, their results were combined for the analysis. In *Gcdh* KO mice, GA, 3OHGA, and C5DC concentrations were elevated in all analyzed tissues and fluids even under standard diet and further increased under exposure to HLD. In *Gcdh/Aass* KO mice, the concentrations of GA and 3OHGA could not be distinguished from those of WT mice. C5DC was upregulated in *Gcdh/Aass* KO group under HLD in all analyzed tissues compared to WT. Concerning QA, no major changes are seen between WT and *Gcdh* KO mice under standard or HLD. However, *Gcdh/Aass* KO group was presenting lower amount of QA under standard diet and an upregulation with the increase of lysine in the diet.

Biochemical analyses comparing the metabolomic fold change between *Gcdh/Aadat* KO and *Gcdh/Aass* KO groups revealed a more robust systemic reduction of GA in *Gcdh/Aass* KO mice. In *Gcdh/Aadat* KO mice, significant reduction in GA was observed in an organ specific pattern. In the brain tissue, it decreased to 50 % under standard diet. While levels remained elevated or even increased in peripheral organs, particularly under HLD (figure 31). While in *Gcdh/Aass* KO a decrease in neurotoxic metabolites concentration ranging from 70% under standard diet and 40–70% under HLD, especially in plasma, urine, kidney, and liver (figure 31) was measured. These results strongly support the notion of the additional *Aass* KO rescues the biochemical and clinical phenotype of *Gcdh* KO mice. Therefore, AASS was shown to be a promising therapeutic target for a substrate reduction therapy for GA1.

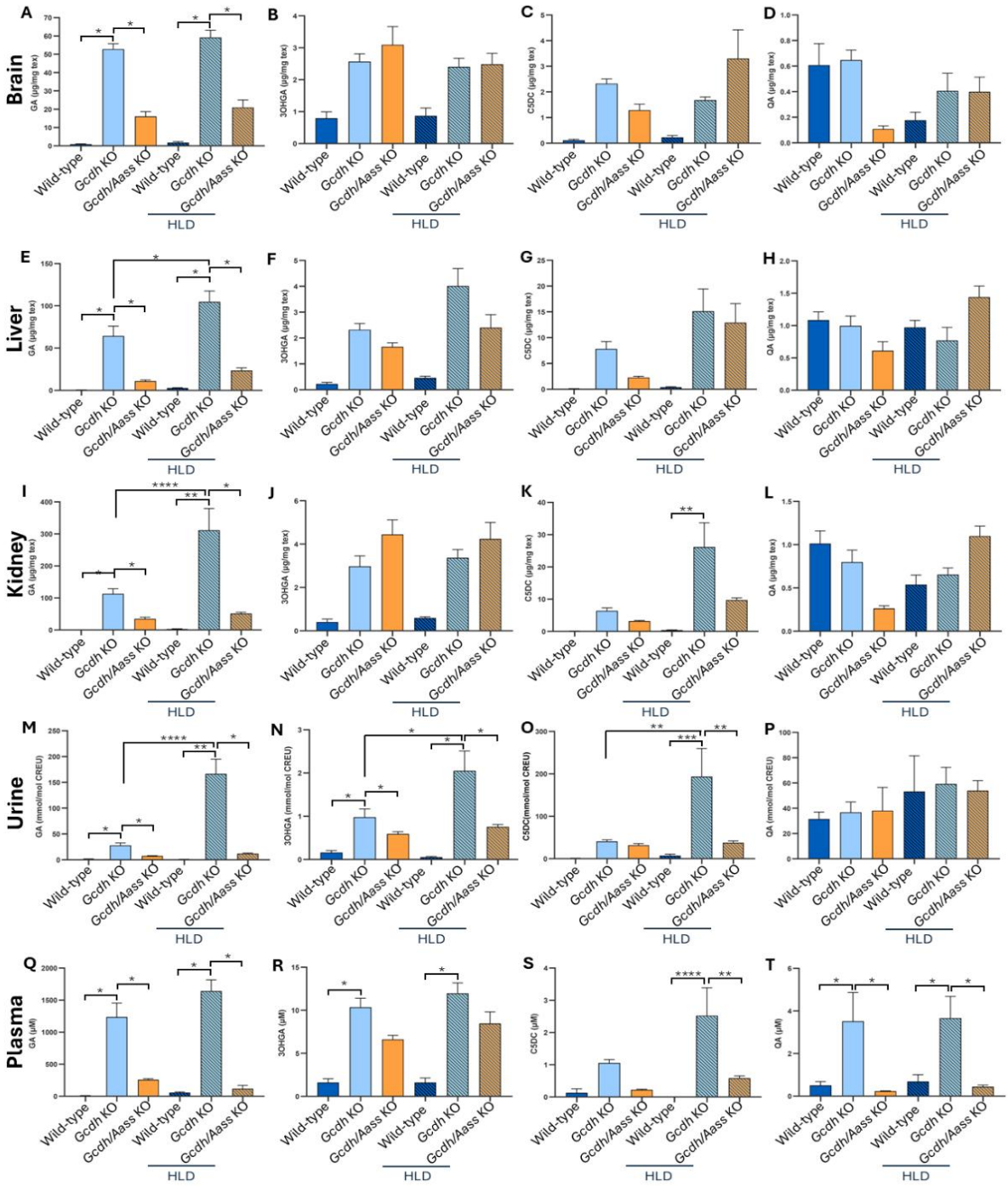

Figure 30. Protection against metabolic derangement in *Gcdh/Aass* double KO mice under standard diet and HLD. The figure shows the metabolomic analysis measured by Prof. Lamarca (Florence, Italy) and analyzed by me of 4-week-old WT, *Gcdh* KO, and *Gcdh/Aass* KO mice. The concentrations were measured in multiple tissues like brain (GA (A), 3OHGA (B), C5DC (C), and QA (D)), liver (GA (E), 3OHGA (F), C5DC (G), and QA (H)), and kidney (GA (I), 3OHGA (J), C5DC (K), and QA (L), and body fluids like urine (GA (M), 3OHGA (N), C5DC (O), and QA (P)), and plasma (GA (Q), 3OHGA (R), C5DC (S), and QA (T)). n=6 for all groups with 3 males and 3 females, since male and female results were statistically nonsignificant, the results were combined. Significance calculated with One-way ANOVA test with * $p < 0.05$; ** $p \leq 0.01$; *** $p \leq 0.001$; **** $p \leq 0.0001$. Abbreviations: striped bar, groups under HLD; KO, knockout; HLD, high lysine diet.

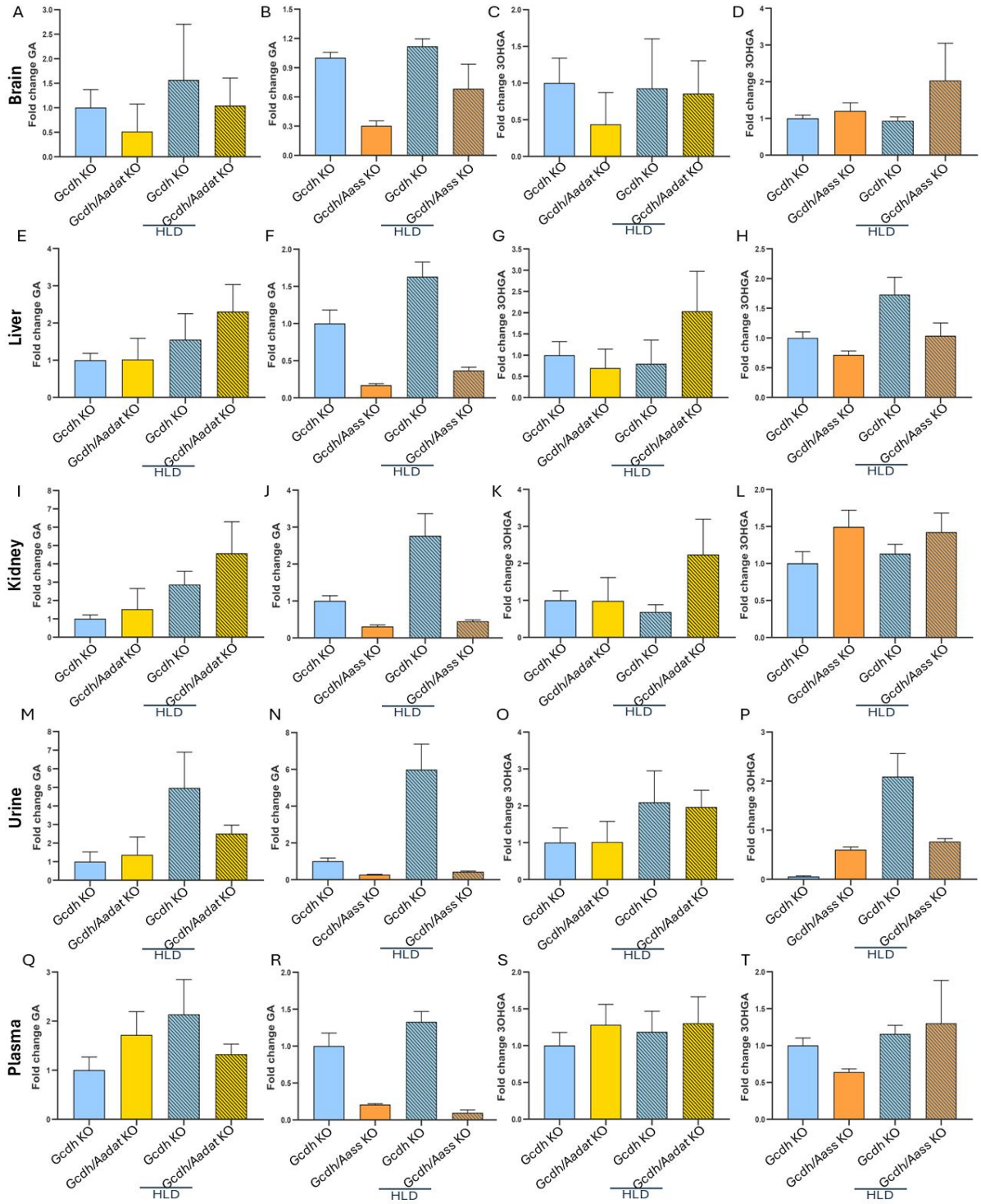

Figure 31. Comparison of biochemical phenotypes in *Gcdh/Aadat* KO and *Gcdh/Aass* KO mice. To validate the efficiency of AASS compared to AADAT, metabolomic measurement measured by Prof. Giancarlo Lamarca (Florence, Italy) and analyzed by me show the fold change of 4-week-old mice tissues and body fluids were compared. The concentrations in brain GA (A, B), 3OHGA (C, D) levels, liver GA (E, F), 3OHGA (G, H) levels, kidney GA (I, J), 3OHGA (K, L) levels, urine GA (M, N), 3OHGA (O, P) levels, and plasma GA (Q, R), 3OHGA (S, T), levels. n=6 for all groups with 3 males and 3 females; male and female results were statistically nonsignificant; thus, the results were combined. Abbreviations: striped bar, groups under HLD; KO, knockout; HLD, high lysine diet.

3.2.8. Influence of the microbiome on lysine metabolism

To evaluate whether the gut microbiome is involved in lysine metabolism and can influence disease severity in GA1, *Gcdh* KO and WT mice were treated with the broad-spectrum antibiotic enrofloxacin for 10 days in the drinking water with or without HLD. Despite antibiotic administration, no improvement in clinical outcome was observed upon HLD. As shown in figure 32, *Gcdh* KO mice from C57BL/6N on HLD displayed a progressive loss of body weight compared to WT controls. In addition to weight loss, *Gcdh* KO mice showed markedly reduced locomotor activity, poor grooming, and occasional seizure-like episodes, indicating increased physiological distress. These symptoms were comparable between antibiotic-treated and untreated *Gcdh* KO mice, suggesting that microbiom depletion does not alleviate long-term metabolic or neurological manifestations of GA1 under high-lysine challenge.

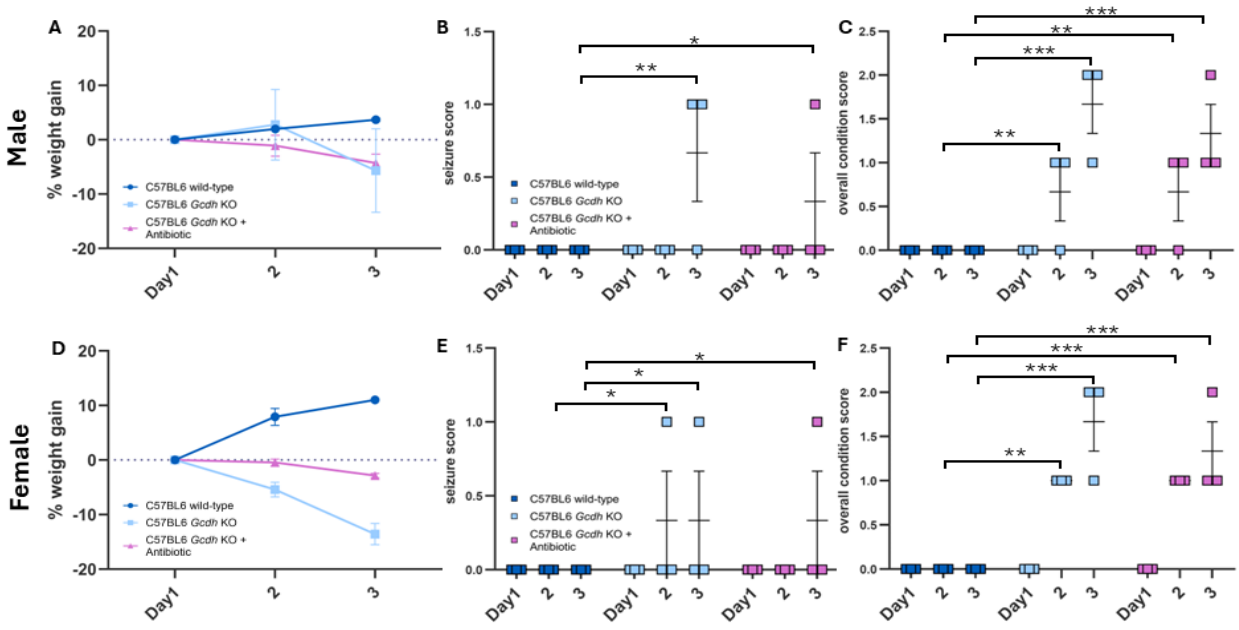

Figure 32. Antibiotic treatment does not ameliorate disease severity in GA1. Mouse score sheet in 4-week-old mice measuring during HLD the weight change in male (A) and females (D), seizure-like behavior development in male (B) and females (E), and overall condition in males (C) and females (F). The overall condition measurement includes averaged score of the percentage of weight loss, seizure like behavior, and the decrease in movement. Significance was calculated with One-way ANOVA test with * p <0.05; ** p ≤0.001; *** p ≤0.0001; n=3 for all groups. Abbreviations: KO, knockout; striped bar, groups under HLD.

To test the hypothesis, that the gut microbiome might contribute to disease severity by producing GA, treated *Gcdh* KO mice under standard or HLD, the levels of GA, 3OHGA and C5DC were measured in collaboration with Prof. Giancarlo Lamarca (Florence, Italy) in plasma, urine and tissues (brain, kidney, liver). As shown in figure 35, there is a slight decrease in the concentrations of GA, 3OHGA, and C5DC in urine and plasma with antibiotic treatment under standard diet. Furthermore, with HLD this change is significantly enhanced. No significant difference was observed between male and female mice. Thus, these results were combined for statistical analysis. On the other hand, in brain, liver and kidney, the concentration of neurotoxins in treated *Gcdh* KO mice is similar or slightly enhanced to the untreated group. Thus, antibiotic treatment leads to a small decrease in the measured concentrations of GA and 3OHGA in body fluids but not in organs.

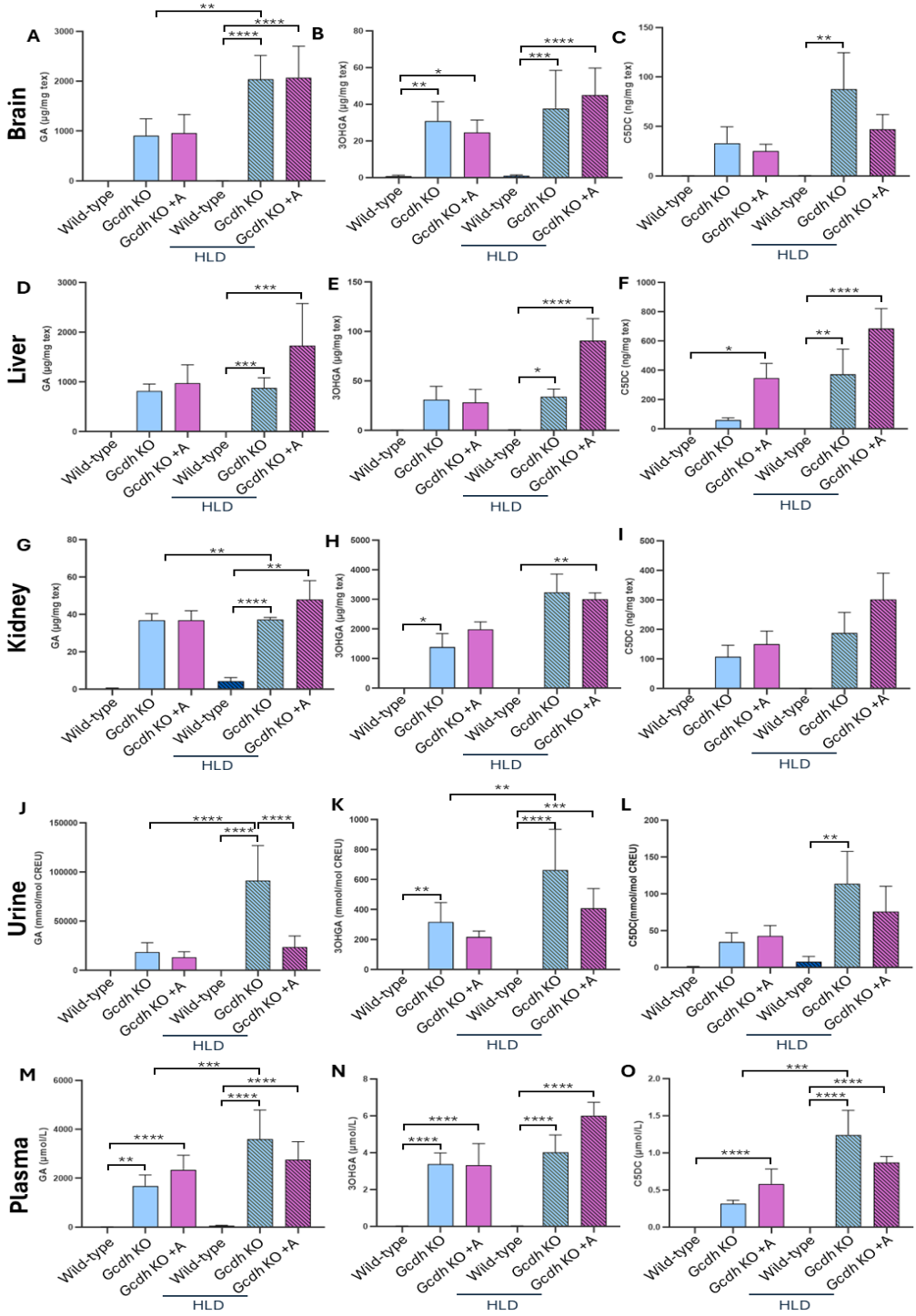

Figure 33. Role of the microbiome on the concentration of GA, 3OHGA, and C5DC. Metabolomic analysis measured by Mayer's Lab, Italy and analyzed by me was performed on 4-week-old mice tissues and body fluids. Metabolite concentrations were measured in brain GA (A), 3OHGA (B), C5DC (C), liver GA (D), 3OHGA (E), C5DC (F), kidney GA (G), 3OHGA (H), C5DC (I), urine GA (J), 3OHGA (K), C5DC (L), and plasma GA (O), 3OHGA (P), C5DC (Q). n=6 for all groups with 3 males and 3 females and since male and female results were statistically nonsignificant, the results were combined. Significance was calculated with One-way ANOVA test with * p <0.05; ** p ≤0.01; *** p ≤0.001; **** p ≤ 0.0001. Abbreviations: striped bar, groups under HLD; A, antibiotic treatment; KO, knockout; HLD, high lysine diet.

Discussion

GA1 remains a significant therapeutic challenge, as current standard management based on dietary lysine restriction and emergency treatment does not reliably prevent striatal injury or long-term neurological disability. Targeting lysine degradation upstream of glutaryl-CoA accumulation has emerged as a promising SRT strategy. In this study, the therapeutic potential of inhibiting upstream enzymes of GCDH using both *Gcdh/Aadat* and *Gcdh/Aass* KO mouse models was evaluated. It is demonstrated that AASS inhibition confers systemic metabolic benefits, improves survival and clinical condition, and reduces toxic metabolite formation in key organs. These findings support AASS as a viable therapeutic target for SRT in GA1.

Genetic background modifies the phenotype of the murine mouse model for GA1

To advance the standardization of a reliable murine model for GA1, I conducted a comparative analysis of two commonly used genetic backgrounds: C57BL/6N and SV129. The findings highlight significant strain-dependent differences in the biochemical and clinical manifestation of GA1, as well as genotype-related effects that are important for the interpretation of translational animal studies.

C57BL/6N WT mice maintained physiological levels of lysine metabolites and did not develop pathological features even under HLD, confirming the metabolic robustness of this strain. In contrast, SV129 WT mice exhibited an unexpected biochemical phenotype: under normal dietary conditions, they displayed low or absent *Gcdh* expression, both transcript and protein, with accompanying accumulation of GA and 3OHGA. This is particularly intriguing, as it suggests a natural hypomorphic regulation of *Gcdh* in SV129 mice, which has not been reported. However, this finding is consistent with known strain-dependent gene expression variability in metabolic enzymes [70, 71]

After analyzing the metabolomics results, elevated levels of toxic metabolites in WT SV129 confirmed that no other enzyme was breaking down the intermediates, causing their accumulation. Notably, in SV129 WT mice, exposure to HLD induced expression of

Gcdh, as evidenced by reduced accumulation of GA and 3OHGA. This implies that dietary lysine may upregulate *Gcdh* via an inducible mechanism, possibly through substrate-mediated transcriptional control, as seen in other amino acid metabolic pathways [72]. This adaptive response, however, complicates the use of SV129 as a GA1 model, because it introduces dietary feedback that could hide genotype-dependent effects.

This led to focusing on the genome and possible differences at the DNA level. As shown previously (figure 16), there are 177 single nucleotides polymorphism when comparing the *Gcdh* gene between the two backgrounds in question. These changes are mostly concentrated in the promoter region, which could explain the activation under HLD. Thus, the second hypothesis arose that under standard condition, the *Gcdh* promoter region in SV129 mice is acetylated on the histone level and therefore un-transcribed. However, with a higher lysine availability, lysine N-acetyltransferase enzyme uses this excess of lysine and transfers the acetyl group allowing the transcription of *Gcdh* and its protein expression.

In both genetic backgrounds, *Gcdh* KO mice displayed marked elevations in GA, 3OHGA, and C5DC under standard diet (figure 16), validating previous findings that *Gcdh* KO mice recapitulate the biochemical phenotype of GA1 [10, 73]. When subjected to HLD as a metabolic stressor, both strains of KO mice developed neurological symptoms, including weight loss, motor abnormalities, and behavioral distress (figure 13), paralleling the clinical features observed in human patients during catabolic crises [14]. However, only C57BL/6N *Gcdh* KO mice consistently displayed seizure-like behaviors under HLD stress, a finding not observed in SV129 KO mice (figure 13). This suggests that strain-specific neurophysiological susceptibility may underline seizure phenotypes, which align with prior studies indicating that seizure thresholds and cortical excitability vary by strain [74].

Histopathological analysis revealed that vacuolization in striatal and hippocampal regions was seen in C57BL/6N *Gcdh* KO mice (figure 9), providing further evidence that this strain mirrors the neuronal injury patterns reported in GA1 patients [75]. Vacuolization, particularly in the striatum, is highly reminiscent of the hallmark selective vulnerability of basal ganglia in GA1, supporting the use of C57BL/6N KO mice as a pathophysiological relevant model.

These findings emphasize the importance of genetic background selection in the design and interpretation of GA1 animal studies. While SV129 mice exhibit atypical regulation of *Gcdh*, C57BL/6N *Gcdh* KO mice exhibit robust neurochemical and histological changes under lysine challenge that better replicate the human disorder [4].

Notably, when comparing male and female mice throughout the study, no main differences were noted. On the molecular level, both sexes expressed genes and proteins in similar amounts. Moreover, under HLD conditions, both developed symptoms and showed decrease in movement, seizure-like behavior and a tendency to decrease in weight.

Next, gut microorganisms play a crucial role in nutrient metabolism, an area still not fully understood in many metabolic disorders. Specific gut bacteria are also capable of catabolizing lysine into glutarate, raising GA levels in the gut lumen and circulation [26, 76]. L-lysine is catabolized into glutarate using GabD enzyme through multiple intermediates including 5-aminovalerate. Under limited conditions enzymes downstream convert glutarate to succinate [26]. In line with this, this study revealed that treating *Gcdh* KO mice with broad-spectrum antibiotics for 10 days significantly reduced plasma and urinary levels of GA and 3OHGA (figure 33). This suggests that inhibiting gut microbial metabolism can attenuate systemic neurotoxin levels, consistent with observations in a separate model, where antibiotic treatment in *Sugct* KO mice normalized metabolic markers by eliminating microbial-derived metabolites [25]. Notably, GA and 3OHGA levels in the organs of treated groups were unchanged post-treatment, indicating that while systemic microbiota-derived metabolites contribute to background neurotoxin exposure, endogenous production in those tissues remains the primary source (figure 33).

Antibiotic-mediated microbiota depletion can reduce baseline neurotoxin load. For acute metabolic stress conditions, combining microbiome targeting strategies with dietary therapy, could be a valuable adjunct therapy to reduce systemic burden; however, it cannot replace strategies targeting organ-specific production. Future work should test targeted pro- and prebiotics that reduce microbial GA production without disrupting beneficial microbial communities.

Thus, the results validate the C57BL/6N *Gcdh* KO mouse as a more suitable preclinical model for GA1 research. This model not only reproduces key biochemical and neuropathological features of the disease but also responds predictably to dietary and metabolic challenges. These properties make it highly suitable for mechanistic studies and preclinical testing of novel therapies, including substrate reduction or gene therapy approaches currently under development [77].

Knocking out upstream enzymes of GCDH: Which is a better target AADAT or AASS

After validating the C57BL/6N *Gcdh* KO as GA1 mouse model, therapeutic strategies were performed on this model. Also, while current dietary and supportive treatments are moderately effective, a significant proportion of patients still experience irreversible motor deficits, primarily dystonia, despite early detection through NBS [13, 52]. These shortcomings underscore the need for more targeted, mechanism-based therapies.

Current research has shifted attention to enzyme upstream GCDH in the lysine degradation pathway. In GA1, two promising upstream enzymatic targets have emerged: AADAT and AASS. These enzymes participate in the saccharopine and pipecolic acid pathways, both of which contribute to lysine catabolism [23]. Importantly, loss-of-function of either enzyme in humans appears clinically benign, supporting their potential suitability as therapeutic targets. No monogenic disorder caused by isolated AADAT deficiency has been described [56]. Similarly, AASS deficiency, which leads to hyperlysinemia, does not result in a severe clinical phenotype despite markedly elevated plasma lysine levels, and individuals are typically asymptomatic [59]. Together, inhibiting these enzymes could reduce the production of glutaryl-CoA, thus lowering the flux of toxic intermediates such as GA and 3OHGA.

The saccharopine pathway is the predominant lysine degradation pathway in humans and rodents, unlike the pipecolic acid pathway, which is more active in peroxisomal metabolism and is poorly characterized in humans [78]. Moreover, the enzymatic composition of the pipecolic pathway in humans remains ambiguous, with limited data on substrate specificity and distribution. The first known enzyme in this pathway is pipecolate oxidase (PIPOX), which acts on L-pipecolate, as described previously in the lysine

degradation pathway [23]. This gap in knowledge suggests that the upstream steps of pipecolate formation may differ fundamentally between species. Based on these uncertainties, researchers have proposed that in humans, L-pipecolate may not be generated via a conventional forward pathway but instead accumulates through a reverse flux when the mitochondrial saccharopine pathway is saturated [78]. This hypothesis underscores the limited understanding of the pathway's regulation and physiological relevance. In contrast, the saccharopine pathway is better defined, and its enzymatic steps are conserved across species, making it a more reliable target for translational research. If the saccharopine pathway is functional in the brain, then its inhibition could play a crucial role in reducing local production of neurotoxic metabolites in GA1 and thus may build the basis for an innovative substrate reduction therapy.

Previous work targeting DHTKD1, another enzyme downstream in the saccharopine pathway, yielded inadequate results [55]. Despite successful genetic inhibition in mice, substrate flux was maintained via bypass through alternative dehydrogenase complexes like OGDHC, rendering the intervention ineffective [79]. DHTKD1 functions as the E1 subunit of the mitochondrial 2-oxoadipate dehydrogenase complex (OADHc), where it preferentially metabolizes 2-oxoadipate; however, when DHTKD1 is absent, the structurally related OGDHc substitutes its E1 component, thereby shifting substrate preference toward 2-oxoglutarate while retaining residual catalytic capacity for 2-oxoadipate [79]. This metabolic redundancy likely preserves glutaryl-CoA formation, preventing meaningful biochemical rescue in GA1. This emphasizes the need for more proximal targets like AASS and AADAT.

AADAT is involved in the lysine degradation pathway and participates in the kynurenine pathway of tryptophan metabolism [57]. It facilitates the transamination of 2-aminoadipate to 2-ketoadipate and converts kynurenine to kynurenic acid, a neuroprotective metabolite with NMDA receptor antagonistic properties [23]. Despite these roles, AADAT mutations have not been conclusively linked to human disease, and knockout studies in rodents show no severe phenotype, indicating it may be a safe therapeutic target [80].

AASS, on the other hand, is a bifunctional mitochondrial enzyme that catalyzes the first two steps of the saccharopine pathway, converting lysine to saccharopine and

subsequently to 2-aminoadipic semialdehyde [23]. Its role in lysine catabolism is well-defined in peripheral tissues, but recent work suggests low or undetectable expression in the brain under physiological conditions [81]. Notably, Sauer et al. [82] and Sacksteder et al. [83] reported that AASS expression is low to undetectable in adult murine brain tissues under basal conditions, although expression may be induced under metabolic stress. Similarly, it has been discussed potential metabolic compartmentalization in the brain [81], highlighting the relevance of local versus systemic lysine metabolism. These observations suggest that cerebral metabolism of lysine could vary by developmental stage, cell type, and physiological context. Individuals with AASS deficiency, displaying hyperlysinemia, exhibit a benign clinical phenotype, further supporting the notion that targeting AASS is safe and well-tolerated [84].

To systematically evaluate the effects of AADAT and AASS inhibition in GA1, I used double knockout mice generated by crossing *Gcdh* KO mice with either *Aadat* KO or *Aass* KO strains. Before proceeding with phenotypic analysis, gene expression verification was essential. Transcript analysis confirmed the absence of *Aadat* in all organs of the *Gcdh/Aadat* KO model, including the brain, where it was surprisingly not expressed even in WT or *Gcdh* KO controls. For AASS, expression was also not observed in brain tissue on the protein level. These findings show both these enzyme with brain-specific area expression and not in whole homogenate which could have led to no detection in the protein measurement analysis.

The first layer of assessment involved physical and behavioral stress response. Upon exposure to HLD, *Gcdh* KO mice rapidly lost weight, developed seizure-like activity, and showed higher mortality rates. In contrast, both double KO models (*Gcdh/Aass* KO and *Gcdh/Aadat* KO) showed significantly improved survival, weight maintenance, and reduced behavioral abnormalities, suggesting that both strategies confer overall clinical benefit (figure 22 and 31).

Biochemical analyses revealed a more robust systemic reduction of GA in *Gcdh/Aass* KO mice, with decreases ranging from 70% under standard diet and 40–70% under HLD, especially in plasma, urine, kidney, and liver (figure 33). Conversely, in *Gcdh/Aadat* KO mice, significant reduction in GA was observed in an organ specific pattern. In the brain

tissue, it decreased to 50% under standard diet. While levels remained elevated or even increased in peripheral organs, particularly under HLD (figure 33).

Levels of 3OHGA were not significantly changed as seen in GA. The present study supports earlier reports that GA levels in urine and tissues, including the brain, are consistently higher than those of 3OHGA and more closely correlate with residual GCDH activity [14, 75]. Thus, GA remains the most reliable biomarker for disease monitoring in GA1, due to its stability, abundance in urine and plasma, and strong correlation with metabolic status. Also, increased levels of nontoxic C5DC indicate the body's enzymatic mechanisms to detoxify glutaryl-CoA (figure 1) [85]. Additionally, neurotoxic QA, a metabolite from the tryptophan pathway, is downregulated in *Gcdh/Aass* KO group under standard diet systemically (figure 30). This could indicate the role of targeting AASS in protecting acute striatal damage [86] when combined with low lysine diet.

This differential effect suggests that AADAT inhibition exerts a brain-specific protective effect, potentially by limiting localized production of glutaryl-CoA or indirectly boosting neuroprotective kynurenine metabolism. While AASS inhibition offers a broader, system-wide reduction.

Earlier animal studies, including McMillan et al. [87], described the fruit-eating bat *Rousettus aegyptiacus* as an example of selective hepatic GCDH enzyme deficiency with preserved cerebral enzyme function. Despite excessive urinary excretion of GA and 3OHGA, these bats do not exhibit neurological symptoms, presumably because of absent cerebral metabolite accumulation. This previous model helps to understand how the AADAT inhibition causing brain specific protection led to recovery of neurological symptoms in the mouse model.

However, in the long term the increase in these metabolites could have a detrimental effect on the organs. Thus, a systemic or at least a liver and brain targeted treatment strategy should be considered, indicating AASS could be a more suitable candidate.

In recent years, substrate reduction therapy (SRT) has been investigated as a complementary therapeutic strategy for GA1. PF-04859989, a potent and selective inhibitor of AADAT developed by Pfizer, was initially characterized by its ability to reduce

KA formation in the brain, with potential application in schizophrenia research [61]. Given its reported specificity and CNS penetration, PF-04859989 is repurposed in this study to evaluate its efficacy in GA1 models. However, *in vivo* findings have demonstrated a lack of therapeutic benefit and in some cases, exacerbation of metabolite accumulation, raising concerns about its applicability in GA1 treatment (figure 25).

The *in vivo* administration of PF-04859989 in *Gcdh* KO mouse models failed to demonstrate a therapeutic effect even after exposure at pharmacologically relevant doses. Mice were treated systemically with PF-04859989, and subsequent analysis of brain and plasma metabolites showed no significant reduction in GA or 3OHGA levels (figure 27). In some organs, metabolite concentrations were elevated. This suggests a potential disruption of compensatory amino acid pathways.

This result could be explained by the dual functionality of AADAT in multiple metabolic pathways [81]. Inhibiting AADAT may lead to shunting of upstream intermediates toward alternative transamination routes, possibly enhancing flux through other enzymes that promote GA and 3OHGA accumulation. Thus, inhibiting AADAT may be insufficient to significantly alter the metabolic flux toward glutaryl-CoA.

In conclusion, targeting genetically and pharmacologically AADAT inhibition as GA1 therapy has not translated into effective metabolic correction *in vivo*. Future SRT strategies in GA1 may benefit from targeting earlier and more lysine-specific enzymes such as AASS, which has shown promising results in the double KO mouse model. Moreover, AASS has potential as a therapeutic target in other lysine-related disorders, including pyridoxine-dependent epilepsy (PDE). In PDE, excessive lysine catabolism leads to toxic accumulation of 2-aminoadipic semialdehyde and its derivatives, which sequester vitamin B6. Studies have proposed that limiting lysine degradation through AASS inhibition may enhance the efficacy of B6 supplementation [88, 89].

This study presents strong preclinical evidence for the use of AASS as a druggable target in GA1. Inhibiting this enzyme offers systemic benefits, improves survival and behavior, and reduces neurotoxic metabolite levels across critical organs. Ultimately, combining SRT strategies with existing dietary may offer the most comprehensive protection against neurological and systemic disease progression in GA1.

Further work will focus on developing pharmacological AASS inhibitors, testing combination therapies with microbiota modulation, and evaluating long-term outcomes in larger animal models.

Limitations

While this study provides novel insights into the metabolic mechanisms underlying GA1, several limitations must be acknowledged. First, histopathological assessment was restricted, a more comprehensive morphological evaluation would be required to assess region-specific vulnerability and the temporal evolution of neurodegeneration. In addition, the study did not investigate chromatin-level regulation of *Gcdh* expression and therefore cannot confirm whether epigenetic differences contribute to the divergent metabolic phenotypes observed between C57BL/6N and SV129 genetic backgrounds. Finally, due to technical constraints, the study did not include real-time brain recording during HLD stress, which could have provided deeper functional validation of the observed physical changes.

Conclusion

This study presents strong preclinical evidence for the use of AASS as a druggable target for substrate reduction therapy in GA1. Inhibiting this enzyme upstream of GCDH in the lysine degradation pathway offers systemic benefits, improves survival and behavior, and reduces neurotoxic metabolite levels across critical organs in *Gcdh* KO mice, a worldwide used animal model for GA1. Ultimately, combining substrate reduction strategies with existing dietary and supportive therapies may offer reliable protection against the accumulation of neurotoxic metabolic as well as neurological and systemic disease manifestation in GA1. In order to study efficiently future AASS SRT, *GCDH* KO iPSC lines were successfully generated and validated. By directing the edited clones toward NPCs, this model faithfully preserves the developmental potential required to investigate GA1-associated neurodevelopmental alterations. In contrast to AASS, inhibition of AADAT may be considered as a candidate for complementary or combined therapy rather than for standalone therapy.

Original Publications

Major results of the present work have been summarized for publication. Currently, the first part of it, describing AASS as a novel target for substrate reduction therapy, has been submitted to Scientific Report. The latter two manuscripts, which describe novel IPSC-based in vitro models for GA1, are in preparation:

1. Celine Saad[1,#], Sabine Jung-Klawitter[1,#], Bianca Dimitrov[1], Juan Antonio Aguilar-Pimentel[2], Lore Becker[2], Patricia da Silva-Buttkus[2], Nathalia RV Dragano[2,3], Lillian Garrett[2], Sabine M Hölter[2], Birgit Rathkolb[2,3,4], Adrián Sanz-Moreno[2], Nadine Spielmann[2], Helmut Fuchs[2], Valerie Gailus-Durner[2], Christian P. Schaaf[6], Giancarlo la Marca[7,8], Roberta Damiano[7], Udo Engelke[9], the CHARLIE Consortium, Martin Hrabe de Angelis[2,3,5*], Sander M. Houten[10*], and Stefan Kölker[1*] (2025). **Aminoadipate-semialdehyde synthase, a potential target for substrate reduction therapy in glutaric aciduria type 1**. Scientific reports, submitted.

2. Celine Saad[a], Larissa Motsch[a], Blaž Lupse[a], Verena Backendorf[a], Samuel Hoffman[a], Stefan Kölker[a], and Sabine Jung-Klawitter[a, *](2025) **Generation of Glutaric aciduria type 1 GCDH5(1) induced pluripotent stem cell lines**. Stem Cell Research, in preparation.

3. Celine Saad[a], Larissa Motsch[a], Blaž Lupse[a], Verena Backendorf[a], Samuel Hoffman[a], Stefan Kölker[a], and Sabine Jung-Klawitter[a, *](2025). **Generation of Glutaric aciduria type 1 GCDH6(3) induced pluripotent stem cell lines.** Stem Cell Research, in preparation.

References

1. Gordon, N., *Glutaric aciduria types I and II.* Brain Dev, 2006. **28**(3): p. 136-40.
2. Sauer, S.W., et al., *Intracerebral accumulation of glutaric and 3-hydroxyglutaric acids secondary to limited flux across the blood-brain barrier constitute a biochemical risk factor for neurodegeneration in glutaryl-CoA dehydrogenase deficiency.* J Neurochem, 2006. **97**(3): p. 899-910.
3. Harting, I., et al., *Dynamic changes of striatal and extrastriatal abnormalities in glutaric aciduria type I.* Brain, 2009. **132**(Pt 7): p. 1764-82.
4. Bjugstad, K.B., S.I. Goodman, and C.R. Freed, *Age at symptom onset predicts severity of motor impairment and clinical outcome of glutaric acidemia type 1.* J Pediatr, 2000. **137**(5): p. 681-6.
5. Stefan Kolker MD, N.B.M., *Glutaric aciduria.* Medlink Neurology, 2024.
6. Yoldas Celik, M., et al., *Glutaric aciduria type 1: Insights into diagnosis and neurogenetic outcomes.* Eur J Pediatr, 2024. **184**(1): p. 72.
7. Patil, M.G., et al., *Glutaric Aciduria Presenting With an Acute Encephalitic Crisis: A Case Report.* Cureus, 2024. **16**(7): p. e65722.
8. Strauss, K.A. and D.H. Morton, *Type I glutaric aciduria, part 2: a model of acute striatal necrosis.* Am J Med Genet C Semin Med Genet, 2003. **121C**(1): p. 53-70.
9. Martner, E.M.C., et al., *The biochemical subtype is a predictor for cognitive function in glutaric aciduria type 1: a national prospective follow-up study.* Sci Rep, 2021. **11**(1): p. 19300.
10. Heringer, J., et al., *Use of guidelines improves the neurological outcome in glutaric aciduria type I.* Ann Neurol, 2010. **68**(5): p. 743-52.
11. Boy, N., et al., *Newborn screening: A disease-changing intervention for glutaric aciduria type 1.* Ann Neurol, 2018. **83**(5): p. 970-979.
12. Viau, K., et al., *Glutaric acidemia type 1: outcomes before and after expanded newborn screening.* Mol Genet Metab, 2012. **106**(4): p. 430-8.
13. Boy, N., et al., *Extrastriatal changes in patients with late-onset glutaric aciduria type I highlight the risk of long-term neurotoxicity.* Orphanet J Rare Dis, 2017. **12**(1): p. 77.
14. Kolker, S., et al., *Natural history, outcome, and treatment efficacy in children and adults with glutaryl-CoA dehydrogenase deficiency.* Pediatr Res, 2006. **59**(6): p. 840-7.
15. D. I. Zafeiriou1, J.Z., P. Augoustidou-Savvopoulou1, and A.S. I. Mauromatis3, E. Kontopoulos1, G. Katzos1, G. F. Hoffmann2, *Atypical and Variable Clinical Presentation of GA1.* Neuropediatrics, 2000. **31: 303±306**.
16. Schmiesing, J., et al., *Disease-Linked Glutarylation Impairs Function and Interactions of Mitochondrial Proteins and Contributes to Mitochondrial Heterogeneity.* Cell Rep, 2018. **24**(11): p. 2946-2956.
17. Popek, M., et al., *Two inborn errors of metabolism in a newborn: glutaric aciduria type I combined with isobutyrylglycinuria.* Clin Chim Acta, 2010. **411**(23-24): p. 2087-91.
18. Johannes Pfeil1, S.L., 3, Georg F Hoffmann1, Stefan Kölker1, Martin Lindner1 and Peter Burgard1*, *Newborn screening by tandem mass spectrometry for*

glutaric aciduria type 1: a cost-effectiveness analysis. Orphanet Journal of Rare Diseases 2013. **8:167**.
19. BRANDT, E.C.a.N.J., *STUDIES ON GLUTARYL-A DEHYDROGENASE IN LEUCOC~ES, FIBROBLASTS AND AMNIOTIC FLUID CELLS. THE NORMAL ENZYME AND THE MUTANT FORM IN PATIENTS WITH GLUTARIC ACIDURIA.* Clinica Chimica Actu, 1978. **88, 267-276**.
20. Lin, Y., et al., *Biochemical and molecular features of Chinese patients with glutaric acidemia type 1 detected through newborn screening.* Orphanet J Rare Dis, 2021. **16**(1): p. 339.
21. Bijarnia, S., et al., *Glutaric aciduria type I: outcome following detection by newborn screening.* J Inherit Metab Dis, 2008. **31**(4): p. 503-7.
22. Boy, N., et al., *Recommendations for diagnosing and managing individuals with glutaric aciduria type 1: Third revision.* J Inherit Metab Dis, 2023. **46**(3): p. 482-519.
23. Leandro, J. and S.M. Houten, *The lysine degradation pathway: Subcellular compartmentalization and enzyme deficiencies.* Mol Genet Metab, 2020. **131**(1-2): p. 14-22.
24. Jones, P., K. Patel, and D. Rakheja, *Chapter 2 - Disorder: Glutaric acidemia type 1*, in *A Quick Guide to Metabolic Disease Testing Interpretation (Second Edition)*, P. Jones, K. Patel, and D. Rakheja, Editors. 2020, Academic Press. p. 17-20.
25. Niska-Blakie, J., et al., *Knockout of the non-essential gene SUGCT creates diet-linked, age-related microbiome disbalance with a diabetes-like metabolic syndrome phenotype.* Cell Mol Life Sci, 2020. **77**(17): p. 3423-3439.
26. Knorr, S., et al., *Widespread bacterial lysine degradation proceeding via glutarate and L-2-hydroxyglutarate.* Nat Commun, 2018. **9**(1): p. 5071.
27. Pardridge, W.M., *Blood-Brain Barrier Carrier-Mediated Transport and Brain Metabolism of Amino Acids.* Neurochemical Research, 1998. **Vol. 23, No. 5**.
28. Chang, F.M., *Update current understanding of neurometabolic disorders related to lysine metabolism.* Epilepsy Behav, 2023. **146**: p. 109363.
29. R. A. CHALMERS, C.R.R., T. E. STACEY, AND C. L. HOPPEL, *Urinary Excretion of 2-Carnitine and Acylcarnitines by Patients with Disorders of Organic Acid Metabolism: Evidence for Secondary Insufficiency of 2-Carnitine.* PEDIATRIC RESEARCH, 1984. **18**.
30. Christiane Obleda, I.P.a.D.B.b., *Metabolic bases of amino acid requirements in acute diseases.* Current Opinion in Clinical Nutrition and Metabolic Care 2002.
31. Jafari, P., et al., *The unsolved puzzle of neuropathogenesis in glutaric aciduria type I.* Mol Genet Metab, 2011. **104**(4): p. 425-37.
32. Zinnanti, W.J. and J. Lazovic, *Mouse model of encephalopathy and novel treatment strategies with substrate competition in glutaric aciduria type I.* Mol Genet Metab, 2010. **100 Suppl 1**: p. S88-91.
33. Sauer, S.W., et al., *Bioenergetics in glutaryl-coenzyme A dehydrogenase deficiency: a role for glutaryl-coenzyme A.* J Biol Chem, 2005. **280**(23): p. 21830-6.
34. Seminotti, B., et al., *Acute lysine overload provokes protein oxidative damage and reduction of antioxidant defenses in the brain of infant glutaryl-CoA*

dehydrogenase deficient mice: a role for oxidative stress in GA I neuropathology. J Neurol Sci, 2014. **344**(1-2): p. 105-13.
35. Wajner, M., et al., *Pathogenesis of brain damage in glutaric acidemia type I: Lessons from the genetic mice model.* International Journal of Developmental Neuroscience, 2019. **78**(1): p. 215-221.
36. Paria, P., et al., *Identification of novel pathogenic variants in the GCDH gene and assessment of neurodevelopmental outcomes in 24 children with glutaric aciduria type 1.* Eur J Paediatr Neurol, 2022. **39**: p. 49-58.
37. Sauer, S.W., et al., *Glutaric aciduria type I and methylmalonic aciduria: simulation of cerebral import and export of accumulating neurotoxic dicarboxylic acids in in vitro models of the blood-brain barrier and the choroid plexus.* Biochim Biophys Acta, 2010. **1802**(6): p. 552-60.
38. Kolker, S., et al., *Pathomechanisms of neurodegeneration in glutaryl-CoA dehydrogenase deficiency.* Ann Neurol, 2004. **55**(1): p. 7-12.
39. David M. Koeller1, Michael Woontner2, Linda S. Crnic2,3, Bette Kleinschmidt-DeMasters4,5, Janet Stephens5, Edgar L. Hunt5 and Stephen I. Goodman2, *Biochemical, pathologic and behavioral analysis of a mouse model of glutaric acidemia type I.* Human Molecular Genetics, 2002. **Vol. 11, No. 4**.
40. Keyser, B., et al., *Transport and distribution of 3-hydroxyglutaric acid before and during induced encephalopathic crises in a mouse model of glutaric aciduria type 1.* Biochim Biophys Acta, 2008. **1782**(6): p. 385-90.
41. Mori, M.A., et al., *A systems biology approach identifies inflammatory abnormalities between mouse strains prior to development of metabolic disease.* Diabetes, 2010. **59**(11): p. 2960-71.
42. Qiao, Q., et al., *Metabolomic analysis of normal (C57BL/6J, 129S1/SvImJ) mice by gas chromatography-mass spectrometry: detection of strain and gender differences.* Talanta, 2011. **85**(1): p. 718-24.
43. K. Maeda, R.H., and K.-A. Hossmann1, *Regional Metabolic Disturbances and Cerebrovascular Anatomy after Permanent Middle Cerebral Artery Occlusion in C57Black/6 and SV129 Mice.* NeurobiologyofDisease, 1999.
44. Fujii, M., et al., *Strain-related differences in susceptibility to transient forebrain ischemia in SV-129 and C57black/6 mice.* Stroke, 1997. **28**(9): p. 1805-10; discussion 1811.
45. Mozhui, K., et al., *Strain differences in stress responsivity are associated with divergent amygdala gene expression and glutamate-mediated neuronal excitability.* J Neurosci, 2010. **30**(15): p. 5357-67.
46. Varul, J., et al., *Dopamine System, NMDA Receptor and EGF Family Expressions in Brain Structures of Bl6 and 129Sv Strains Displaying Different Behavioral Adaptation.* Brain Sci, 2021. **11**(6).
47. STEWARD*, P.E.S.A.O., *Genetic determinants of susceptibility to excitotoxic cell death: Implications for gene targeting approaches.* Proc. Natl. Acad. Sci. USA, 1997.
48. Erickson, R.P., *Mouse models of human genetic disease: which mouse is more like a man?* Bioessays, 1996. **18**(12): p. 993-8.

49. Sauer, S.W., et al., *Multifactorial modulation of susceptibility to l-lysine in an animal model of glutaric aciduria type I.* Biochim Biophys Acta, 2015. **1852**(5): p. 768-77.
50. Strauss, K.A., et al., *Safety, efficacy and physiological actions of a lysine-free, arginine-rich formula to treat glutaryl-CoA dehydrogenase deficiency: focus on cerebral amino acid influx.* Mol Genet Metab, 2011. **104**(1-2): p. 93-106.
51. Singanamalla, B., et al., *The Challenge of Severe Acute Malnutrition in Inborn Errors of Metabolism: Does Medical Food Alone Suffice?* J Pediatr Genet, 2023. **12**(2): p. 175-178.
52. Kolker, S., et al., *Diagnosis and management of glutaric aciduria type I--revised recommendations.* J Inherit Metab Dis, 2011. **34**(3): p. 677-94.
53. Boy, N., et al., *Impact of newborn screening and quality of therapy on the neurological outcome in glutaric aciduria type 1: a meta-analysis.* Genet Med, 2021. **23**(1): p. 13-21.
54. Rajanala, K., F. Dotiwala, and A. Upadhyay, *Geographic atrophy: pathophysiology and current therapeutic strategies.* Front Ophthalmol (Lausanne), 2023. **3**: p. 1327883.
55. Biagosch, C., et al., *Elevated glutaric acid levels in Dhtkd1-/Gcdh- double knockout mice challenge our current understanding of lysine metabolism.* Biochim Biophys Acta Mol Basis Dis, 2017. **1863**(9): p. 2220-2228.
56. Denise L.M. Goh, a., b Ankita Patel,c George H. Thomas,a,c Gajja S. Salomons,d Danielle S.M. Schor,d Cornelis Jakobs,d and Michael T. Geraghtya,*, *Characterization of the human gene encoding a-aminoadipate aminotransferase (AADAT).* Molecular Genetics and Metabolism 2002. **76 172–180**.
57. Buchli, R., et al., *Cloning and functional expression of a soluble form of kynurenine/alpha-aminoadipate aminotransferase from rat kidney.* J Biol Chem, 1995. **270**(49): p. 29330-5.
58. Han, Q., et al., *Substrate specificity and structure of human aminoadipate aminotransferase/kynurenine aminotransferase II.* Biosci Rep, 2008. **28**(4): p. 205-15.
59. Sander M Houten1, Heleen te Brinke1, Simone Denis1, Jos PN Ruiter1, Alida C Knegt3, Johannis BC de Klerk4, and J.H. Persephone Augoustides-Savvopoulou5, Matthias R Baumgartner6, Turgay Coşkun8, Johannes Zschocke9, Jörn Oliver Sass7,10, Bwee Tien Poll-The2, Ronald JA Wanders1,2 and Marinus Duran1,2, *Genetic basis of hyperlysinemia.* Orphanet Journal of Rare Diseases 2013. **8:57**.
60. Leandro, J., et al., *Deletion of 2-aminoadipic semialdehyde synthase limits metabolite accumulation in cell and mouse models for glutaric aciduria type 1.* J Inherit Metab Dis, 2020. **43**(6): p. 1154-1164.
61. Dounay, A.B., et al., *Discovery of Brain-Penetrant, Irreversible Kynurenine Aminotransferase II Inhibitors for Schizophrenia.* ACS Med Chem Lett, 2012. **3**(3): p. 187-92.
62. Noorbakhsh, A.A.-O., et al., *Designing a natural inhibitor against human kynurenine aminotransferase type II and a comparison with PF-04859989: a*

computational effort against schizophrenia. Journal of biomolecular structure & dynamics, 2022. **40(15), 7038–7051**(1538-0254 (Electronic)).
63. Erhardt, S., et al., *The kynurenic acid hypothesis of schizophrenia.* Physiol Behav, 2007. **92**(1-2): p. 203-9.
64. Wu, H.Q., et al., *Targeting kynurenine aminotransferase II in psychiatric diseases: promising effects of an orally active enzyme inhibitor.* Schizophr Bull, 2014. **40 Suppl 2**(Suppl 2): p. S152-8.
65. Thomas C. Lehman, D.E.H., Ajay Bhala, and Colin Thorpe, *An Acyl-Coenzyme A Dehydrogenase Assay Utilizing the Ferricenium Ion.* ANALYTICALBIOCHEMISTRY 1990. **186,280-284**.
66. Livak, K.J. and T.D. Schmittgen, *Analysis of Relative Gene Expression Data Using Real-Time Quantitative PCR and the 2−ΔΔCT Method.* Methods, 2001. **25**(4): p. 402-408.
67. Lowry, O., et al., *Protein Measurement with the Folin Phenol Reagent.* Journal of Biological Chemistry, 1951. **193**(1): p. 265-275.
68. Dimitrov, B., et al., *Organic acidurias: Major gaps, new challenges, and a yet unfulfilled promise.* J Inherit Metab Dis, 2021. **44**(1): p. 9-21.
69. Kozak, R., et al., *Reduction of brain kynurenic acid improves cognitive function.* J Neurosci, 2014. **34**(32): p. 10592-602.
70. Rudeck, J., et al., *Liver lobe and strain differences in the activity of murine cytochrome P450 enzymes.* Toxicology, 2018. **404-405**: p. 76-85.
71. Wang, S., et al., *Strain differences between CD-1 and C57BL/6 mice in expression of metabolic enzymes and DNA methylation modifications of the primary hepatocytes.* Toxicology, 2019. **412**: p. 19-28.
72. Xiao, F., et al., *Effects of essential amino acids on lipid metabolism in mice and humans.* J Mol Endocrinol, 2016. **57**(4): p. 223-231.
73. Zinnanti, W.J., et al., *A diet-induced mouse model for glutaric aciduria type I.* Brain, 2006. **129**(4): p. 899-910.
74. Ferraro, T.N., et al., *Differential Susceptibility to Seizures Induced by Systemic Kainic Acid Treatment in Mature DBA/2J and C57BLI6J Mice.* Epilepsia, 1995. **36**(3): p. 301-307.
75. Strauss, K.A., et al., *Type I glutaric aciduria, part 1: natural history of 77 patients.* Am J Med Genet C Semin Med Genet, 2003. **121C**(1): p. 38-52.
76. Dodd, D., et al., *A gut bacterial pathway metabolizes aromatic amino acids into nine circulating metabolites.* Nature, 2017. **551**(7682): p. 648-652.
77. Lamanna, W.C., et al., *A genetic model of substrate reduction therapy for mucopolysaccharidosis.* J Biol Chem, 2012. **287**(43): p. 36283-90.
78. Struys, E.A. and C. Jakobs, *Metabolism of lysine in alpha-aminoadipic semialdehyde dehydrogenase-deficient fibroblasts: evidence for an alternative pathway of pipecolic acid formation.* FEBS Lett, 2010. **584**(1): p. 181-6.
79. Leandro, J., et al., *DHTKD1 and OGDH display substrate overlap in cultured cells and form a hybrid 2-oxo acid dehydrogenase complex in vivo.* Hum Mol Genet, 2020. **29**(7): p. 1168-1179.
80. Yu, P., et al., *Biochemical and phenotypic abnormalities in kynurenine aminotransferase II-deficient mice.* Mol Cell Biol, 2004. **24**(16): p. 6919-30.

81. Hallen, A., J.F. Jamie, and A.J. Cooper, *Lysine metabolism in mammalian brain: an update on the importance of recent discoveries.* Amino Acids, 2013. **45**(6): p. 1249-72.
82. Sauer, S.W., et al., *Therapeutic modulation of cerebral L-lysine metabolism in a mouse model for glutaric aciduria type I.* Brain, 2011. **134**(Pt 1): p. 157-70.
83. Sacksteder, K.A., et al., *Identification of the alpha-aminoadipic semialdehyde synthase gene, which is defective in familial hyperlysinemia.* Am J Hum Genet, 2000. **66**(6): p. 1736-43.
84. Yeganeh, M., et al., *A case of hyperlysinemia identified by urine newborn screening.* JIMD Rep, 2023. **64**(6): p. 440-445.
85. Tortorelli, S., et al., *The urinary excretion of glutarylcarnitine is an informative tool in the biochemical diagnosis of glutaric acidemia type I.* Mol Genet Metab, 2005. **84**(2): p. 137-43.
86. Amaral, A.U., et al., *Induction of Neuroinflammatory Response and Histopathological Alterations Caused by Quinolinic Acid Administration in the Striatum of Glutaryl-CoA Dehydrogenase Deficient Mice.* Neurotox Res, 2018. **33**(3): p. 593-606.
87. McMillan, T.A., et al., *Conservation of central nervous system glutaryl-coenzyme A dehydrogenase in fruit-eating bats with glutaric aciduria and deficient hepatic glutaryl-coenzyme A dehydrogenase.* Journal of Biological Chemistry, 1988. **263**(33): p. 17258-17261.
88. van Karnebeek, C.D., et al., *Lysine-Restricted Diet as Adjunct Therapy for Pyridoxine-Dependent Epilepsy: The PDE Consortium Consensus Recommendations.* JIMD Rep, 2014. **15**: p. 1-11.
89. Coughlin, C.R., 2nd, et al., *Triple therapy with pyridoxine, arginine supplementation and dietary lysine restriction in pyridoxine-dependent epilepsy: Neurodevelopmental outcome.* Mol Genet Metab, 2015. **116**(1-2): p. 35-43.

List of Figures

List of Tables

Appendix

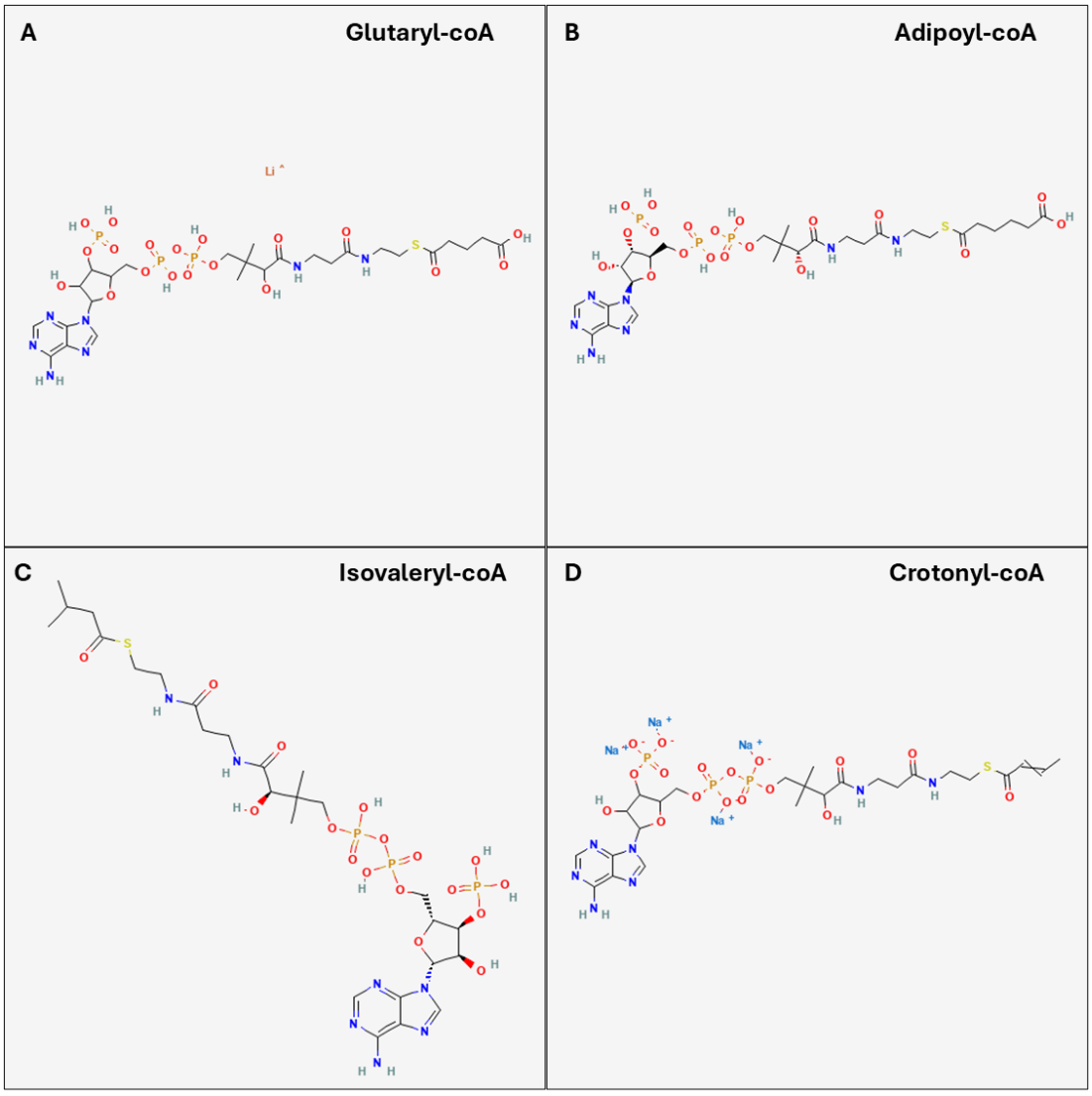

Figure 34. Molecular structures of the different substrate showing resemblance in carbon backbone to Glutaryl-CoA generated from NCBI Pubchem website.

Acknowledgments

Completing this doctoral thesis has been one of the most challenging and meaningful journeys of my life, and it would not have been possible without the support, guidance, and kindness of many people to whom I owe my deepest gratitude.

First and foremost, I would like to express my sincere appreciation to my supervisor, Prof. Stefan Kölker, for your unwavering guidance and the time you invested in helping me grow as a scientist and a person. I am truly grateful for the opportunity to learn from you. My deepest thanks go to Prof. Christian Schaaf for your insightful discussions, your constructive criticism, and your steady support, your expertise has been invaluable.

I am profoundly grateful to all members of the AG neurotransmitter's lab for creating a stimulating, supportive, and warm environment. Thank you for the scientific exchanges, the technical help, the shared frustrations, and the shared laughter. I am happy to have gained your friendship throughout this journey.

To my dear friends Salome, Charlotte, Daniel, Aiste and the many others who stood by me in big and small ways, thank you for reminding me of life beyond the lab. Your encouragement, your messages in difficult moments, and your presence, whether in person or through texts, gave me strength when this journey felt overwhelming.

Most importantly, I extend my deepest gratitude to my family. To my parents, Odette and Georges Saad, your unconditional love, sacrifices, and prayers are the foundation of everything I have achieved. No words can express how grateful I am for your constant support throughout all the highs and lows. To my brother Serge, thank you for your patience and your encouragement. Your belief in my abilities, especially in the moments when I doubted myself, has shaped this work more than you know. To John, you have been my motivation and my safe place through this process despite the challenges.

This dissertation is dedicated to all of you. Each page reflects not only my effort, but also the support, love, and resilience you have given me throughout this journey. I am humbled and deeply grateful to every person who walked alongside me and helped me become who I am today. Thank you.